A Review on Removal of Carbon Dioxide (CO_2) using Zeolitic Imidazolate Frameworks: Adsorption and Conversion via Catalysis

Hani Nasser Abdelhamid[1,2,3]*

[1]Advanced Multifunctional Materials Laboratory, Department of Chemistry, Assiut University, Assiut, 71516, Egypt

[2]Proteomics Laboratory for Clinical Research and Materials Science, Department of Chemistry, Assiut University, Assiut, 71516, Egypt

[3]Nanotechnology Research Centre (NTRC), The British University in Egypt, El-Shorouk City, Suez Desert Road, P.O. Box 43, Cairo 11837, Egypt

***** Email: hany.abdelhamid@aun.edu.eg; **Tel**:+201029952642; **Fax**: 0020-88.234222

Abstract

Carbon dioxide (CO_2) is one of the culprit causes of global climatic changes. Furthermore, the efficient separation of CO_2 from other gaseous mixtures using ZIFs-based materials is vital for several processes such as flue gas separation, gas sweetening, and natural gas processing. Zeolitic imidazolate frameworks (ZIFs)-based materials are emerging adsorbents and catalysts for CO_2 gas removal via adsorption and conversion into valuable chemicals. ZIFs-based adsorbents with high adsorption/conversion efficiencies and tunable properties can be achieved by judicious synthesis and fabrication methods. We reviewed ZIF-based materials for CO_2 removal via adsorption and catalysis (e.g., cycloaddition, carboxylation, hydrogenation, N-formylation, electrocatalysis, and photocatalysis). In addition, recent development methods such as membrane synthesis and ways to improve the gas separation performance of ZIF membranes were highlighted. The prospective point of view to promote industrial applications and commercialization of ZIF-based materials was briefly discussed. Once challenges such as low performance and reproducibility for ZIFs-based materials are solved, scalability and cost-effectiveness should not become issues.

Keywords: Zeolitic Imidazolate Frameworks; Metal-organic Frameworks; Carbon dioxide; Cycloaddition; Photocatalysis.

1. Introduction

Global climate changes represent a serious threat to humans. The Intergovernmental Panel on Climate Change (IPCC) report expected that the mean global temperature will rise by 1.9 °C in 2100 (https://www.ipcc.ch/). It is estimated that the concentration of CO_2 in the atmosphere will be increased to 950 ppm by 2100 (the present value of 400 ppm; https://www.ipcc.ch/). The changes in the climate temperature are irreversible, causing a real threat to the environment and humankind. The emission of gases is one of the most causes of global climate change[1-11]. Gases can be classified as incondensable inorganic gases (i.e., hydrogen (H_2), carbon dioxide (CO_2), carbon monoxide (CO), nitrogen (N_2), oxygen (O_2), and noble gases such as He-Kr) and condensable organic gases (i.e., methane (CH_4), ethane (C_2H_6), ethene (C_2H_4)). Greenhouse gases, e.g., CO_2, and NO_x, are mainly responsible for global climate changes. Among these gases, CO_2 emission to the atmosphere from human activities such as breathing, industrial processes, and the burning of fossil fuels is one of the leading causes of global warming[1-11]. Thus, several methods were reported for CO_2 capture and utilization (CCU), including adsorption and sequestration[12].

Metal-organic frameworks (MOFs) are organic-inorganic crystalline porous materials[13–22]. They have well-defined pore structures with high porosity as high as 50% of the crystal volume, offering low density (0.2–1 g/cm^3) and high specific surface areas (> 10,000 m^2/g for some cases)[23]. They can be produced via a reticular synthesis procedure, creating ordered networks or framework structures with strong bonds between organic and organic moieties[24]. The construction networks between both moieties tune the geometry of MOFs via designing the secondary building units (SBUs) with suitable organic linkers[25]. The functional groups and the porosity of MOFs can be changed via methods such as post-synthetic modification (PSM)[26]. Multivariate MOFs (MTV-MOFs) with different metal nodes or clusters and other organic functionalities can also be

synthesized [27]. Many MOF materials have strong bonds between their moieties, offering high chemical and thermal stability in the temperature range of 250 °C to 500 °C[28]. The high chemical stability of MOFs, especially against water molecules, is usually required for applications such as gas adsorption of CO_2 from the atmosphere or hot-flue gases[29]. MOFs were applied for several applications, including CO_2 adsorption[30], chemical conversion/fixation of CO_2[31–40], catalysis[41–43], photovoltaic devices[44], sensors[45–48], hydrogen production[18,49–53], dye sensistizing solar cells (DSSCs)[54], water treatment[55–57], energy[58,59], and osmotic power generators[60].

Zeolitic imidazolate frameworks (ZIFs) [28,61,62] or metal-azolate frameworks (MAFs)[63] are a subclass of MOFs with similar topological morphology to inorganic porous materials zeolites[13,47,64–66]. They are composed of tetrahedrally coordinated transition metal ions, e.g., Co, Cu, Zn, and imidazole-based linkers, e.g., 2-methyl imidazole (Hmim), or benzimidazole (Bmim). ZIFs crystals are porous materials with high chemical and thermal stabilities (up to 400 °C). They have similar properties to porous MOFs with a full exposition of imidazole-based ligand edges and faces [67]. ZIFs have the potential to improve several applications such as biomedical applications [20,65], gene delivery [68–70], biomedicine[71,72], environmental [15,73–76], and energy-based applications [50,51,77–79]. They are also promising materials for gas separation/storage. ZIF-8 (Zn-based ZIFs) was reported as a colorimetric sensor for the simple detection of CO_2 [80].

Herein, ZIFs-based applications were reviewed to remove CO_2 via adsorption, fixation, and chemical conversion (**Figure 1**). This review address most of the current opportunities and challenges for the topic. We highlighted the innovative synthesis methodologies and discussed the challenges of the existing synthesis procedures. Adsorption of CO_2 from pure gas and mixed gas was summarized using various forms of ZIFs materials, including powder, membrane, thin-film, foams, and three-dimensional (3D) objects. ZIFs-based materials exhibit high adsorption

capacities and excellent selectivity compared to other porous materials. These features open the door for industrial applications and commercialization.

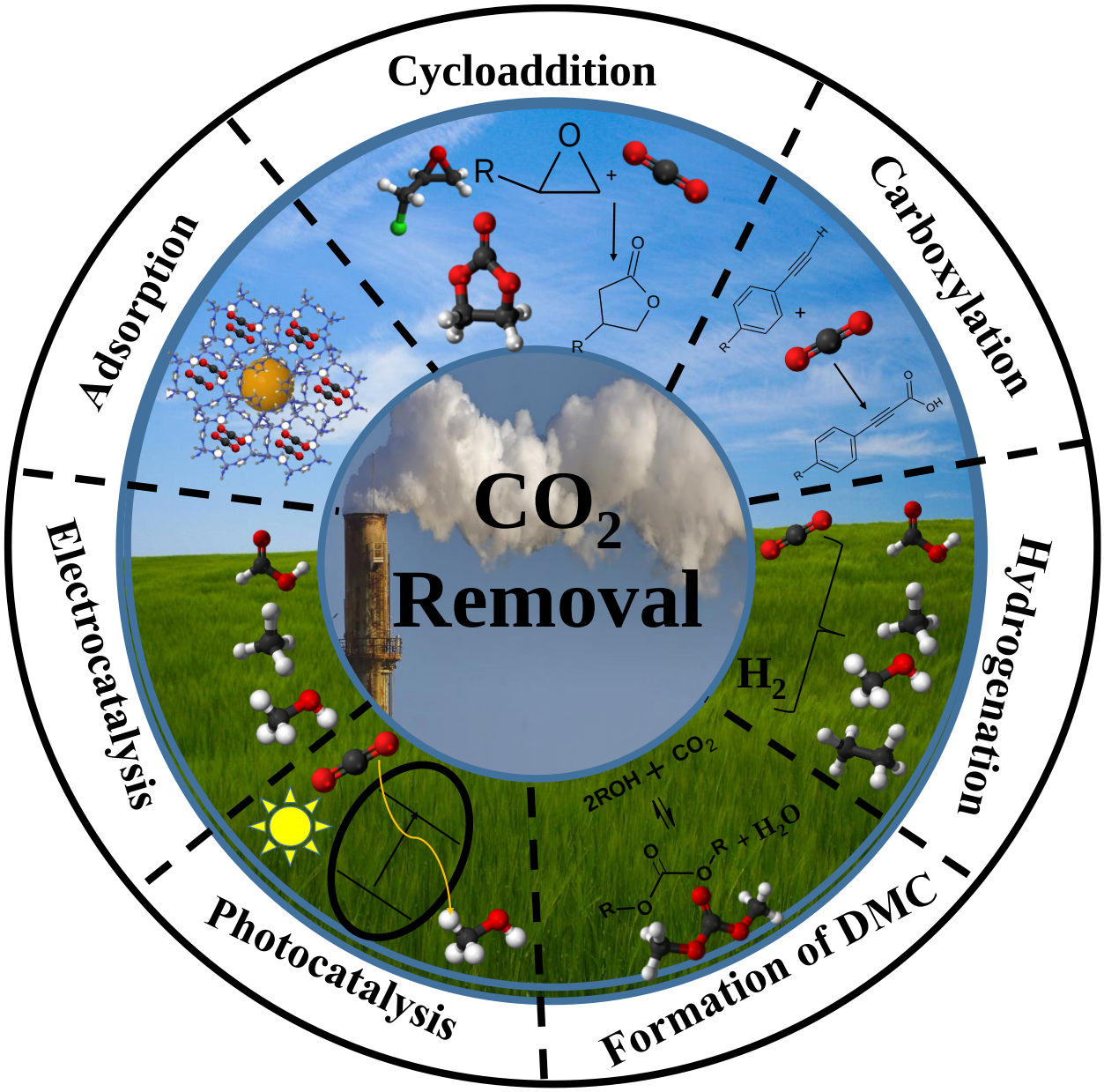

Figure 1 Overview of CO_2 removal methods covered in this Review.

2. Properties of ZIFs materials

The 3D structures of ZIFs crystals consist of transition metal cations (M) such as Zn^{2+}, and Co^{2+}, which are coordinated to an imidazole-based (Im) linker (**Figure 2**). The coordination bonds are formed between the tetrahedral metal centers and nitrogen atoms in the 1,3-positions of the imidazolate linker [81]. The nature between the N atom and the metal node is not well known. However, the crystal combines both types of covalent and coordination bonds. The bond angle of M-Im-M is 145°, similar to the Si–O–Si bond angle (145°) in zeolites. Thus, the name was 'Zeolitic Imidazaolte Frameworks', meaning 'zeolite-like materials based on imidazolate. ZIFs exhibit zeolite topology such as SOD, RHO, or LTA. ZIFs crystals show the framework's flexibility concerning gas adsorption. More than 105 ZIF topologies are in the literature (**Figure 2**) [63,82].

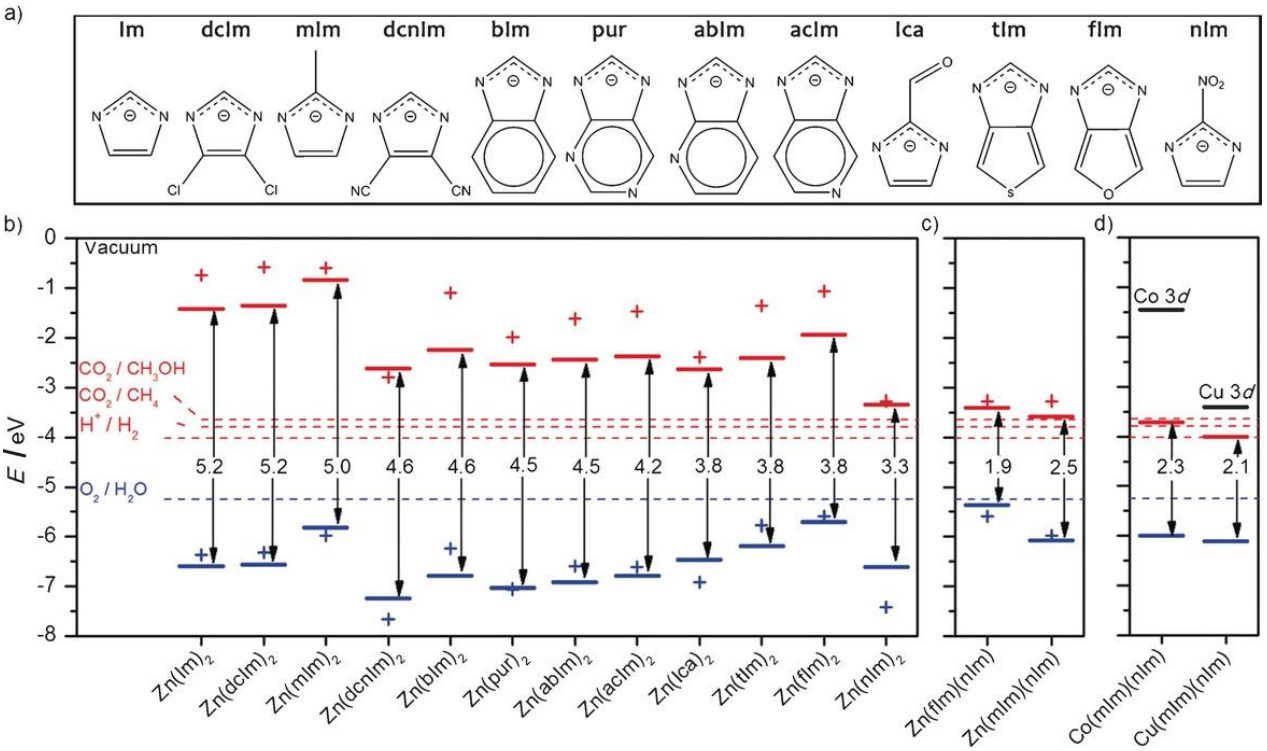

Figure 2 Common structure of linker used for the synthesis of ZIFs materials, and the positions of the highest occupied energy levels (blue) and lowest unoccupied energy levels (red) of the ZnX_2, X refers to the organic linker. Figure reprinted from Ref. [83]. This is an Open Access.

ZIFs exhibit high chemical and thermal stability (up to 400 °C). ZIFs are stable under harsh conditions such as refluxing with organic solvents, water, and aqueous alkaline solutions [28]. However, several studies reported the instability of ZIFs materials. A study stated that ZIF-8 crystallites were unstable in water under ambient conditions [84]. ZIF-8 crystals were dissolved in water, forming zinc and imidazolate ions [84]. They undergo a phase shift to a dense structure and a leaf-like morphology [84]. However, it is essential to mention that the conversion depends on the ratio of ZIF-8/water [84]. The degradation of ZIF-8 is higher in culture media than in deionized water [85]. This observation could be due to the reaction between the released zinc ions with phosphate ions in phosphate-buffered saline (PBS) or with organic moieties in Luria Bertani (L.B.) media. The degradation of ZIF-8 in L.B. and PBS media was 70–80 wt.%, which is higher than in pure water (22 wt.%) [85]. The stability of ZIFs materials can be enhanced by shielding the metal-ligand bond from the attack of water molecules [86].

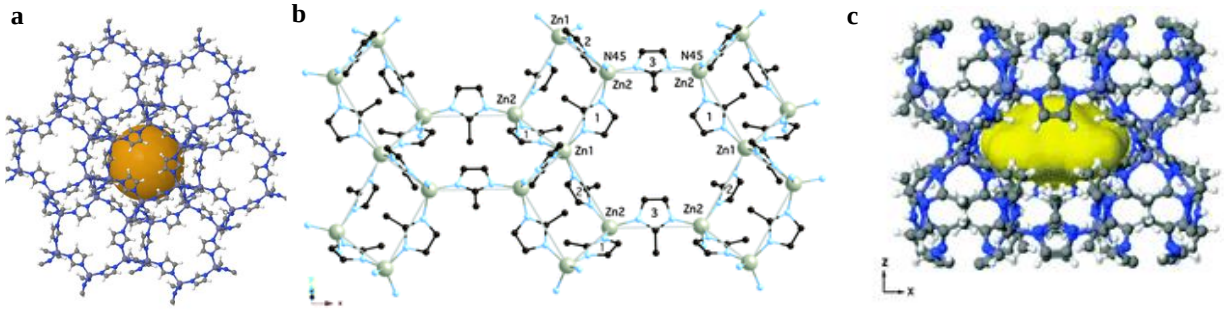

Figure 3 Crystal structure of a) ZIF-8 and b-c) ZIF-L and c) their pore shape.

ZIFs materials are porous and have flexible structures. Most of the reported ZIFs are micropore materials, i.e., pore size less than 2 nm. However, several synthesis procedures create mesopore (pore size 2-50 nm) and macropore (>50 nm) inside ZIFs crystals producing 'hierarchical porous' ZIFs. Pore size properties of ZIFs materials are essential for gas adsorption. ZIF-8 is a micropore material with diameters of 11.6 Å, connected by apertures. They are efficient materials for the

separation of gas, as well as for size-selective catalysis due to their pore size (< 5 Å) [28,82]. A study using thermodynamically corrected diffusivities of probe molecules at 35 °C showed that the adequate aperture size of ZIFs materials such as ZIF-8 was 4.0-4.2 Å [87]. These values are significantly larger than pore apertures estimated using X-ray diffraction (XRD), showing an aperture size of 3.4 Å [87]. This observation indicates that ZIF-8 showed an aperture size similar to well-known porous materials such as zeolite 4A (3.8 Å) and 5A (4.3 Å). The structures of most of the reported ZIFs are flexible. The aperture diameter of ZIF-8 increases from 3.4 to 4.0 Å after gas adsorption [88].

3. Synthesis of ZIFs

The synthesis of ZIFs materials is state-or-art. Several methods were reported to synthesize ZIFs materials, including solvothermal, hydrothermal, stirring at room temperature, mechanochemical method, microwave-assisted method, and ultrasonic-assisted method.

ZIFs materials were synthesized via solvothermal methods. The synthesis procedure involved using an organic solvent such as dimethylformamide (DMF) at a temperature above 100^{o}C for a few hours. The amide solvent such as DMF is decomposed to generate amines that deprotonate the imidazole, forming imidazolate. The resultant materials are pure phases with big crystal sizes. Hydrothermal synthesis was also reported using a solvent such as water [89–91], methanol [92,93], ethanol [94], and isopropanol [95]. However, these methods require the use of a base such as a pyridine [96], triethylamine (TEA)[97], sodium formate [98], and NaOH [73,99] to deprotonate the imidazolate.

A water-based method was reported to synthesize ZIFs materials at room temperature. The procedure involved the addition of chemical precursors such as zinc salts and organic linkers into

water. The crystallization can be accelerated via deprotonation using a base that deprotonates the organic linker to initiate the coordination. The organic base plays a dual role; deprotonation and creates a metal oxide or metal hydroxide that offers sacrificial templates for crystal formation. Several deprotonation reagents such as sodium hydroxide (NaOH), trimethylamine (TEA), and ammonium hydroxide (NH4OH) were reported.

Mechanochemical methods advanced the synthesis of MOFs [100,101]. ZIF-8 was synthesized via one-step mechanochemical processing using a stoichiometric ratio of ZnO nanoparticles and Hmim [102]. The procedure showed the complete conversion of ZnO nanopowders into ZIF-8 with a particle size of ca. 80 nm in diameter with minimal agglomeration. The materials have a surface area of 1885 m^2/g [102]. The grinding process can be assisted with different chemicals such as NaOH [103] and ionic liquids [101]. The synthesis involved adding a small amount of NaOH powder before grinding at a temperature of 343 K for 24 h [103]. The mechanochemical synthesis procedure is simple, fast, and can be used for large-scale production. However, the products lack high purity and contain residual inorganic materials such as ZnO.

4. Synthesis and Fabrication of ZIFs-based membrane

ZIFs-based membranes can be fabricated via in-situ growth, ex-situ growth, and innovative approaches (**Figure 4**). There are several fabrication methods for synthesizing ZIFs-based membranes (**Figure 4**). Each of these methods shows advantages and disadvantages. The following paragraph summarizes most of the main points of these methods.

ZIFs crystal can be grown via in-situ procedure using modified and unmodified supports. The in-situ method involves the growth of ZIFs crystals into porous support. This technique includes the immersion of support into the solution of ZIFs precursors. After a period at a specific temperature, the nucleation of ZIFs crystals starts producing layers of ZIFs crystals. However, the use of

unmodified support lacks a high nucleation rate due to functional groups that serve as nucleation sites.

The in-situ synthesis of ZIF-8 membranes on the support of α-alumina disks was reported using a *contra-diffusion* method [104]. The *contra-diffusion* procedure involves immersing α-alumina in a solution of zinc metal followed by immersion in a solution containing Hmim and HCOONa. The growth of ZIF-8 crystal was achieved under energy sources such as solvothermal or microwave conditions. The *contra-diffusion* method can be used for the defective heal membranes because they can be recycled using ligand and metal solutions [105]. It is a cost-effective method compared to conventional synthesis methods.

Ex-situ synthesis procedures or secondary growth procedures were reported for ZIFs-based membrane. ZIFs crystals can be attached to the support via a physical method using ZIFs seeds. Physical methods such as manual rubbing or electrospinning were reported. Rubbing-mediated seeding can be performed repeatedly by applying pressure onto the substrate's surface or sandpaper. These processes render the surface of the smooth support surface. They are suitable for substrates such as polyethersulfone (PES) disks [106] or tubular α-alumina [29].

An automatic procedure such as electrospinning was also reported using a high voltage electrical charge to draw a seed from a syringe containing a ZIF's seed solution. In the electrospinning procedure, droplets on the capillary tip can be formed by inducing a surface charge on the solution by the applied potential. The electrostatic forces of the charged droplet overcome the surface tension of the solution producing charged jets of the solution into a substrate. The solvent of the deposited droplet undergoes rapid evaporation producing ZIFs crystals on the substrates. The electrospinning method was used to create ZIF-8 crystals from a polyvinyl pyrrolidone (PVP) solution containing seed crystals, followed by a solvothermal procedure on the SiO_2 substrate [107].

PVP polymer allows uniform dispersion of the ZIF-8 seeds on the substrate, offering a strong adhesion between the substrate and the membrane. Electrospinning procedures produce pure crystals of ZIFs materials. It has been recognized as a reliable method for producing ZIFs-based membranes. It can be applied for large-scale production and industrial scale.

Chemical attachment of ZIFs seeds on substrates can be achieved using several methods such as dip coating [108], slip-coating [109], thermal seeding, reactive seeding, and microwave-induced thermal deposition (MITD)[110]. The dip-coating procedure involves the dipping of a substrate such as α-alumina disks in a solution of ZIFs/PEI seeding solution for the fabrication of ZIF-7 membranes [111] and ZIF-8 membranes [112]. PEI promotes the linkage between seeds and support using their functional groups. It also accelerates crystal formation via the linker's deprotonation.

An ex-situ synthesis procedure was also reported for the fabrication of ZIFs-based membranes. The method involved the secondary or seeded growth of ZIFs crystal into the support that contained attached seeding crystals (**Figure 4**). A seed crystal of ZIFs materials can be attached to the membrane supports via physical or chemical treatments. The method is different from the in-situ synthesis method. There is no crystal nucleation, growth, and intergrowth in secondary growth synthesis. The choice of ex-situ procedure is critical for the membrane's performance. Generally speaking, ZIF8-based membranes synthesized using rubbing seeding produce higher gas permeability than the electrospinning seeding procedure.

The rapid thermal deposition (RTD) method is based on the evaporation-induced crystallization concept. It consists of immersing the porous support in the precursor solution of ZIFs materials followed by heating the soaked support in an oven at temperatures of 180–200 ^{o}C for a short time (15 min). This step promotes the flow of the precursor solution inside the support. The precursor

solution is then evaporated for crystallization homogeneously inside and heterogeneously outside the support.

Electrospray deposition offers a uniform distribution of minute droplets containing ZIFs precursors generated via an electrostatic force applied on a capillary. This method forms fine-charged precursor droplets that travel through a thermal gradient zone due to an electrical potential gradient. The droplets land and spread on the substrate surface before evaporation-induced nucleation and crystallization of ZIFs crystals to form continuous membranes. This method offers a significant reduction in the synthesis time and precursor consumption. It can be used for easy control of the membrane's thickness. It also simplifies the activation process of the membrane for gas adsorption. The rate of evaporation is a crucial feature during membrane fabrication. It is essential to obtain continuous pore channels in ZIF membranes. The temperature of evaporation for the hot plate should be optimized based on the solvent's boiling point (bp.). At high temperatures, most of the solvent in the electrospray droplets was dried quickly before the successive droplets reached the substrate surface. Thus, the deposited droplet will form single crystals rather than creating a continuous layer of ZIFs materials. On the other hand, low evaporation temperature makes the precursor solution wet the substrate surface. The droplet smears into the interior of the substrate without considerable formation of ZIF crystal.

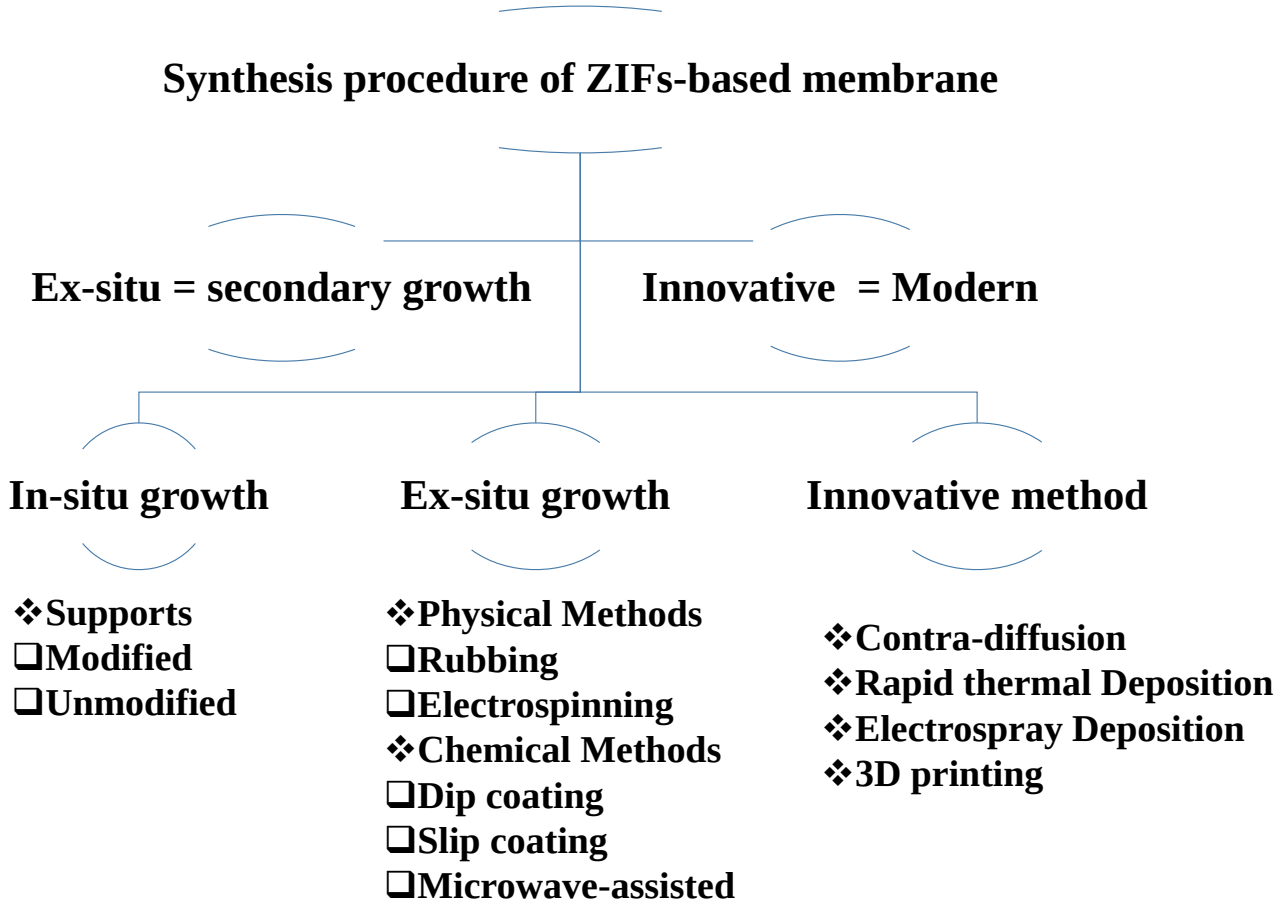

Figure 4 General method used for the synthesis of ZIFs-based membranes.

5. Adsorption of CO_2

5.1. ZIFs-based powder

ZIFs materials exhibit higher adsorption properties toward CO_2 [113]. The diffusivity of CO_2 is two times higher than that of CH_4 [114]. However, there are strong interactions between CO_2 molecules and the functional groups of ZIFs, including hydrogen bond formation. These properties lead to high adsorption capacity and selectivity toward CO_2 over other gases. Furthermore, modification can further enhance adsorption capacity and selectivity via an amendment (**Table 1**)[115,116]. ZIFs can be synthesized using an environmentally friendly solvent such as water. They exhibit high

recyclability [117]. Several ways were reported to improve adsorption capacity and enhance the selectivity toward CO_2 gases (**Figure 5**)[118]. The following paragraphs discuss these methods.

Figure 5 Strategies to enhance the adsorption capacity and selectivity toward CO_2 using ZIFs-materials.

ZIF-8 and leaf-like ZIF (ZIF-L) were synthesized using a water-based template-free method [73]. The synthesis involves using sodium hydroxide (NaOH) that induces a sacrificial template for zinc

hydroxide nitrate. The high adsorption of CO_2 using ZIF-L compared to ZIF-8 crystal is due to the presence of a cushion-shaped cavity between the layers with a dimension of 9.4 Å × 7.0 Å × 5.3 Å [119]. The adsorption capacity of CO_2 increases by 3-10% with the increase of the NaOH concentration used during the synthesis [73]. The synthesis procedure can be improved using large biomolecules such as 2,2,6,6-tetramethylpiperidine-1-oxyl radical (TEMPO)-mediated oxidized nanocellulose (TOCNF) [120]. The materials were coined as CelloZIF-L and CelloZIF-8 for ZIF-L and ZIF-8. CelloZIF-L and CelloZIF-8 exhibited CO_2 adsorption capacity of 0.58-1.1 mmol•g^{-1} and 0.33-0.57 mmol•g^{-1}, respectively[120]. ZIF-68 and ZIF-69 exhibited a CO_2 adsorption capacity of 7.5 and 5.5 mmol•g^{-1}, respectively, at 20 bar[121].

The adsorption of ZIF-8 was enhanced via amine functionalization[122]. The adsorption capacity of ZIF-8 can be improved up to 43% at 1 bar via amine functionalization using 3-aminopropyl-triethoxy silane (APTES) and graphene oxide (GO)[123–133] of ZIF-8 compared to unmodified ZIF-8 [134]. Polyethylenimine (PEI) was used to modify ZIF-8 producing PEI@ZIF-8 adsorbent [135]. PEI@ZIF-8 exhibited higher CO_2 adsorption capacity and selectivity by 6.2 and 27 times that of ZIF-8 [135]. The presence of cation ions such as K^+ enhanced the adsorption and selectivity of CO_2 [116].

Adsorption of CO_2 using ZIFs can be improved using ionic liquids (ILs)[136–139]. Ionic liquids (ILs) such as 1-Butyl-3-methylimidazolium Acetate [Bmim][Ac] and 1-Ethyl-3-methylimidazolium Acetate [Emim][Ac] were impregnated into ZIF-8 for CO_2 adsorption [140]. [Bmim][Ac]@ZIF-8 with a loading of 30 wt.% IL exhibited high selectivity toward CO_2 adsorption. [Bmim][Ac]@ZIF-30 showed higher CO_2 uptake with excellent selectivity for all investigated temperatures (303, 313, and 323 K). It offered up to 7 times higher CO_2 capacity than the pristine ZIF-8 at 0.2 bar and 303 K [140]. CO_2 can be dissolved into ILs. Thus, ZIFs materials containing ILs provided high

adsorption capacity. The use of binary ILs enhanced the CO_2 selectivity by 3.5-fold compared to simple ILs@ZIF-8 [141]. A binary ILs with both hydrophobic-hydrophobic properties exhibited higher CO_2 selectivity. This observation can be attributed to the strong interactions between CO_2 and IL anions. Adsorption using simple and binary mixtures of ILs in ZIF-8 was investigated via density functional theory (DFT) and grand canonical Monte Carlo (GCMC) methods. Data analysis revealed that ILs with fluoride and hydrophobic properties exhibited high adsorption of CO_2 [142]. ILs encapsulated ZIFs materials exhibited higher adsorption capacity [143].

Dye encapsulated ZIFs materials were reported for CO_2 adsorption. Dye molecules enhanced the adsorption capacity of CO_2[144]. Dye@ZIF-8 showed a superior capacity for CO_2 of 1.46 $mmol \bullet g^{-1}$ at 273 K. It provided a 42 % higher adsorption capacity than that of ZIF-8 (0.84 $mmol \bullet g^{-1}$) under the same conditions [144]. The guest molecules such as dyes improved the adsorption capacity of CO_2.

A dual-metal ZIF crystal was synthesized via metal substitution from ZIF-108 (Zn(2-nitroimidazolate)$_2$, SOD topology) as the parent material [145]. Among metals substitutions, including Co^{2+}, and Cu^{2+}, Ni^{2+}-substituted ZIF-108 shows high adsorption selectivity toward CO_2 over N_2 by up to 227 [145].

Table 1 Adsorption of CO_2 using ZIFs-based powder.

ZIFs	Guest	Synthesis procedure	Content (%)	Pressure (bar)	Capacity (mmol/g)	Selectivity	T (°C)	Ref.
		Stirring at 298 K for 4 h			0.94	CO_2/CH_4 (7.2)		[119]
ZIF-L		Stirring at RT for 30 min	0		0.96	CO_2/N_2 (4.7–6.5)		[73]
ZIF-7		Solvothermal, 373 K for 48 h			2.76			[146]
		Solvothermal, 413 K for 24 h		1	1.63		25	[147]
ZIF-8		Stirring at 298 K for 24 h			0.45	CO_2/CH_4 (7)		[115]
	K^+	Heating at 413 K for 24 h	22-28		0.68	CO_2/N_2 (20)		[116]
ZIF-L	TOCNF	Stirring at RT for 1h	0.28-0.48[a]		0.58–1.1			[120]
					0.33–0.57			
	ILs	Incipient wetness	30	0.2	0.45			[140]
ZIF-8	$[bmim^+][Tf_2N^-]$	Encapsulation	0.02–0.38	100	8	CO_2/CH_4 (41) CO_2/N_2 (100)		[143]
	Dyes	Stirring at RT, 30 min	10-20	1	1.46		0	[144]
		Stirring at 85 °C for 5 min	0	15% CO_2	3.04		35	[117]
ZIF-68 ZIF-69		Solvothermal, 100 °C for ZIF-68 and 85 °C for ZIF-69) for 96 h		20	7.5 5.5		38	[121]
ZIF-68		Solvothermal, 100 °C for		1	2.28		25	[82]
ZIF-68	-C_6H_6	Solvothermal, 85 °C for 52 h		1	1.68		25	[148]
ZIF-91-OLi	n-BuLi	n-BuLi, -78 °C, 20 min	0.4%	10	10	CO_2/N_2 (16)	25	[149]
ZIF-DIA	DIA)	➢ Stirring at 25 °C for 24 h ➢ Solvothermal at 50 °C for 2 h	DIA:2-MeIM 1: 7	1	5.83		55	[122]
APTES-GO@ZIF-8	GO	Refluxing at 343 K for 5 h	35	1	0.85		30	[134]
PEI@ZIF-8	PEI	➢ Heating at 423 K for 12 h ➢ Drying at 313 K ➢ Heating at 373 K for 12 h	45	1	0.95	CO_2/N_2 (2.3)	25	[135]

Notes: 2,5-diimidazolylaniline, DIA; *a,* carboxylic content mmol/g.

5.2.ZIFs-based membrane

Membrane-based technologies are an attraction for the adsorption of CO_2 (**Table 2**). They offer a cost-effective solution with a high ability for CO_2 adsorption. They circumvent some of the challenges of other technologies, such as multiple stages procedures that include pressurizing, depressurizing, and purging. They provide high efficiencies compared to other methods such as conventional pressure swing adsorption systems or cryogenic separation methods. The membranes should exhibit pore continuity (interconnectivity) with defect-free structure and high adherence to the substrate surface for high-adsorption performance.

The high stability of ZIFs-based membranes ensures reliability and reproducibility in the separation performance for CO_2, which are necessary for industrial applications. The chemical and thermal stability of ZIFs-based membranes are not widely investigated compared to ZIF crystals [28]. There are only a few reports on the strength of ZIFs-based membranes[150]. ZIF-69 membrane exhibits high chemical stability [151]. It showed good composure under boiling with methanol and benzene [151]. However, the membranes were unstable in boiling water.

Membrane-based technologies are not widely used due to the challenges in manufacturing. The current fabrication methods produce small and medium-scale membrane units. There is a high need for throughput methods for large-scale production. The membrane fabrication requires dense polymeric materials that usually exhibit high selectivity but with low permeability. Several materials were reported to improve the gas adsorption using membrane technologies, including MOF such as MOF-5 [152,153] and ZIF [154] (**Table 2**). There are several fabrication methods for synthesizing ZIFs-based membranes (**Figure 4**). There is no general fabrication method that can be suitable for all membranes. In-situ and ex-situ growth of ZIFs materials on a substrate was reported. Modern or innovative technologies such as electrospray and three-dimensional (3D)

printing were investigated (**Figure 4**). The general fabrication method facilitates the scaled-up processes. The in-situ growth c-oriented ZIF-69 membranes use α-alumina substrates for CO_2/CO separation [151].

Electrospray deposition was used to prepare ZIF-8 [155] and ZIF-7 [156] membranes for H_2/CO_2 separation. The membranes were synthesized via preparing two solutions of the metal salts and the linker separately and then mixing them to obtain ZIFs precursor solutions. The mixed solution was then fed into a nozzle with an applied potential for electro-spraying on a hot α-alumina substrate (**Table 2**).

Developing a fabrication strategy for ZIF-based membranes with low energy consumption is vital. Methods such as RTD and electrospray deposition require high temperatures to promote crystallization and shorten the synthesis time. The synthesis procedures should meet some requirements, making it standard for most ZIFs-based membranes. They should offer conditions such as control structures, thickness, and ZIFs-loadings. They should have high reproducibility for effective gas separation.

ZIFs-based membranes using polymers were reported for CO_2 adsorption. Mixed matrix membrane (MMM) of ZIFs was reported using co-polyimide (6FDA-bisP) consisting of 4,4′-(hexafluoroisopropylidene)diphthalic anhydride (6FDA) and 4,4′-(1,4-phenylenediiso propylidene) bisaniline (bisP)[157]. 6FDA-bisP offered higher performances of CO_2 with permeability and selectivity of 35.3 Barrer and 25.6, respectively (**Table 2**). It showed higher CO_2/CH_4 selectivity compared to several commercial polymer-based membranes. A poly(ethylene oxide)-based membrane was reported using poly(ethylene glycol) diacrylate (PEGDA) and poly(ethylene glycol) methyl ether acrylate (PEGMEA) for ZIF-8 [158]. The loading of ZIF-8 affected the gas transport properties in MMMs at 35 °C. ZIF-8 loading of 10 wt.% using cross-

linked PEGDA increased the permeability of CO_2 from 130 Barriers to 320 Barriers, i.e., 170% increment without any observation for the reduction of the selectivity of CO_2 adsorption [158]. Several polymers and their blend were reported, including polyether-block-amide (PEBA2533) polymer[159], Pebax-1657[160], Pebax® 2533[161], Matrimid®[162], polysulfone[163], and Matrimid®/polysulfone blend[164]. Polymer and inorganic supports were also reported for poly(vinyl chloride)-poly(oxyethylene methacrylate) (PVC-POEM)/alumina[165]. The CO_2 permeability of the thin PVC-POEM membrane was 1652% (17.5 fold) higher than that of the free-standing membrane [165]. Polymer enhances the adsorption capacity and selectivity and can also be used as a binder to strengthen the adhesion between ZIFs and the substrate. ZIF-78 improved CO_2 permeability's up to 39% in the Matrimid® membrane without a significant decrease in the selectivity of pure Matrimid® membranes[162].

Table 2 Adsorption of CO_2 using ZIFs-based membranes.

ZIFs	Support	Methods	Fabrication conditions	Thickness (μm)	Separation Selectivity	T (°C)	Permeance [mol•s^{-1}•m^{-2}•Pa^{-1}]	Ref.
ZIF-8	TiO_2 disks	In-situ growth	Solvothermal at 100 °C for 4 h	30	CO_2/CH_4 (3.4) CO_2/CH_4 (2.0) CO_2/CH_4 (1.7) CO_2/CH_4 (3.6) CO_2/CH_4 (2.1) CO_2/CH_4 (1.7)	25 100 200 25 100 200	CO_2: 2.6×10^{-8} (50% in CH_4) CO_2: 1.56×10^{-8} (50% in CH_4) CO_2: 1.14×10^{-8} (50% in CH_4) CO_2: 2.73×10^{-8} (s) CO_2: 1.68×10^{-8} (s) CO_2: 1.20×10^{-8} (s)	[166]
ZIF-69	α-Al_2O_3 disks		Solvothermal at 100 °C for 72 h	50	CO_2/CO (3.5)	RT	CO_2: 3.6×10^{-8} (50% in CO)	[167]
ZIF-8	α-Al_2O_3 tubes		Solvothermal at 25–200 °C for 5 h	6	H_2/CO_2 (7.1) H_2/CO_2 (32.2) N_2/CO_2 (12.9) CH_4/CO_2 (11.9)	RT	H_2: 1.7×10^{-7} (45% in CO_2) H_2: 9.9×10^{-7} (s) N_2: 3.1×10^{-7} (s) CH_4: 2.5×10^{-7} (s)	[168]
ZIF-22	APTES-modified TiO_2 disks		Solvothermal at 150 °C for 72 h	40	H_2/CO_2 (7.2)			[169]
ZIF-90	APTES-modified α-Al_2O_3 disks		Solvothermal at 100 °C for 18 h	20	H_2/CO_2 (7.3)	200	H_2: 2.37×10^{-7} (50% in CO_2)	[150]
ZIF-95	APTES-modified α-A_2O_3 disks		Solvothermal at 120 °C for 72 h	30	H_2/CO_2 (25.7)	325	H_2: 7.59×10^{-8} (50% in CO_2)	[170]
ZIF-8	APTES-modified α -Al_2O_3 particles on α -Al_2O_3 tubes		Contra-diffusion at 150 °C for 5 h	2	H_2/CO_2 (17)			[171]

	α-Al_2O_3 tubes	Ex-situ growth	➢ Rubbing seeding ➢ Hydrothermal at 150 ^oC for 5 h	5-9	CO_2/CH_4 (4–7)	RT	CO_2: 2.4 $\times 10^{-5}$ (50% in CH_4)	[172]
	α-Al_2O_3 tubes		➢ In situ deposition of seeds ➢ Rubbing ➢ Solvothermal at 110 ^oC for 4 h	5	H_2/CO_2 (5.2)	RT	H_2: 1.1 × 10^{-6} (s)	[108]
	SiO_2 disks		➢ Electrospinning seeding ➢ Solvothermal at 120 oC for 24 h	100	H_2/CO_2 (7.31)	R.T.	H_2: 3.23 $\times 10^{-7}$ (50% in CO_2)	[173]
ZIF-7	α-Al_2O_3 disks		➢ Dip-coating seeding ➢ Microwave-assisted ➢ Solvothermal at 100 ^oC for 3 h	1.5	H_2/CO_2 (6.48)	RT	H_2: 7.71 × 10_{-8} (50% in CO_2)	[174]
ZIF-7	α-Al_2O_3 disks		➢ Dip-coating seeding ➢ Microwave-assisted ➢ Solvothermal at 100 ^oC for 2.5 h	2	H_2/CO_2 (13.6)	220	H_2: 4.55 × 10_8 (50% in CO_2)	[175]
ZIF-69	α-Al_2O_3 disks		➢ Dip-coating seeding ➢ Solvothermal at 100 ^oC for 72 h	40	CO_2/N_2 (6.3) CO_2/CO (5.0) CO_2/CH_4 (4.6) CO_2/N_2 (2.2) CO_2/CO (2.9) CO_2/CH_4 (2.7)	RT	CO_2: 1.034 × 10^{-7} (50% in N_2) CO_2: 1.031 $\times 10^{-7}$ (50% in CO) CO_2: 1.023 $\times 10^{-7}$ (50% in CH_4) CO_2: 2.36 × 10^{-8} (s)	[111]
ZIF-7	α-Al_2O_3 disks		➢ Dip-coating seeding with PEI ➢ Microwave method at 100 ^oC for 225 min	1.9	H_2/CO_2 (8.4)	200	H_2: 9 $\times 10^{-9}$ (50% in CO_2)	[112]
ZIF-8	α-Al_2O_3 disks		➢ Dip-coating seeding with PEI ➢ Microwave method at 100 ^oC for 2 h	12	H_2/CO_2 (6)	25	H_2: 1 × 10^{-7} (50% in CO_2)	[109]
ZIF-90	Torlon1 hollow fibers		➢ Dip-coating seeding ➢ Solvothermal at 65 ^oC for 4 h	5	CO_2/CH_4 (1.5) H_2/CO_2 (1.8) CO_2/N_2 (3.5)	35	CO_2: 1.065 × 10^{-7} (s)	[176]
ZIF-78	ZnO disks		➢ Reactive seeding ➢ Solvothermal at 120 ^oC for 12 h	25	H_2/CO_2 (9.5)	25	H_2: 9.7 × 10^{-8} (50% in CO_2)	[107]

ZIF-90	APTES-modified α-Al_2O_3 disks	Ex-situ method	Imine functionalization with ethanolamine via refluxing methanol at 60 ^oC for 10 h	20	H_2/CO_2 (15.3)	200	H_2: 2.02×10^{-7} (50% in CO_2)	[177]
	APTES-modified α-Al_2O_3 disks		APTES functionalization by refluxing in at 110 ^oC for 1 h	20	H_2/CO_2 (20)	225	H_2: 2.9×10^{-7}	[178]
	APTES-modified α-Al_2O_3 disks		Refluxing in methanol and APTES solution at 110 ^oC for 0.5 h	20	CO_2/CH_4 (4.7) H_2/CO_2 (21)	225	CO_2: 1.26×10^{-8} (50% in CH_4)	[179]
ZIF-108	polysulfone (PSF)		➢ Stirred for 24 h, ➢ Dip-coated, dried at 25^oC for 24 h, 80 ^oC for 6 h, and 80 ^oC for 24 h under a vacuum	2	CO_2/CH_4 (15.9) CO_2/N_2 (16)	25	150 barrers	[145]
ZIF-8	6FDA-bisP		➢ Stirred 2 h ➢ Casting	50–70	CO_2/CH_4 (35)	25	25.6 barrers	[157]
ZIF-8	PEGMEA		➢ Stirring fo 2h and ➢ Sonication fo 30 min, ➢ Exposure to UV light at 254 nm and 3.0 mW/cm^2 for 5 mins	100–150	CO_2/H_2 and CO_2/N_2	35	320 barrers	[158]
Zn/Ni-ZIF-8	PEBA2533		➢ Sonication for 2 h, ➢ Stirred for 8 h at 67 °C, ➢ Vacuum oven at 30 °C for 24 h, ➢ Dried at 50 °C for 24 h	30	CO_2/N_2 (42.8)	25	321 barrer	[159]
ZIF-8	Matrimid®/polysulfone blend		➢ Sonication for 1 h, ➢ Dry under nitrogen for 3 days at room temperature, ➢ Dried at 100 °C under nitrogen flow for 2 days,	60-70	CO_2/CH_4 (40)	35	20 barrer	[164]

			➢ Vacuum dried at 150 °C for 2 days					
ZIF-8	PVC-POEM)/ α-Al_2O_3		➢ Heating at 90 °C for 24 h, ➢ Dried in a vacuum oven at 50 °C for 24 h, ➢ spin-coated onto the α-alumina disk for 20 s at 3000 rpm	5.5	CO_2/CH_4 (14.4)	25	CO_2: 8.9×10^{-9} mol s^{-1} Pa^{-1} m^{-2} CH_4: 6.2×10^{-10} mol s^{-1} Pa^{-1} m^{-2}	[165]
ZIF-7	α-Al_2O_3 disks	Innovative	Electrospray deposition at 160 °C for 8 min	4.5	H_2/CO_2 (9.59) H_2/CO_2 (10.74) H_2/CO_2 (13.79) H_2/CO_2 (14.90) H_2/CO_2 (16.75) H_2/CO_2 (18.30)	25 50 75 100 125 150	H_2: 4.57×10^{-7} (50% in CO_2) H_2: 4.06×10^{-7} (50% in CO_2) H_2: 3.76×10^{-7} (50% in CO_2) H_2: 3.56×10^{-7} (50% in CO_2) H_2: 3.28×10^{-7} (50% in CO_2) H_2: 3.05×10^{-7} (50% in CO_2)	[155]
ZIF-8	α-Al_2O_3 disks		Electrospray deposition at 70 °C for 55.71 min	28.1	H_2/CO_2 (20.29)	25	H_2: 4.23×10^{-7} (50% in CO_2)	[180]

Notes: barrer, 10^{-10} cm^3(STP) cm cm^{-2} s^{-1} $cmHg^{-1}$.

5.3.Factors affecting the adsorption using ZIFs-based membranes

5.3.1. Effect of ZIFs' properties: structure, porosity, guest molecules, and morphology

Adsorption of CO_2 can be improved using the hard structure of ZIF-90 via sequential reduction using $NaBH_4$ [78]and lithiation reaction (i.e., formation of ZIF-91-OLi) [149]. ZIFs materials with high rigid structures ensure that the pore size will be preserved without change during the fabrication process [181]. The rigid membranes can be achieved through post-synthetic modification and functionalization with imine [171] and APTES [177,178]. However, it is essential to note that there is no diffusive motion for CO_2 and CH_4 in rigid ZIF-8 [182]. MMM with tiny defects in ZIF-8 enhanced the CO_2/N_2 separation [183].

Dual-metal (bimetallic) ZIF crystals exhibited high adsorption capacity with high selectivity compared to a single-metal ZIF crystal. Ni^{2+}-substituted ZIF-108 (Zn(2-nitroimidazolate)$_2$ shows high adsorption selectivity toward CO_2 [145]. The Zn/Ni-ZIF-8-PEBA MMM (ZIFs loading of 10%) exhibited a CO_2 permeability and selectivity (CO_2/N_2) of 321 Barrer and 42.8, respectively, at 2 bar [159]. While, ZIF-8-PEBA MMM showed only permeability and selectivity of 266 Barrer and 33.8, respectively [159]. Bimetallic (Ce,Zn)ZIF-8 and (Ce,Co)ZIF-67 showed CO_2 uptake value of 3.77 mmol/g and 3.55 mmol/g, respectively[184]. Bimetallic Co–Zn-based ZIF ($Co_{75}Zn_{25}$-ZIF-8) showed higher CO_2 uptakes of 30% compared to single metal ZIF adsorbent[185]. The CO_2 adsorption can be further improved to 4.55 mmol/g after loading with 15% diethanolamine (DEA) [184].

The functional groups of the organic linker in ZIFs materials play an important role in the adsorption capacity and the selectivity of the materials (**Figure 6**)[186]. Adsorption properties of ZIF materials can be tuned via a mixed linker [187]. ZIFs of a linker with electron-withdrawing and donating groups have enhanced CO_2 adsorption[186]. Density functional theory (DFT) calculation

was used to quantify the binding ability of CO_2 for ZIF materials for 137 linkers[188]. The presence of asymmetrical functional groups, e.g., NO_2/OH, CN/OH, and Cl/OH in imidazolate improved the CO_2 adsorption[188]. Amino-functionalized ZIF-8 materials using 2,5-diimidazolyl aniline (ZIF-DIA) exhibited superior CO_2 adsorption [122]. It can be used for CO_2 capture in humid flue gas [189]. Grand Canonical Monte Carlo (GCMC) simulations for ZIF-69 revealed that the electronegative –Cl functional group in the organic linker of ZIF-69 displayed an inductive effect. The effect of the functional groups is correlated to the heat of adsorption and selectivity [190]. The electronegative functional group such as Cl offers electrostatic interactions with the polar gas molecules such as CO_2 molecules that can be trapped at the pore opening. On the other side, non-polar gas such as (CH_4) undergoes penetration through the pore without adsorption. Thus, the materials offer high selectivity. Using DFT and GCMC, theoretical calculation revealed that the terminal group's rotation tunes the linker swing motion ZIF-90 [191]. The Nitro group of 2-nitroimidazole linkers offers a strong Lewis acid-base interaction [192]. On the other side, the interaction of H atoms of the benzimidazole and the oxygen atoms of CO_2 enabled high selectivity[192]. Adsorption of CO_2 was enhanced two-fold after solvent assisted ligand exchange (SALE) of ZIF-8 with an imidazole linker containing electron withdrawing groups such as -NO_2 and -SH [193]. Electron withdrawing groups in the linker of ZIF crystal enhanced the acidity for the hydrogen atoms on linker offering hydrogen bond interactions with the oxygen atoms of CO_2 (**Figure 6**)[194].

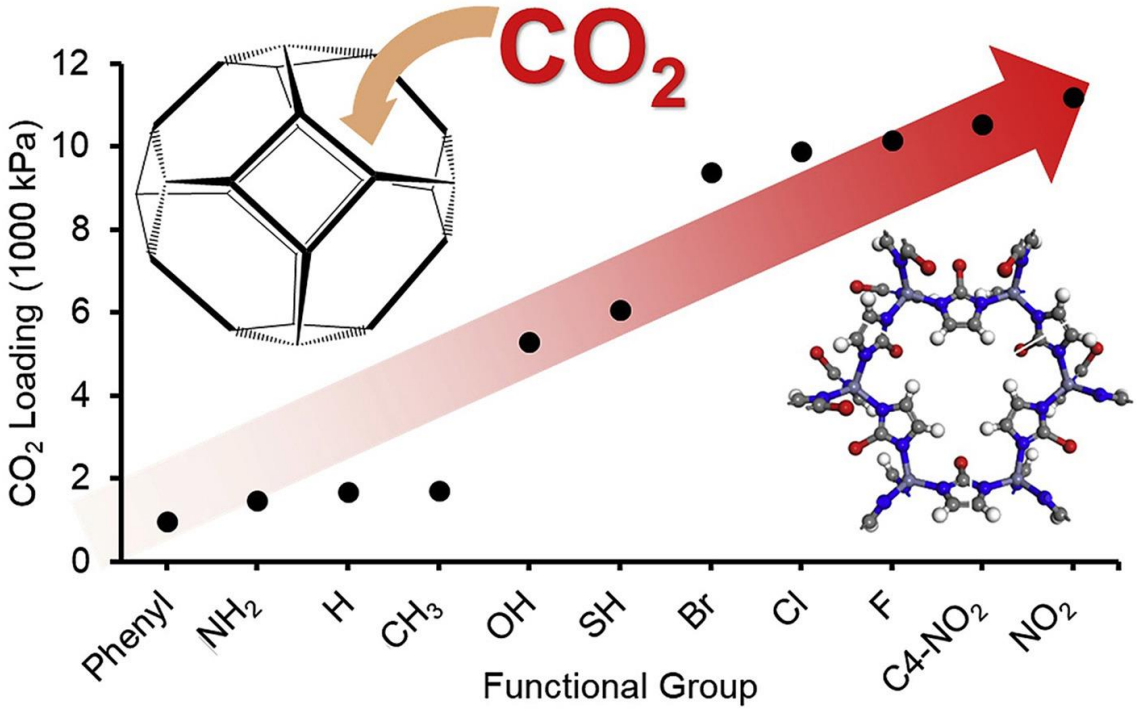

Figure 6 Effect of linker's functional group on the adsorption capacity of CO_2. Figure reprinted with permission from Ref. [186]. Copyrights belong to Elsevier.

Besides the functional groups of the linker, the ligand dipole moment is also a key factor for CO_2 adsorption (**Figure 7**) [195]. Data analysis showed an exponential relationship between the ligand dipole moments and the isosteric heat of adsorption (q_{st}) of CO_2 (**Figure 7**). The high ligand dipole moment showed a 5- to 7-fold improvement in the selectivity for CO_2 adsorption for CO_2/CH_4, CO_2/N_2, and CO_2/CO mixtures (**Figure 7**).

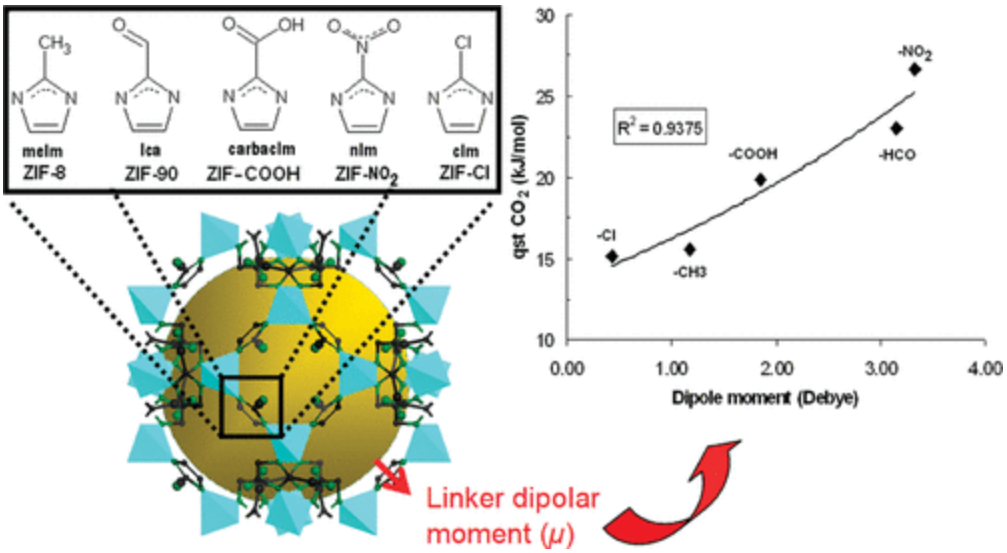

Figure 7 Effect of linker's dipolar moment on the isosteric heat of adsorption of CO_2. Figure reprinted with permission from Ref. [195]. Figure reprinted from American Chemical Society (ACS).

The porosity of ZIFs is a key parameter in gas adsorption. The substrates shouldn't block the porosity of ZIFs crystals. The pore aperture size of ZIFs crystals can be modified using a post-synthetic modification to increase the gas separation performance. Post-synthetic procedures can constrict the pore aperture size, reduce intercrystalline defects, increase the crystal's homogenous distribution inside the membrane, or create active adsorption sites. It is crucial to balance reducing the pore aperture size and the permeability of the gases. Small pore size apertures significantly decrease the gas permeability. On the other side, selectivity is usually enhanced by the pore aperture size reduction and the reduction of grain boundary defects. Consequently, non-selective transport pathways and the ‘‘gate opening effect’’ can be prevented.

Moreover, thermal and hydrothermal stability can be improved via the post-synthetic functionalization step, which may facilitate membrane activation. A study on the porosity effect (windows and cavity) was reported using positron lifetime for ZIFs; ZIF-90, ZIF-93, and ZIF-

94[196]. Data analysis revealed that the smaller pore size (micropore or ultramicropores) of ZIFs is optimal for CO_2 adsorption under ultralow pressure [196]. ZIFs crystals with the smaller pores (e.g., ZIF-7 and ZIF-94) showed higher CO_2 adsorptions than ZIFs materials with larger pores (e.g., ZIF-11 and ZIF-93) at low pressures (<1 bar)[148]. In contrast, the opposite is true at higher pressures, i.e., the larger-pore structures showed significantly higher adsorption[148]. Hollow ZIF-8 containing meso/macro pores showed good adsorption of CO_2 with an adsorption capacity of 1.05 mmol/g at 1 bar[197].

Solvent assisted ligand exchange (SALE) of ZIF-8 was reported using linkers of 2-mercaptobenzimidazole (SHBzIm), 2-aminobenzimidazole (NH_2BzIm), 2-nitroimidazole (NO_2Im) and 2-phenylimidazole (PhIm)[193,198]. CO_2 adsorption increases (from 42.7 to 48.2 cm^3/g) with the rise of the amine percentage from 5% to 16% via the SALE of ZIF-8 (**Figure 8**) [193]. Although SALE reduced the BET surface area of LeZIF8-NH_2BzIm (ligand exchange) derivatives, their CO_2 adsorption increased. Amine modification thus enhanced the CO_2 adsorption of nZIF-8 (**Figure 8**) [193]. SALE for ZIF-8 using halogenated (-Cl, -Br, and -CF_3) and thiol (-SH)- and nitro (-NO_2) imidazole derivatives showed an increase of 11-22%, 32%, and 100% in CO_2 adsorption, respectively[199].

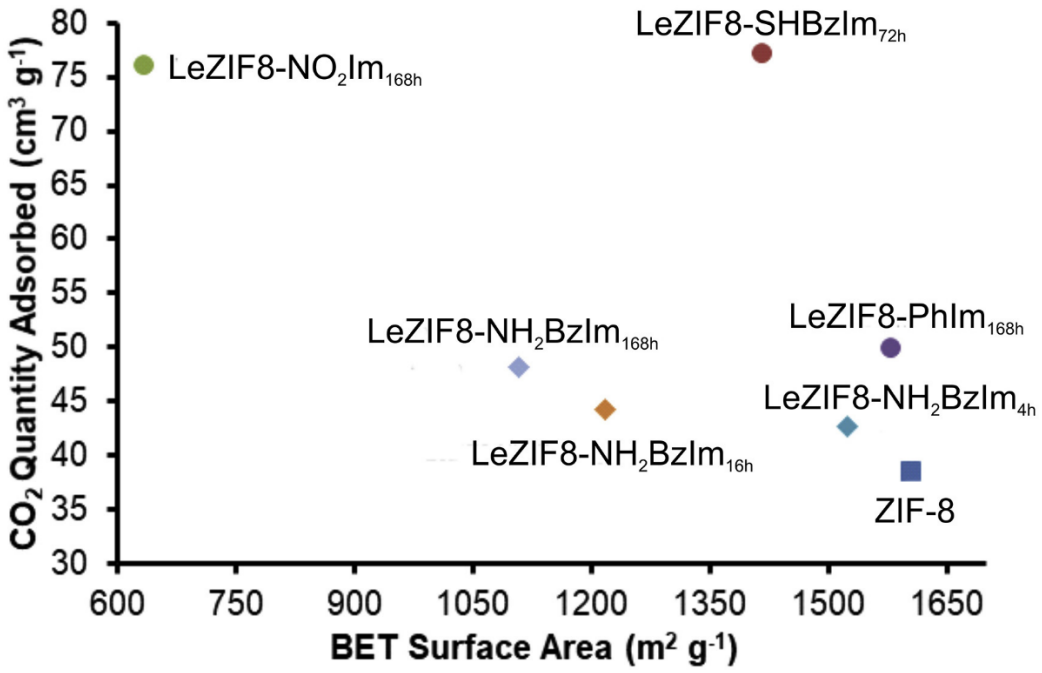

Figure 8. Maximum CO_2 quantity adsorbed at 900 mmHg (cm^3/g) vs. BET surface area (m^2/g) for SALE derivatives of ZIF-8; nZIF-8 (■), NH_2 substituents (♦) and electron-withdrawing substituents (●). Figure reprinted with permission from Ref. [193]. Copyright belongs to Elsevier.

Guest molecules such as ionic liquids [142], dyes, nanoparticles, and alkali metals[200] enhanced the adsorption of CO_2. The effect of the counter ions of ILs 1-butyl 3-methylimidazolium ($[BMIM]^+$) was reported for anions (i.e. $[Cl]^-$(chloride), $[CF_3CO_2]^-$ (trifluoroacetate), $[BF_4]^-$ (tetrafluoroborate), $[OTF]^-$ (trifluoromethane sulfonate) and $[PF_6]^-$ (hexafluorophosphate)) [142]. Fluorine containing 1-butyl 3-methylimidazolium ($[BMIM]^+$) ILs (i.e., $[BMIM]^+$ with counter ions such as $[BF_4]^-$ and $[PF_6]^-$ anions) exhibited high adsorption of CO_2 (**Figure 9**)[142]. It was found that CO_2 molecule interacts with anions of ILs such as $[BMIM][CF_3CO_2]$ and [BMIM][OTF] via carbon of CO_2 with oxygen and fluorine (with distance of 2.75 and 2.89 Å), respectively. In the other side, $[BF_4]$ and $[PF_6]$ anions interacted with CO_2 via the methyl and butyl groups of cation, respectively. Based on the calculation, the binding energies (BEs) can be ordered in the sequence of $[Cl]^- > [CF_3CO_2]^- > [BF_4]^- > [OTF]^- > [PF_6]^-$. The higher BEs for $[CF_3CO_2]^-$ and $[Cl]^-$ are due to

the hydrophilic nature of ILs and the electrostatic interactions with CO_2 molecules. On the other side, $[BMIM]^+$ with $[BF_4]^-$, $[OTF]^-$, and $[PF_6]^-$ anions showed a very less binding with CO_2 (**Figure 9**)[142]. This could be also due to the high dispersion of fluorine-containing anions on the ZIF-8 surface compared to the non-fluorinated anion[201]. The incorporation of ILs in ZIFs materials enhances the adsorption and selectivity of CO_2 [202].

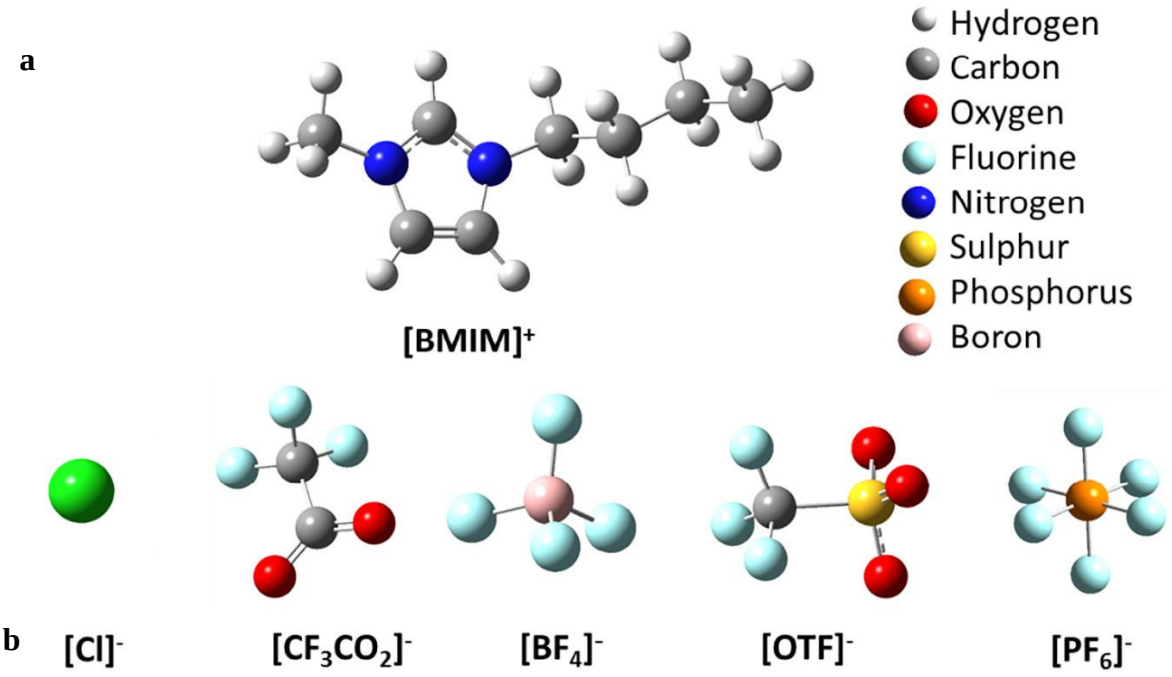

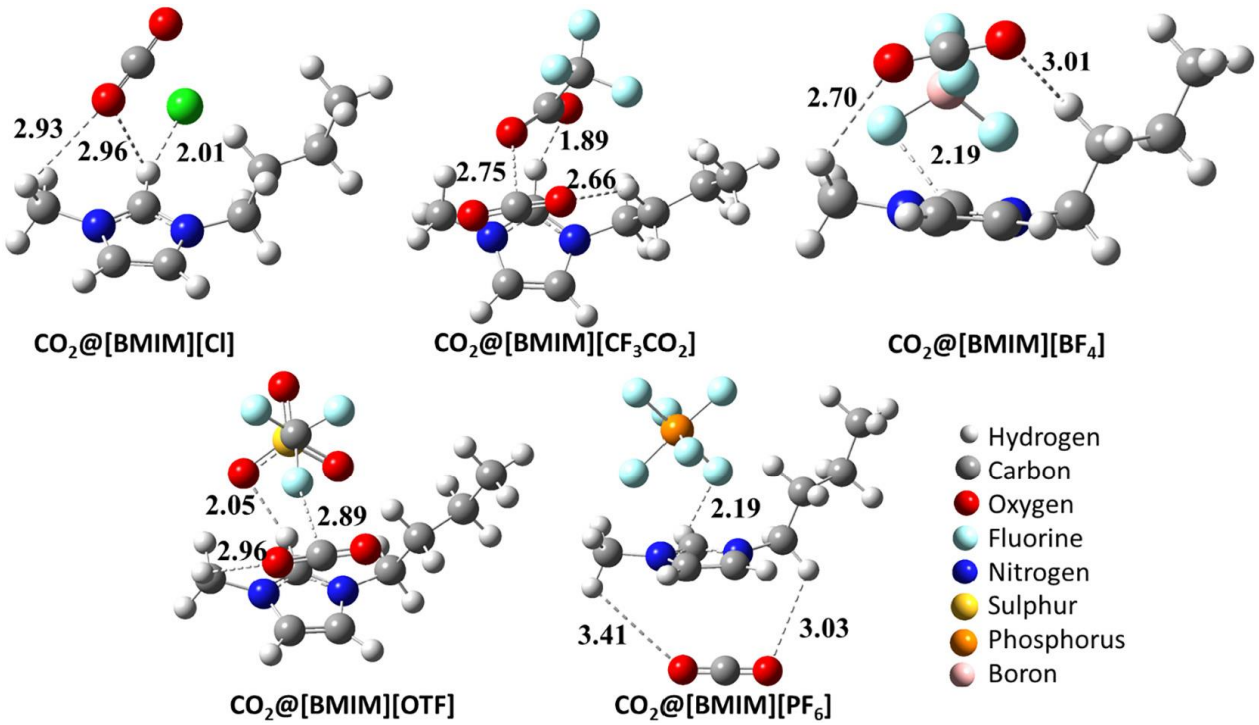

Figure 9 a) structure of the ionic liquid, and b) gas-phase optimized geometries of CO_2@ILs, with shortest interaction distances (in Å). Figure reprinted with permission from Ref. [142]. Copyrigt belongs to Elsevier.

Ethylenediamine (ED) treated ZIF-8 nanoparticles enhanced the selectivity of CO_2/CH_4 by 37% compared to untreated ZIF-8 [203]. It can remove H_2S and CO_2 from natural gas[204]. The use of nanoparticles such as carboxylated carbon nanotubes (CNTs) composite prevented the aggregation of ZIF-8 in the membrane, increased the free volume of the MMM, and enhanced the CO_2 adsorption performance and CO_2/N_2 separation performance[160]. ZIF-8-PEI@IL (15 wt.%) increased the CO_2 permeability of MMMs by 123%, and the selectivity of CO_2/N_2 and CO_2/CH_4 from 17 and 12 to 76 and 25, respectively[161].

The morphology of ZIF materials exhibits an insignificant effect on CO_2 adsorption[162]. The low and high aspect ratio ZIF-78 showed similar CO_2 adsorption behavior [162]. However, leaf-like ZIF (ZIF-L) with 2D morphology exhibited high CO_2 adsorption. This observation is due to the

cushion-like pore of ZIF-L (**Figure 3**). The vibrational properties of ZIFs materials such as ZIF-68 and ZIF-69 [121]. The high CO_2 uptake causes high free-breathing vibrations of the ligands, causing the large ZIF pores [121].

5.3.2. Effect of the substrate

The fabrication of ZIFs-based membranes requires support or substrate. The judicious choice of substrate is important during the synthesis of ZIFs-based membrane. Several substrate were reported including ceramic [107,151,154,166,205,206], ionic liquids membrane[207], and polymeric-based materials. Ceramic supports including α-alumina [151], titania [154,205], yttria-stabilized zirconia (YSZ) [166], ZnO [206], and SiO_2 [107] were reported. α-alumina was the commonly used ceramic substrate. It offers excellent mechanical stability, and for this reason, it is the most commonly preferred ceramic-based substrate. Some of these ceramics show excellent mechanical and thermal stability. Ceramic such as titania can promote heterogeneous nucleation. However, titania is expensive and brittle leading to broken during the gas adsorption [167]. Support of two different substrates such as α-alumina and titania was also described to combine the high mechanical stability of α-alumina and the smooth appearance of titania [173].

The support should promote the heterogeneous nucleation of ZIFs crystals. The bare support lacks heterogeneous nucleation. Thus, surface modification of the support is usually required to create active sites for crystal nucleation. In fact, α-alumina supports were modified with organic linkers [208], polymer [150,169,209], or ZnO [179]. ZnO or organic linkers can be used as sacrificial templates for the nucleation and growth of ZIFs crystals[179]. The sacrificial templates enable the formation of smooth layers of ZIFs crystals. The ceramic substrate can also be modified chemically with 3-aminopropyltriethoxysilane (APTES) [170]. APTES molecules act as a binder between the membrane layer, the support, and the ZIF-22 crystals [209]. It forms a covalent bond between the

ethoxy groups of APTES react and the surface hydroxyl groups of cerium support, such as Al_2O_3 [176]. The presence of functional groups of the support and the surface modification ensure effective heterogeneous sites for developing continuous layers of ZIFs materials on the substrate [150].

Polymeric supports were also reported using porous nylon[210], porous polyethersulfone (PES) [106], and Torlon [211]. The functional groups of these polymeric materials strengthen the interaction between the polymeric support and the organic linkers. Polyaniline enhanced thermal stability and CO_2 adsorption property of ZIF-8 [212]. 20 wt.% ZIF-68 MMM increased CO_2 permeability by 116% and 122% for CO_2/N_2 and CO_2/CH_4, respectively, for Matrimid MMMs[213].

Substrates such as hydrotalcite (a magnesium-aluminum hydroxycarbonate, $Mg_6Al_2(OH)_{16}CO_3 \bullet 4H_2O$), MXenes, and graphene oxide (GO) should also be considered because of their ability to adsorb CO_2. Binders such as ILs were also reported for membranes. ILs enhance the binding and adhesion in the MMMs [214].

5.3.4.Effect of promoter and deprotonation

The well-intergrown ZIF crystals are required to obtain high pore continuity, i.e., good interconnectivity in membranes. The homogenous growth of ZIFs layers into the substrate can be promoted using deprotonation. A base such as triethylamine (TEA), sodium formate (HCOONa), ammonium hydroxide (NH_4OH), or sodium hydroxide (NaOH) can be used to deprotonate the organic linker and promotes crystal growth[208]. Thus, the ZIFs crystals can be grown in all substrate directions. The base can also play a dual role; deprotonation and the formation of a sacrificial template via conversion of Zn salts into ZnO. It was also reported that Hmim exhibits a higher degree of deprotonation in water than in organic solvents [109]. Besides the base, polymers such as polyethyleneimine (PEI) were also reported for ZIF7-based membranes[111]. The functional groups of PEI promote the linkage between the seeds and the support. PEI can also

deprotonate the organic ligand [111].The adsorption using ZIF-67 can be improved via the in-situ growth of the adsorbent inside hollow carbon nanospheres (ZIF-67@HCSs) [215]. The CO_2 adsorption capacities of ZIF-67@HCS-40, ZIF-67@HCS-50, and ZIF-67@HCS-60 were 4.6 mmol/g, 3.9 mmol/g, and 3.0 mmol/g, respectively at 273K[215].

5.3.5. Effect of the solvent

Solvothermal and hydrothermal methods are widely used for the synthesis procedures of ZIFs materials. Solvents such as dimethyl formamide (DMF), dimethyl formamide (DEF), methanol, and water were commonly used to synthesize ZIFs materials. They are critical for the synthesis of the desired materials. Water offers several advantages being a low-cost solvent and benign solvents for health and environmental concerns. However, few ZIF-membrane, such as ZIF-8 membranes, were synthesized using water as the solvent.

The solvent affects the synthesis procedure as well as the activation process. Most of the reported ZIFs are microspore materials meaning that large solvents such as DMF or DEF may remain in the final products. Thus, these species should be removed to render the pore empty for gas adsorption.

5.3.4. Effect of activation

The adsorption of gases such as CO_2 requires the presence of an empty pore. The pore structure can be evacuated using a different method. The process is called an activation step that aims to remove all occluded solvent molecules. The activation with low boiling point solvents such as water or ethanol removes solvents such as DMF or DEF present in the pore of the materials. The solvent exchange method requires soaking the materials in a solvent such as ethanol or methanol for a long time to ensure the full exchange of the occlude solvents. The solvent exchange process

may cause damage to the ZIF crystals due to the high mass transfer rate. Thus, it is highly recommended to use a solvent mixture of DMF–methanol to activate ZIF78-based membranes to slow down the diffusion rate of DMF [206]. The process requires several steps. For example, the solvent exchange process can be started by immersing the membranes in a low methanol content of DMF–methanol solvent to reduce the concentration gradient of DMF. Further steps were also performed by increasing the methanol content and ended with using pure methanol at the end of the activation process[206]. The solvent exchange with a highly volatile solvent such as methanol enables the fast removal via the drying process [206]. The synthesis procedures such as electrospray deposition simultaneously synthesize and activate ZIF-based membranes for ZIF-7 [156] and ZIF-8 [155] membranes.

5.3.6. Gases loading and interferences

GCMC simulations reveal that H_2O molecules enhanced the CO_2 adsorption at very low pressures; simultaneously, there is a reduction of CO_2 adsorption at higher pressures[216]. H_2O and SO_2 exhibited a cooperative effect on CO_2 adsorption for ZIF-NO_2 and ZIF-90 containing polar functional groups[217]. The presence of gases such as O_2 shows no impact on the capture of CO_2 [217].

The loading effect for gases, e.g., CH_4 and CO_2, was investigated [218]. The amount of the gases affect the adsorption and selectivity. The gases are usually present as a mixture with different pressure. The interaction energies between CH_4 molecules and ZIF-10 are almost constant regardless of the gas's loading due to the absence of interaction forces such as hydrogen bonds (HBs). On the other side, the interaction energies between CO_2 and ZIF-10 decreased rapidly with the increase of the gas's loading [218]. Gibbs ensemble Monte Carlo (GEMC) and molecular dynamics (MD) simulations were investigated for CO_2 adsorption using ZIF-87 via diffusion[219].

Data analysis revealed that low concentrations showed high selectivity as significant as 140. The authors also found that the selectivity value can be increased further with decreasing CO_2 concentration [219]. It was reported that both CO_2 and CH_4 are preferentially located proximal to the -C=C- bond of the Hmim linker, i.e., near the aperture at a low loading of gas molecules. While, at high loading, CH_4 and CO_2 are mainly located near the aperture, and in the cage center, respectively[182]. The efficient separation of CO_2 from other gaseous mixtures is essential for several processes such as flue gas separation, gas sweetening, and natural gas processing.

Molecular dynamics simulations were investigated for the translational and rotational motions of alkane and alkene (C_2H_6, C_3H_8, and n-C_4H_{10}) and their binary mixtures with CO_2 in ZIF-10 [220]. CO_2 gas molecules significantly promote both the translational and rotational motions of the n-C_4H_{10}/CO_2 mixture in ZIF-10. CO_2 molecules exhibit strong hydrogen bonds with the imidazolate rings leading to weakened interactions between alkanes and ZIF-10. Furthermore, both the translational and rotational motions are small compared to other gases. Thus, there was selective adsorption toward CO_2 molecules compared to alkanes [220].

Non-equilibrium dynamic Monte Carlo (DMC) simulations combined with dual control volume (DCV), denoted as DCV-DMC, were explored for the separation selectivity of a gas mixture of CH_4/CO_2 gas mixtures in ZIF-8 membrane (thickness of 20 nm)[221]. Data analysis revealed that the parts near membrane surfaces at both ends play a crucial role in determining separation selectivity [221].

5.3.7. Adsorption conditions

Low pressure (<1 bar) is optimal for ZIFs crystals with smaller pores (e.g., ZIF-7 and ZIF-94[148]. In contrast, higher pressures is required for ZIFs materials with larger pores (e.g., ZIF-11 and ZIF-93) [148].

The diffusion of CO_2 gases inside ZIF-11 crystals was investigated using multinuclear pulsed field gradient (PFG) nuclear magnetic resonance (NMR) [222]. Data analysis revealed that the intracrystalline diffusivity of CO_2 decreased with an increasing diffusion time. This observation is due to the reflections of diffusing CO_2 molecules from the external crystal surface.

5.4. Mechanism of CO_2 Adsorption into ZIFs Materials

Several mechanisms have been reported for gas adsorption, including the gate-opening mechanism [223,224], the flip motion of the linkers [88], and the linker swing motion [191]. The low-temperature heat capacity measurements of ZIF-8 confirm the structural change of the framework upon adsorption [223]. Data analysis revealed CO_2 rearrangement and lattice expansion[223]. The adsorption mechanism depends on several parameters, including temperature[225]. A study reported no gate opening related in the temperature range of 133 K and 227 K [225]. There are three sites for the binding of CO_2 and ZIF-68 (at 298 K and 1 kPa); the center of the HPR cages (Site I), the corners of the GME cages (Site III), and the nearby bIM linkers of the KNO cages (Site III), as shown in **Figure 10** [148]. Another study was reported using the van der Waals density functional model to study the binding of CO_2 into ZIFs materials [226]. The data analysis reveals the presence of three distinct binding sites for CO_2[226].

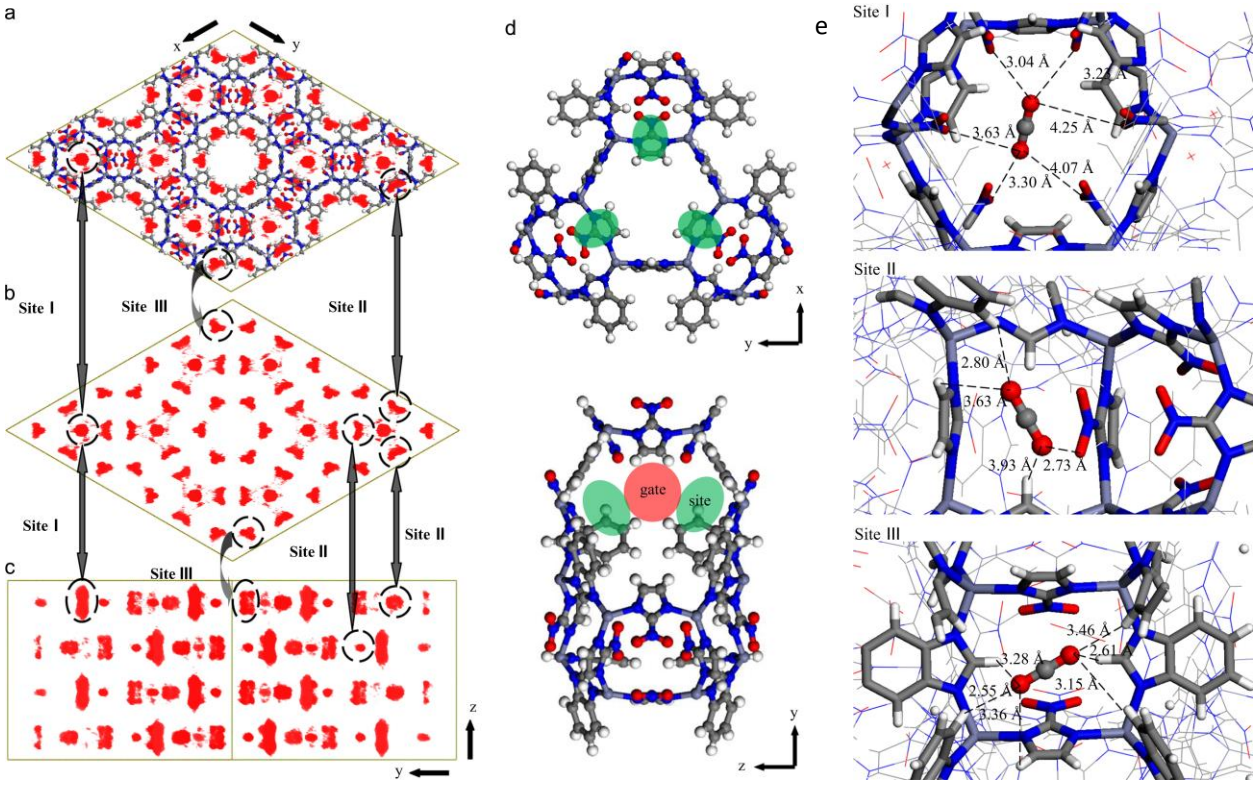

Figure 10. Probability distribution plots (PDPs) of CO_2 in ZIF-68, (a) PDPs with framework atoms in XY planes, (b) PDPs without framework atoms in (b) XY planes, (c) YZ planes, and (d) CO_2 adsorption site II in XY and YZ planes, and e) Simulation snapshots of CO_2 locations on different sites. Atom colors; Zn, light blue; O, red; C, gray; N, blue; H, white. Figure reprinted with permission from Ref. [148]. Copyright belongs to Elsevier.

A computational study using GCMC simulations were reported to study the adsorption of CO_2 and H_2O using the Zinc Triazolate-based Framework (ZTF) [216]. Data analysis reveals that the interactions between ZTF and CO_2 occur via two sites; Lewis acid–Lewis base interactions and hydrogen bonding, together with apparent electrostatic interactions[216]. In situ Raman investigation was reported to study the interactions of ZIFs with CO_2 under pressure (0–10 bar) and temperature regimes (0–64 °C)[227]. Raman spectra show a significant shift (159 cm^{-1}) in the vibration peaks of phenyl bending mode, revealing the presence of hydrogen bond interaction (**Figure 11**)[227]. The presence of electron-withdrawing groups enhanced the acidity of the linker's hydrogen atoms, improving the hydrogen bond interactions with the oxygen atoms of CO_2[194].

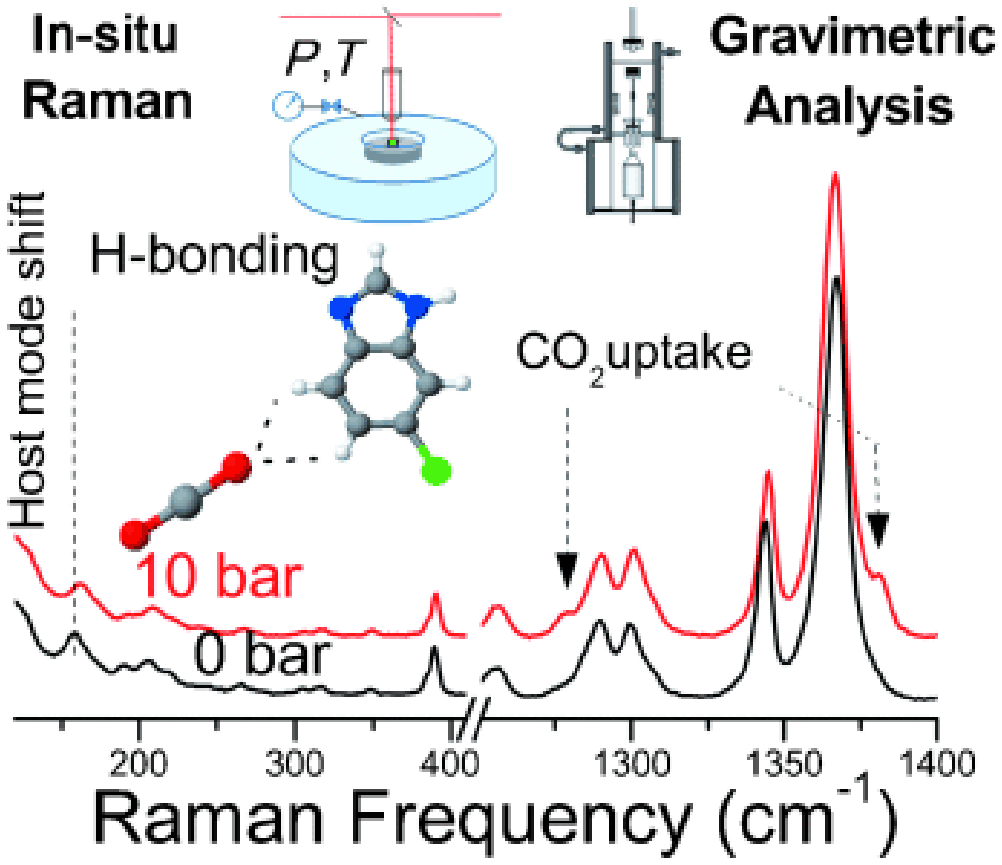

Figure 11 In-situ Raman setup and spectra of ZIF material after interaction with CO_2 under low and high pressure. Figure reprinted with permission from Ref. [227]. Copyright belongs to John Wiley & Sons.

6. Conversion of CO_2 via catalysis

Carbon dioxide (CO_2) can be removed via the conversion of CO_2 into valuable chemicals **(Figure 1)**[228,229]. It can be converted via chemical reaction (**Figure 12**), photocatalysis, and electrochemical methods **(Figure 1**). The chemical transformation of CO_2 can be achieved via cycloaddition with epoxides to produce cyclic carbonates, hydrogenation, N-formaylation [230], and synthesis of dimethyl carbonate (DMC) from CO_2 and methanol **(Figure 12)**. The following sections summarize most of the findings for these topics.

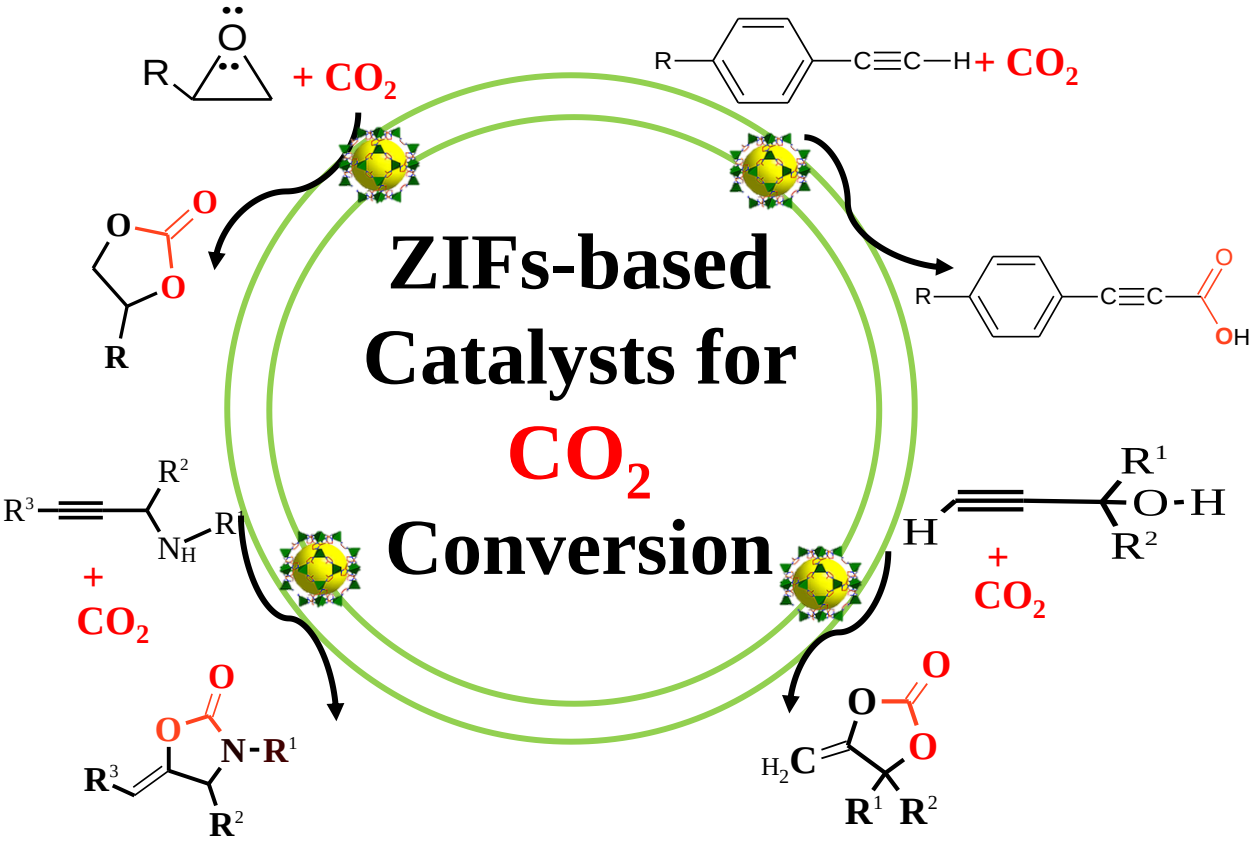

Figure 12 Chemical conversion of CO_2 into valuable compounds.

6.1.Cycloaddition with epoxides

CO_2 is an inert gas molecule (bond enthalpy +805 kJ/mol) with high thermodynamic stability. Thus, the coupling or cyclization between CO_2 and an epoxide molecule is a non-spontaneous reaction. Although, it is a highly exothermic reaction. The activation energy of the cycloaddition reaction is in the range of 50-65 kcal/mol[231–233]. Thus, this reaction requires a catalyst (**Table 3**). There are several ZIFs materials including ZIF-8[234], ZIF-23[235], ZIF-90 [236–238], ZIF-95[239], ZIF-67 [240,241], bimetallic (Zn, Co) ZIF-67[242–244], Co/ZIF-8[245], Fe/ZIF-8[246], and ZIF-68[247]. Bimetallic (Co, Zn)-ZIF-derived magnetic catalyst was also reported (**Table 3**) [248,249].

ZIF-8 has been considered the first catalyst based on ZIFs materials for CO_2 fixation via cycloaddition (**Table 3**) [234]. It catalyzed the cyclic carbonate formation, i.e., styrene carbonate from CO_2 and styrene oxide, with a yield of 53.0% at 100 °C (**Table 3**). Besides, the catalytic activity of the ZIF-8 catalyst was declined after recycling. After the reaction, the material lost its distinctive crystalline nature and catalytic performance. ZIF-68 was reported to remove CO_2 via cyclic carbonate formation using styrene oxide under mild reaction conditions (120 °C and 1.00 MPa) [247]. It yielded > 93.3% after 12 h [247]. Dual-ligand ZIF (ZIF-8-90) was used for CO_2 removal via the formation of five-membered cyclic carbonate with epichlorohydrin (ECH)[250]. ZIF-8-90 exhibited high selectivity (> 99%) compared to ZIF-8[250].

ZIFs materials (ZIF-7, ZIF-8, ZIF-9, and ZIF-67) were used as precursors for the synthesis of metal-based catalysts embedded into N-doped nanoporous carbons via carbonization at elevated temperature for cycloaddition reaction (**Table 3**) [251]. Among the carbonized materials, carbonized ZIF-9 at 600 °C (denoted as C600-ZIF-9) under an inert gas (Ar) showed the highest catalytic activity (yield of 90%) at 80 ºC under 0.6 MPa of CO_2[251]. The increased activity could be due to the uniformly distributed acidic and basic sites of partly oxidized cobalt nanoparticles and nitrogenous species [251]. ZnO nanoparticles encapsulated into N-doped porous carbon were synthesized via the carbonization of ZIF-8 followed by oxidation treatment with sodium hypochlorite (NaClO)[252]. The oxidation of the carbonized materials offered several oxygen-containing functional groups such as carboxyl, lactone, and alkoxy. ZnO@NPC-Ox-700 (NPC: N-doped porous carbon, Ox oxidized, 700 refers to carbonized temperature (º)) exhibited the highest catalytic conversion, selectivity, and recyclability for CO_2 cycloaddition[252]. Bimetallic ZIF containing Co and Zn can be used to synthesize Zn/Co@C magnetic nanoparticles via carbonization process at 900 ºC, denoted as N-doped magnetic porous carbon (NPC-900)[248].

NPC-900 is a recyclable catalyst with a simple separation procedure via an external magnet [248]. ZIF-L- derived catalyst offered high catalytic activities for CO_2 cycloaddition with 83% yield under mild conditions (70 °C and 0.1 MPa CO_2) [253].

The mechanism for cycloaddition of CO_2 and epoxide is shown in **Figure 13**. The epoxide O atom binds at the vacant coordination site of the metal ion, e.g., Zn, in the framework (**Figure 13)**. A nucleophile attacks the coordinated epoxide to activate the reaction. A co-catalyst e.g., tetrabutylammonium bromide, (TBAB) forms a Bromo-alkoxy intermediate [254]. The authors suggested the Zn-N bond dissociation and creation of active sites of Zn-OH species (low-coordinated Zn species) that act as Lewis acid/base for CO_2 cycloaddition. They also claimed that the dissociated N-species (pyrrolic or pyridinic) were inactive sites for the reaction (**Figure 13)**[254].

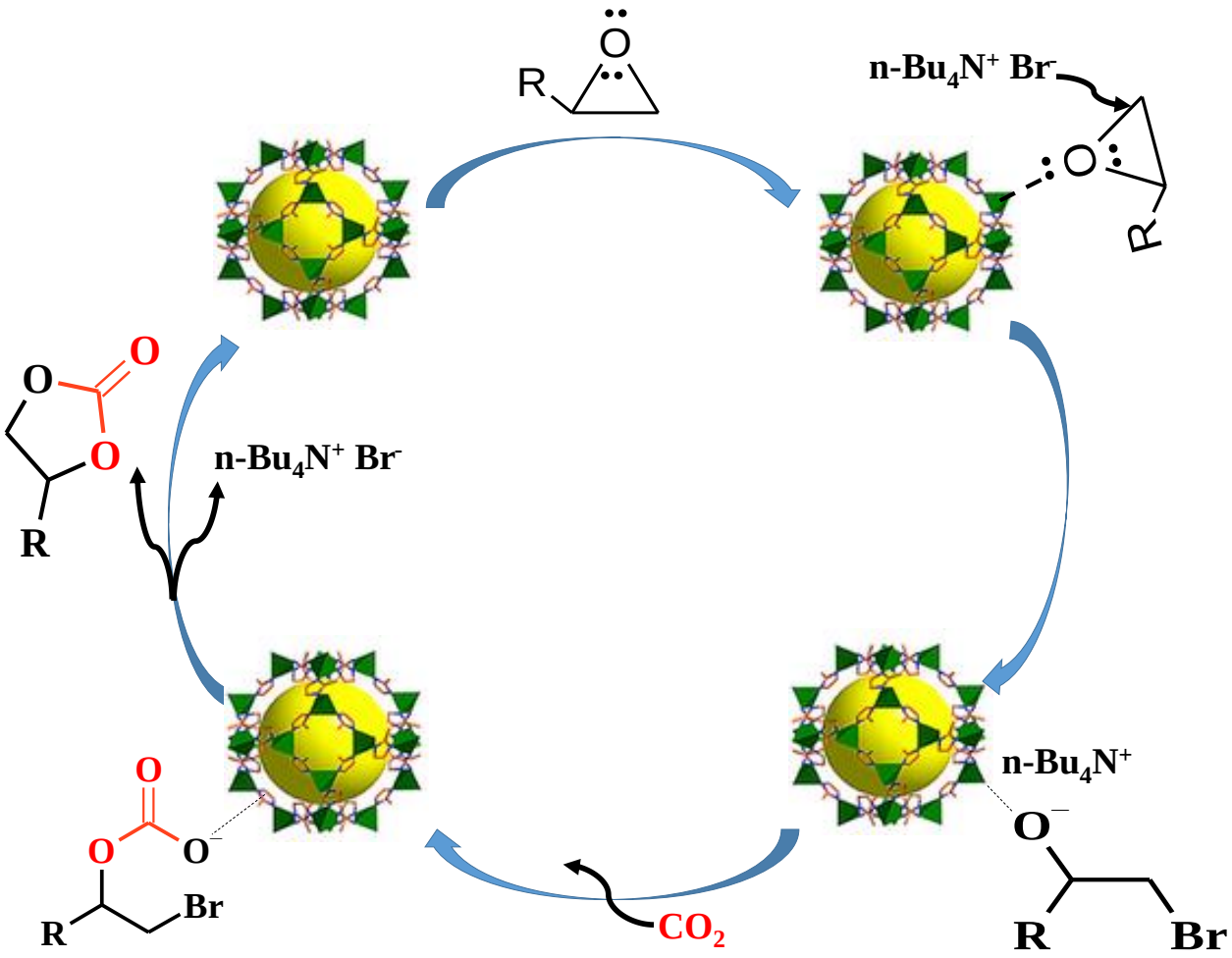

Figure 13 Mechanism of cycloaddition of CO_2 and epoxide using ZIF-8 as a catalyst.

A yolk-shell Cu_2O@ZIF-8 material was synthesized via the in-situ growth of ZIF-8 on Cu_2O modified polyvinyl pyrrolidone (PVP)[255]. It was used to convert CO_2 via the reaction with propargylic alcohols and propargylic amines under mild conditions, offering turnover numbers (TONs) of 12.1 and 19.6, respectively (**Figure 14**). It is a noble metal-free catalyst for synthesizing valuable α-alkylidene cyclic carbonates and oxazolidinones using CO_2 (**Figure 14**)[203]. It can be recycled at least five times.

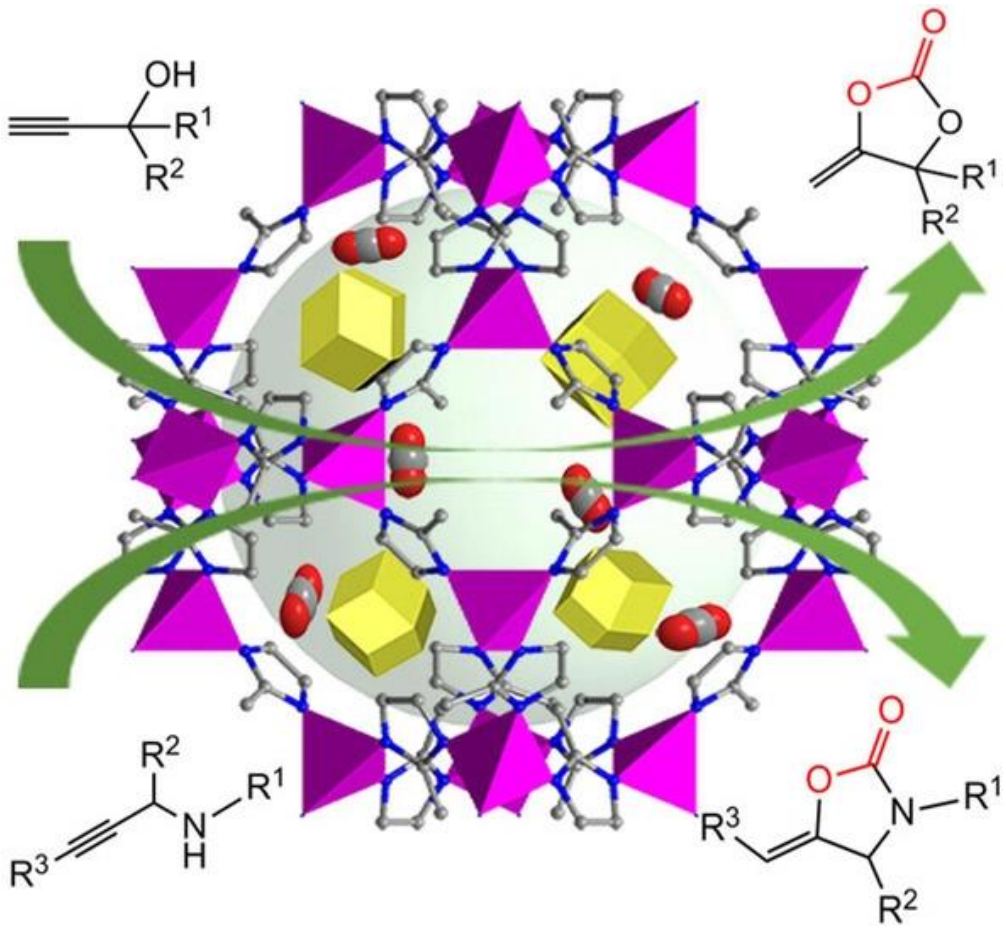

Figure 14 Conversion of propargylic alcohols and propargylic amines with CO_2 activated by Noble-metal-free catalyst Cu_2O@ZIF-8. Figure reprinted with permission from Ref. [255].

6.2. Reaction with Alcohol: Synthesis of Dimethyl Carbonate (DMC) and Carboxylation

CO_2 can be converted into a valuable compound of dimethyl carbonate (DMC) via the reaction with methanol in the presence of a catalyst (**Table 3**) [256]. DMC can be used for several usages, including glue, gasoline additives, medicine, battery electrolyte, and insecticide. It can be used as a green solvent.

Bimetallic Cu–Ni/ ZIF-8 catalyst was applied for the DMC synthesis [257]. ZIF-8 served as support. The optimal loading of Cu-Ni was 5 wt.%. The highest DMC yield was only 6.39%, with a MeOH conversion of 12.79% at 20 bar of CO_2[257]. The catalyst can be recycled for 4 cycles. However,

the yield or conversion is still very low and requires further investigation for improvement. Furthermore, the active catalytic species are Cu and Ni, with an insignificant role in ZIF-8.

ZIF-67 catalyzed the carboxylation of glycerol with CO_2 to form glycerol carbonate[258]. It showed conversion, yield, and selectivity of 32%, 29%, and 92%, respectively, at 210 °C for 12 h using 3 bar of CO_2 in the presence of a dehydrating agent such as acetonitrile (CH_3CN) [258]. Ag@ZIF-8 was reported for the carboxylation of terminal alkynes with CO2 under mild conditions (**Figure 15**)[259]. It can be used for many substrates with 77-97% (**Figure 15**). The high catalytic activity is due to two active species, Ag^+ and Ag^0 (**Figure 15**)[259]. Surface-attached nanoclusters of La_2O_3 to ZIF-8 boosted the catalytic performance of ZIF-8 for the production of glycerol carbonate using CO_2 and glycerol[260]. La^{3+}–O^{2-} pairs improved the Lewis basicity and acidity, leading to selectivity of 95% with a conversion rate of 46.5% [260].

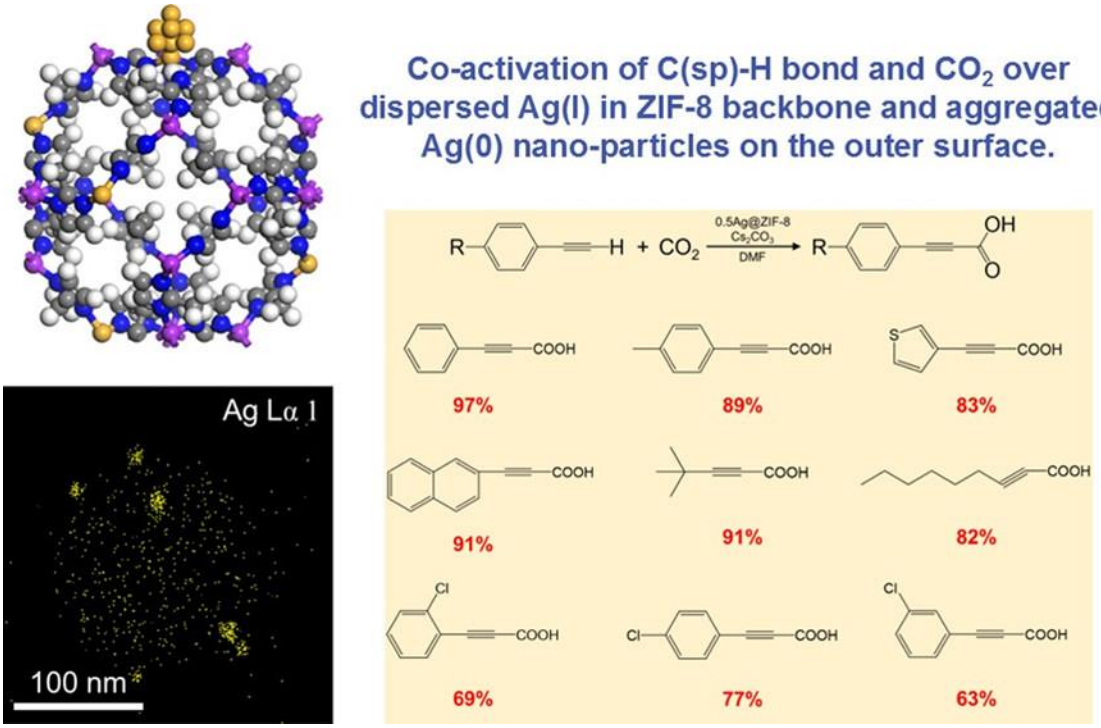

Figure 15 The carboxylation of terminal alkynes with CO_2 using Ag@ZIF-8. Figure reprinted with permission from Ref. [259]. Copyright belong to ACS.

6.3. Hydrogenation for CO_2

The conversion of CO_2 into hydrocarbons via hydrogenation is a promising method of making waste into value-added materials [10,261–270]. This reaction can solve the environmental and energy issues caused due to CO_2 emissions. Hydrogenation of CO_2 can be used to synthesize valuable compounds; 1) hydrocarbons, such as methane (CH_4, the reaction can be called methanation)[267,271], olefins, and gasoline, or 2) other compounds, such as formic acid (HCOOH), alcohol (e.g., methanol), and carbon monoxide (CO)[10,261–270]. Hydrogenation can be promoted via electrochemical [272], thermo-catalysis [273], and photo/thermal [274] methods. ZIFs materials are promising catalysts in terms of efficiency and selectivity among several catalysts.

Hydrogenation of CO2 into HCOOH using a catalyst involves the activation of CO2, rearrangement, formation, and adsorption of intermediate (e.g., HCO2-, or -OCHO). ZIF-8 on Ru was reported for CO2 hydrogenation to formic acid (Table 3) [224]. The catalyst RuCl3@ZIF-8-Mtz(0.29) was synthesized via anchoring RuCl3 on a post-synthetic modified (PSM) ZIF-8 using a linker of 3-methyl-1,2,4-triazole (Mtz). The Mtz linker comprises uncoordinated N-sites to coordinate with Ru3+ ions [224]. RuCl3@ZIF-8-Mtz(0.29) overcomes the high-energy barrier of the reaction.

Fe_2O_3/ZIF-8 was investigated for CO_2 hydrogenation to olefins[275]. MOFs can be a more effective support for active catalysts than traditional support such as α-Al_2O_3. A comparison between ZIF-8 and MIL-53-supported catalysts was reported[275]. Both MOFs were used to support the Fe_2O_3 catalyst (21 wt.%) for synthesizing hydrocarbons via CO_2 hydrogenation[275]. ZIF-8 offered different levels of light olefins selectivity; on the other side, MIL-53 could not improve the obtaining of light olefins. The study also investigated three different sizes for ZIF-8 supports. The authors reported that the selectivity of alkenes decreases with increases in particle size [275]. ZIF-

derived FeZnK-NC was also reported for CO_2 hydrogenation in the production of C_2-C_4 olefins with high stability[276]. It showed C_{2+} selectivity of 63 mol.% [276]. The hydrogenation of CO_2 using ZIF67-derived materials can be promoted using sodium via impregnation with $NaNO_3$[277]. Carbonized ZIF-67 showed the highest CO_2 conversion and selectivity of 52.5% and 99.2% toward CH_4 formation under the 72000 mL• g^{-1}• h^{-1} GHSV (gas hourly space velocity) at 270 °C [278].

Table 3 The removal of CO_2 via cycloaddition, hydrogenation, and formation of DMC.

Catalysts	**Synthesis**	**Removal Methods**	**Conditions**	**T/P/t (°C/bar/h)**	**Conversion (%)**	**Selectivity (%)**	**TOF**	**Ref.**
ZIF-8	➢ Stirred at RT for 24 h ➢ Refluxed for 20 h	Cycloaddition reaction of ECH	Catalyst (100 mg), ECH (18 mmol)	100/7/4	98	33	12	[234]
ZIF-90	Solvothermal at 100 °C for 18 h	Cycloaddition reaction of AGE	Catalyst (20 mg), AGE (18.1 mmol)	120/11.7/18	43		101	[238]
F-ZIF-90					96.7	98.7	547-855	
ZIF-95	Solvothermal at 120 °C for 72 h	Cycloaddition reaction of PO	Catalyst (0.4 mol%), PO (18.6 mmol), TBAB (0.4 mol%)	80/12/2	91	99	104	[239]
ZIF-67	Stirring at RT for 24h	Cycloaddition reaction of ECH	Catalyst (100 mg), ECH (18 mmol)	95/8/8	99	99		[240]
	Stirring at RT for 2-3h	Cycloaddition reaction of ECH	Catalyst (0.7 mol%), ECH (18 mmol)	100/7/6	76	99	38	[241]
Zn-doped ZIF-67	Stirring at RT for 24h	Cycloaddition reaction of ECH	Catalyst (50 mg), ECH (9 mmol)	100/7/2	99	99		[242]
Zn,Co-ZIF	➢ Stirring at RT for 15 min ➢ Aging at RT for 24 h ➢ Stirring with tannic acid for 10 min	Cycloaddition reaction of ECH	Catalyst (1.7 mol%), styrene oxide (4.5 mmol), TBAB (1.7 mol%)	40/7/24	99	99		[244]
Co/ZIF-8	➢ Stirring at 60 °C ➢ Stirring at RT for 24 h	Cycloaddition reaction with styrene oxide	Catalyst (50 mg), epoxide (18 mmol)	120/7/8	96.8	97.9		[245]
Fe/ZIF-8	➢ Stirring at RT for 2h ➢ Aging at RT for 24 h	Cycloaddition reaction with styrene oxide	Catalyst (50 mg), epoxide (2.05 mL)	120/7/8	97.5	99.1		[246]

ZIF-68	Solvothermal for 72h at 100 °C	Cycloaddition reaction with styrene oxide	Catalyst (100 mg), styrene oxide (0.848 g)	120/ 10/12	93.3	99		[247]
NPC-900	➢ Grinding at RT for 2 h ➢ Carbonization at 900 °C for 2h	Cycloaddition reaction of ECH	Catalyst (50 mg), ECH (1 mmol) and TBAB (54 mg, 0.17 mmol), Xenon lamp with an illumination intensity of 320 mW/cm^2	100/ 1/24	97	99		[248]
C600-ZIF-9	➢ Solvothermal ➢ Carbonization at 600 °C	Cycloaddition reaction of ECH	Catalyst (100 mg, 0.34 mol%), ECH (18 mmol)	60/6/6	90			[251]
ZnO@NPC-Ox	➢ Stirring at RT for 24 h ➢ Carbonization at 700 °C for 2h	Cycloaddition reaction with styrene oxide	Catalyst (50 mg), styrene oxide (1 mmol), TBAB (0.2 mmol)	60/1/3	98	100		[252]
ZIF-8-90	➢ Stirring for 30 min at RT ➢ Hydrothermal for 24h at 90 °C	Cycloaddition reaction of ECH	Catalyst (20 mg, 0.34 mol%), ECH (25 mmol)	100/20/4	99	99	60	[250]
ZIF-8	Solvothermal for 48h at 120 °C	Cycloaddition reaction of ECH	Catalyst (80 mg), ECH (20 mmol), TBAB (0.48 g)	25/1/48	99			[279]
ZIF-67	➢ Stirring at RT for 30 min ➢ Aging at RT for 24h	Carboxylation of glycerol	Catalyst (10 mg), glycerol (15 mL), CH_3CN (5 mL)	210/3/12	32	92		[258]
$RuCl_3$@ZIF-8-Mtz	➢ Stirring at RT for 24h ➢ PSM with Mtz at 50 °C for 24 h ➢ Stirring with $RuCl_3$ at 50 °C for 12 h	Hydrogenation of CO_2 to HCOOH	Catalyst (10 mg), H_2 ($P(CO_2)/P(H_2)$ = 1:1), $RuCl_3$ 1.9 wt.%	120/40/2			372	[280]
Fe_2O_3/ZIF-8	➢ Solvothermal at 150 °C for 24 h ➢ Solid grinding method using nano α-Fe_2O_3	CO_2 hydrogenation to hydrocarbons	Catalyst (1 g), Fe_2O_3 (21 wt.%), $n(H_2)/n(CO_2)$ = 3 (molar ratio)	300/30/3600[a]				[275]
Cu–Ni/ZIF-8	➢ Solvothermal at 70 °C for 15 min	Production DMC from	5%Cu–Ni/ZIF-8 (700 mg)	110/20/12	12.79			[257]

	➢ incipient wetness impregnation method	CO_2 and methanol						
Cu_2O@ZIF-8	➢ Ultrasonic treatment for 1 h ➢ Stirring at 50°C for 1 h	Propargylic alcohols and propargylic amines with CO_2	Catalyst (10 mg, 5 mol% based on Cu), propargylic amines (0.5 mmol), atmospheric pressure of CO_2 at 40 °C, 0.5 mL CH_3CN	40/1/6	99		3.025 h^{-1}	[255]

Notes: a, $mL \cdot g^{-1} \cdot h^{-1}$; Allyl glycidyl ether, AGE; Propylene oxide, PO; Tetrabutylammonium bromide, TBAB; TOF was calculated based on the yields per equivalent of the metal ion.

6.4. Electrochemical-based method

MOFs advanced electrochemical reduction of CO_2[281–291] and electro-carboxylation[292]. Electrochemical CO_2 reduction reaction (CO_2RR) is promising for CO_2 conversion to valuable chemical compounds. These reactions require electro-active catalysts to enable the transformation of CO_2. ZIFs-based electrocatalysts should be stable under measurements, including high electrolyte concentration. ZIFs materials exhibit good electrochemical properties compared to other MOFs materials (**Table 4**).

Several ZIF materials, including ZIF-8[293], and $Ni(Im)_2$[294], were reported for electro-reduction of CO_2 to CO. ZIF-8 was used as an effective catalyst for electrochemical reduction of CO_2 to CO[293]. ZIF-8 exhibited the highest electrochemical reduction compared to other ZIFs materials, including ZIF-108, ZIF-7, and SIM-1 [295]. It provided the highest CO Faradaic efficiency of 81.0% at − 1.1 V (vs. reversible hydrogen electrode, RHE) with a CO current density of 12.8 mA/cm^2 at − 1.3 V (vs. RHE)[295]. The Zn center and imidazolate ligands of ZIFs play an essential role in CO_2RR during the process. ZIF-8 can be synthesized via in-situ electrochemical deposition into a Zn foil to produce a ZIF-8/Zn-40 electrode [296]. The ZIF-8/Zn-40 electrode exhibited fast diffusion of CO_2 with high electroreduction efficiency of CO_2 to CO in an ionic liquid-based electrolyte[296].

ZIF-based nanocomposites were reported as electrocatalysts for CO_2RR. Cu-doped ZIF-8 was prepared via the one-pot method for electroreduction of CO_2 [297]. It exhibited high selectivity for CH_4 and CO compared to other Cu electrodes[297]. ZIF/Co-C_3N_4 was investigated for the electrocatalytic reduction of CO_2[298]. It showed a Faraday efficiency of 90.34% at −0.67 V *vs.* RHE under the light. The electroreduction of CO_2 to CO was 30% higher under light than under darkness with 200 mV lower overpotential [298]. A core-shell ZIF-8@Co/C catalyst exhibited good photo-activation for the electrocatalysis of CO_2 toward reduction [299]. It can be

used under light irradiation with a positive shift of 200 mV and 5.2-fold higher electroreduction efficiency at a potential of −0.9 V *vs.* RHE[299].

ZIF8-derived ZnO was used as an efficient CO_2 electroreduction[300]. ZIF-derived carbon doped with Fe-N sites, and Fe-N-C, were prepared via ammonia treatment[301]. Fe-N-C was synthesized via the post-impregnation method, followed by a carbonization step at 900 ºC and ammonia treatment. The treatment with ammonia facilitates the sublimation of residual Zn species and the etching of unstable carbon moieties, increasing the active sites of Fe-N active sites. It enhanced the electroreduction efficiency by 2.65 times[301]. $Cu(OH)_2$@ ZIF-8 was used as a precursor for synthesizing a hollow Cu@Cu–N–C via carbonization[302]. Cu@Cu–N–C showed high electroreduction activity due to the synergistic effect of Cu^0 (from Cu NPs) and Cu-N_x sites.

Tin (Sn)-modified ZIF-based composites were applied as catalysts for the electrochemical reduction of CO_2 to formic acid with a faradaic efficiency and current density of 76.70% and −9.81 mA/cm^2, respectively, at −1.16 V *vs.* RHE[303]. It exhibited the highest selectivity toward the formation of HCOOH. N-doping carbonized ZIF-8 at 800 ºC was used to support the earth-rich Sn catalyst (denoted as Sn- ZIF-8-800-20%) [272]. It improved the electron transfer and CO_2 adsorption capacity of Sn. Sn-ZIF-8-800-20% showed the highest reaction rate and Faraday efficiency of HCOOH and CO's hydrogenation product. The Faraday efficiency increased from 29.1% to 41.8%, from 15.9% to 27.1%, respectively, for HCOOH and CO at −1.14 V vs. RHE. On the other side, the reaction onset potential decreased from −0.74 V to −0.54 V vs. RHE[272]. The high electrochemical performance of Sn- ZIF-8-800-20% is due to the electroactive sites e.g., pyridinic nitrogen.

Electrocarboxylation of olefins with CO_2 is a promising approach to producing valuable compounds of carboxylates (**Figure 16**). Nitrogen-coordinated single-atomic Cu sites on carbon

framework (Cu/N-C) was synthesized via the carbonization of $Cu(acac)_2$@ZIF-8[292]. Cu/N-C served as an excellent electrocatalyst for electrocarboxylation of styrene with CO_2. It contains two different valence states of Cu^+ and Cu^{2+}, offering a higher charge density. The electron-rich single-atomic Cu sites exhibited effective activation of CO_2 into CO_2^- that attack styrene to produce phenyl succinic acid (**Figure 16**). Cu/N-C offered high Faradaic efficiency, good selectivity, and a high production rate of 92%, 100%, 216 mg•cm^{-2}•h^{-1}, respectively[292].

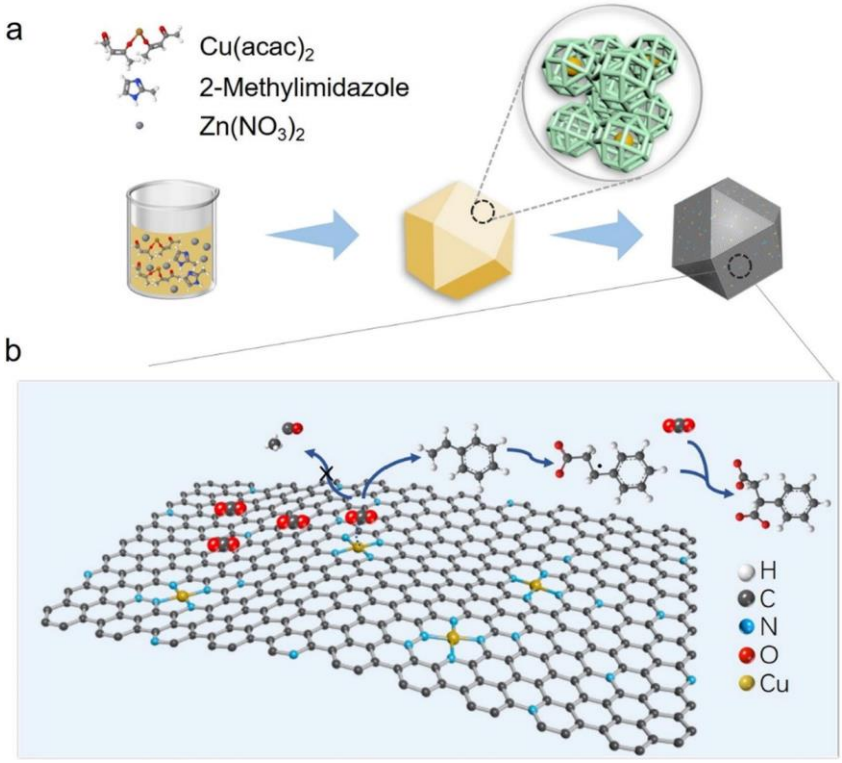

Figure 16. Synthesize of $Cu(ac.ac)_2$@ZIF-8 and their carbonization into Cu/N-C for the carboxylation of styrene into phenyl succinic acid. Figure reprinted with permission from Ref. [292]. Copyright belongs to Elsevier.

Electrochemical conversion of CO_2 can be improved using ZIFs-based catalysts with high electric conductivity (**Table 4**). The performance of the electrocatalyst depends on the metal centers of the ZIF materials[304]. The performance can also be enhanced under light using photoactive components in the investigated electrocatalysts [298].

Table 4 Electrochemical-based method for CO_2 conversion using ZIFs-based materials.

Catalysts	Synthesis	Reaction	Conditions	Faradaic Efficiency (%)	Current Density (mA/cm)	Ref.
ZIF-8	Stirring at RT for 10h	Reduction of CO_2 to CO	Catalysts (10 mg), carbon black (2 mg), Nafion solution (5 wt.%), ethanol (1 mL), diameter glassy carbon electrode, Pt wire (counter electrode) and saturated calomel reference electrode (SCE, Reference)	65 at −1.8 V (vs. SCE)	1.75 at −1.8 V (vs. SCE)	[293]
ZIF-8	Stirring at RT for 2.5h	Reduction of CO_2 to CO	Catalyst (1.0 ± 0.05 mg/cm^2) 5 wt% Nafion, Vulcan XC-72R carbon black and polytetrafluoroethylene, Vulcan XC-72R:catalyst of 1:1, Pt counter electrode and an Ag/AgCl	81 at − 1.1 V		[295]
ZIF-8/Zn-40	In-situ electrochemical deposition	Reduction of CO_2 to CO	Catalyst (36 mg), Nafion D-521 dispersion (20 µL, 5 wt %), carbon black (Vulcan XC 72, 4 mg), Toray carbon paper	91.8 at −1.9 V vs. Ag/Ag^+	12.6 at −1.9 V vs. Ag/Ag^+	[296]
Cu-doped ZIF-8	➢ Stirred at RT for 90 min ➢ Aging at RT for 24 h	Reduction of CO_2 to CH_4 and CO	Catalyst (25 mg), Nafion (40 µL), glassy carbon working electrode, Pt counter electrode and an Ag/AgCl	80 at -1.2 V	-40 at -2.1 V	[297]
ZIF8-derived ZnO	➢ Stirring at RT for 24h ➢ Carbonization at 500 ^oC for 5h	Reduction of CO_2 to CO	Catalyst (2 mg/cm), CO_2-saturated 0.25 M K_2SO_4), Zn foil, Ag/AgCl electrode and Pt wire	86.7 at −1.2 V (vs. RHE)	16.1 at −1.2 V (vs. RHE)	[300]
Fe-N-C	➢ Stirring at RT for 1 h, ➢ Aging at RT for 7 days ➢ Stirring for 24 h with ammonium ferric citrate	Reduction of CO_2 to CO	Catalyst (2.0 ± 0.1 mg/cm^2), Nafion (10 wt%.), CO_2-saturated 1 M $KHCO_3$, carbon paper (Toray TGP-H-060), Ag/AgCl and Pt	95 at −0.34 V (vs. RHE)	16 86.7 at −0.83 V (vs. RHE)	[301]

	➢ Carbonization 900 °C for 2h ➢ Pyrolysis under flowing NH_3 at 900 °C					
Cu@Cu–N–C	➢ Stirring at RT for 24 h ➢ Sonication at RT for 0.5h ➢ Stirring at RT for 12h ➢ Carbonization at 1000 °C for 2 h	Reduction of CO_2 to CO	Catalyst (0.6 mg/cm^2), glass carbon a rotating disk electrode (RDE, 3 mm in diameter) or rotating ring disk electrode (RRDE), Ag/AgCl electrode, Pt wire electrode	90% at −0.5 V vs RHE	16 at −0.5 V vs RHE	[302]
Sn-ZIF-8-800-20%	➢ Stirring for 20 min ➢ Aging at RT for 24h ➢	Electrochemical reduction to HCOOH	20% (mass) ZIF-8-800, catalyst loading 0.5 mg/cm^2 Pt/C	49.3		[272]
Cu/N-C	➢ Heated at 120 ^oC for 24 h ➢ Carbonization at 900 ^oC for 3h	Electrocarboxylation of styrene and CO_2	TBABr (0.2 M), Metallic Mg and Ag/AgI (with 0.01 M I^-)	92		[292]

6.5.Photocatalytic Reduction of CO_2

MOFs have advanced photoreduction of CO_2[284,305–322]. The reaction requires a ZIF materials with good light absorption. Most of the reported ZIF materials lack high visible-light absorption. For example, ZIF-8 has bandgap of 4.3 eV[74]. Thus, it shows zero rate of photocatalytic reduction of CO_2[323–325]. The common applications of ZIF for photo-reduction are co-catalysts or support (**Table 5**)[326,327]. ZIFs materials were conjugated with several materials including $[Ru(bpy)_3]Cl_2 \cdot 6H_2O$ (bpy = 2,2-bipyridine)/ZIF-67[326,328], $CsPbBr_3$@(Zn,Co)ZIF-67[327], Au@PtAg/ZIF-8[329], Ag@ZIF-8@g-C_3N_4[330], CdS/ZIF-8[331], CdS@ZIF-67[332], CdSe@ZIF-8[333], ZnO/ZIF-8[325,334], ZnO@Pt/ZIF-8[335], ZnO/Au@ZIF-8 [336], Au@ZIF-67[337], TiO_2/ZIF-8[338,339], TiO_2/Co-ZIF-90[340], Cu/ZIF-8[323], Zn_2GeO_4/ZIF-8[324], and WO_3/$CsPbBr_3$/ZIF-67 [341] (**Table 5**). ZIFs materials were also used as precursor for the synthesis of metal oxide embedded into carbon such as ZIF-67/MIL-125-derived Co_3O_4/TiO_2 (**Figure 17**) [342][215]. Photocatalytic reduction of CO_2 leads to formation of methanol [334], CO[329], or CH_4[336].

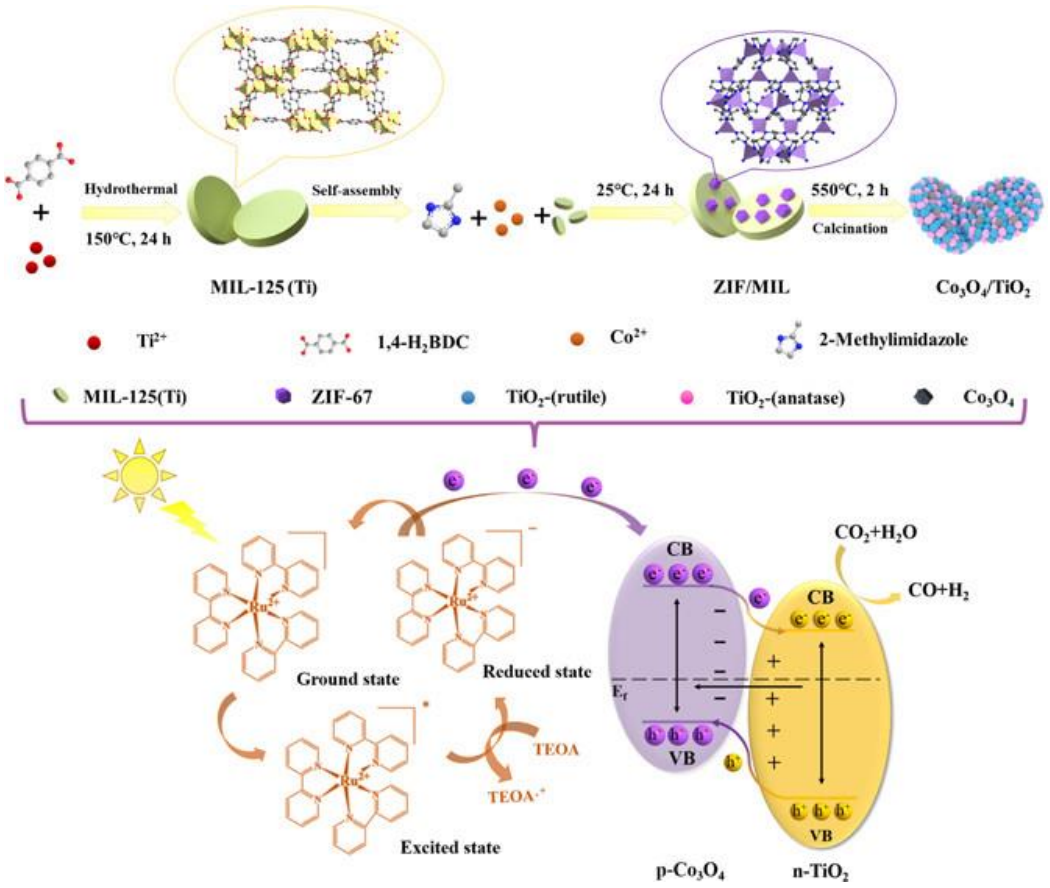

Figure 17. Fabrication procedure of the Co_3O_4/TiO_2 composites. Schematic illustration of charge transfer over Co_3O_4/TiO_2 under simulated solar light. [342]

Ru-dye/ZIF-67 was reported for photocatalytic CO_2 reduction under mild conditions [326]. The catalyst was prepared vid dispersion of photosensitizer $[Ru(bpy)_3]Cl_2 \cdot 6H_2O$ and co-catalyst ZIF-67 in a solution of triethanolamine (TEOA)/water/acetonitrile. It offered photo-reduction using a 300 W xenon lamp with 420 nm cut-off filter. It exhibited CO generation rate of 37.4 μmol/30 min. The catalyst can be recyclable with good stability[326].

A core@shell $CsPbBr_3$@(Zn, Co) ZIF-67 was reported as an efficient photocatalytic CO2 reduction[327]. The photocatalyst was synthesized via a facile in-situ procedure. The synthesis method involves the direct growth of a bimetallic zinc/cobalt- ZIF on the surface of

$CsPbBr_3$ quantum dots. Co centers in ZIF-67 accelerated the charge separation process and activated the adsorbed CO_2 molecules leading to high catalytic CO_2 reduction activity [327].

ZIF-67 was used as a precursor for synthesizing ultrathin holey Co_3O_4 nanosheets (thickness of 1.8 nm) [343]. The synthesized Co_3O_4 nanosheets was used as a co-catalyst and support for photosensitizer $[Ru(bpy)_3]Cl_2 \cdot 6H_2O$. $[Ru(bpy)_3]Cl_2 \cdot 6H_2O/Co_3O_4$ nanosheets showed CO generation rate and selectivity of 4.52 μmol/h and 70.1%, respectively. Co_3O_4 nanosheets offered a large specific surface area, high affinity to promote CO_2 adsorption, enhanced the separation and transport of charge carriers, and offered several active sites for CO_2 photoreduction[343]. The Zn_2GeO_4/ZIF-8 with 25 wt.% ZIF-8 showed 3.8 times higher CO_2 adsorption capacity than the bare Zn_2GeO_4 nanorods, offering a 62% enhancement in the photocatalytic reduction of CO_2 into CH_3OH [324].

ZIF-8 prevent photocorrosion of CdS enable good photocatalysis [331]. TiO_2/Co-ZIF-90 showed 2.1 times higher CO_2 photoreduction than pure TiO_2[340]. ZIF-based catalyst can be combined with Au nanoparticles and assembled into 3D Ni foam (**Figure 18**) [336]. NF@ZnO/Au@ZIF-8 photocatalyst showed 270.02 μmol/g with high selectivity of 89.72%. It exhibited high stability. The main product using ZnO, NF@ZnO, and NF@ZnO@ZIF-8 were CO. While, in the presence of Au, CO is further reduced, forming –CHO, $-CH_2O$, finally leading to the production of CH_3OH and CH_4. The reduction of Au is due to the high adsorption performance and high surface electron density of gold. Then -CHO gained protons and photogenerated electrons to form $-CH_2O$. Afterward, the $-CH_2O$ further obtains protons and photogenerated electrons to form $-OCH_3$. Finally, the $-OCH_3$ reacts with protons and photogenerated electrons to CH_4 (**Figure 18**) [336].

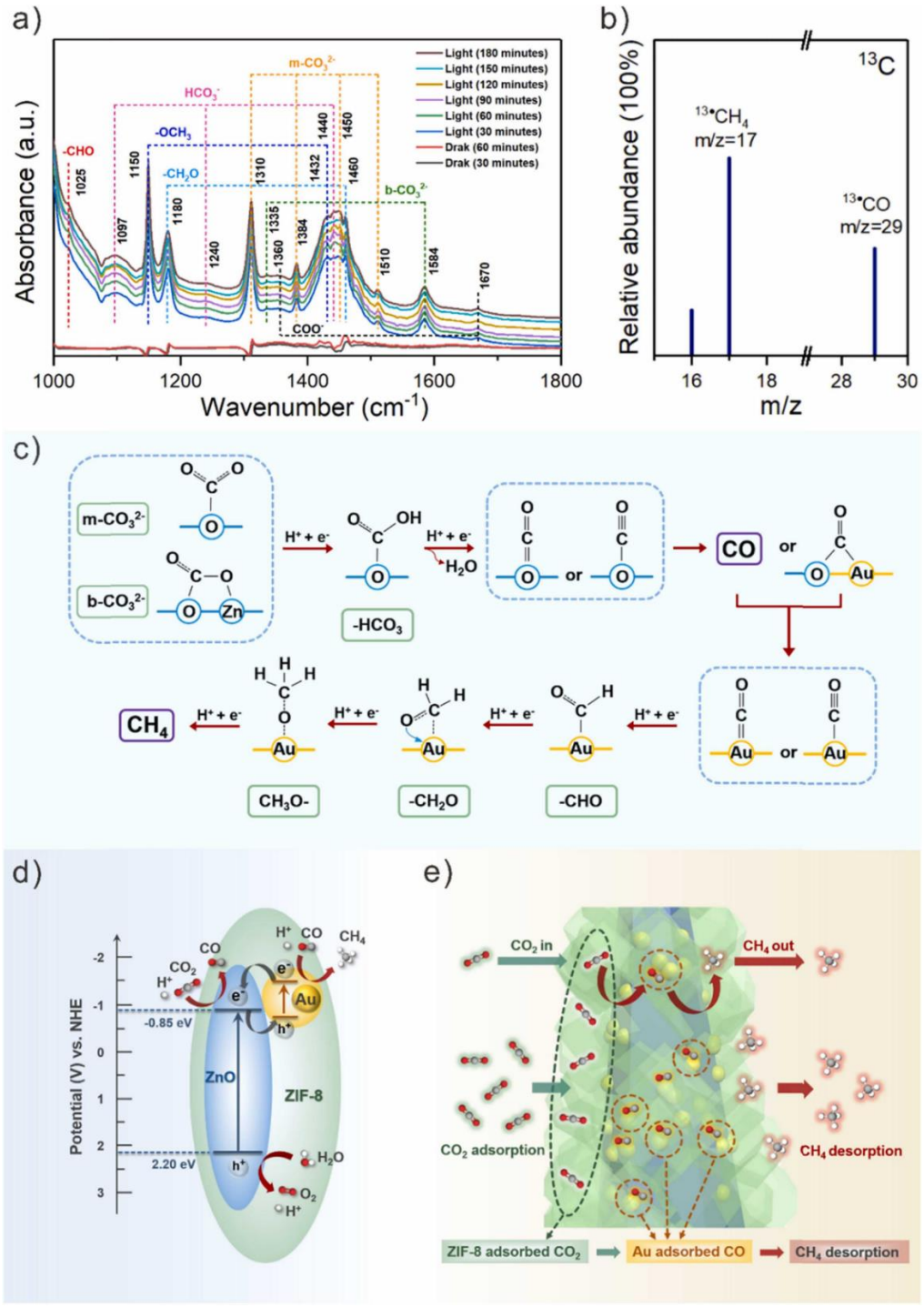

Figure 18. (a) In-situ FT-IR spectra of a mixture of CO_2 and H_2O vapor mixture under dark (0–60 min) and illumination (180 min) using NF@ZnO/Au@ZIF-8, (b) GC−MS analysis of the products generated using $^{13}CO_2$ isotope, (c) pathway for the reduction to CO and CH_4 on the surface of NF@ZnO/Au@ZIF-8, (d) the band structure and charge transfer process of NF@ZnO/Au@ZIF-8 catalyst under UV-Vis light, and (e) a diagram for CO_2 photocatalytic reduction using NF@ZnO/Au@ZIF-8 catalyst. Figure reprinted with permission from Ref.[336]. Copyright belongs to Elsevier.

Table 5 Photocatalysis reduction of CO_2 using ZIFs-based materials.

Catalysts	➢ **Synthesis**	**Conditions**	**Reactor Condition**	**Rate (μmol/h)**	**Selectivity (%)**	**Ref.**
Ru-dye/ZIF-67	➢ Aging at RT for 24h ➢ Dispersed in a solution of triethanolamine	Catalyst (1 mg), $[Ru(bpy)_3]Cl_2$ (8 mg)	300 W xenon lamp with 420 nm cut-off filter	37.4	66.7	[326]
CdS/ZIF-8	➢ Solvothermal at 120 °C for 12 h ➢ Stirring at RT for 4h	Catalyst (40 mg), 2,2′-bipyridine (200 mg), TEOA (10 mL), $CoCl_2$ (10 μmol), CH_3CN/H_2O = 2:1	300 W Xe lamp equipped with a 420 nm cut-off filter	32.13	83.96	[331]
ZnO/Pt@ZIF-8	➢ Solvothermal at 180 °C for 12 h ➢ Solvothermal at 130 °C for 24 h ➢ Solvothermal at 70 °C for 1 h	Catalyst (100 mg), in situ production of CO_2 and H_2O vapor by the reaction of $NaHCO_3$ powder and aqueous H_2SO_4 solution	300 W Xe arc lamp	1.13		[335]
TiO_2/ZIF-8	➢ Grinding for 30 min ➢ Solvothermal at 120 °C for 12 h	Catalyst (1 mg), H_2O vapor	40 W LED lamp	21.74	99	[339]
	➢ Solid-state method, at 180 °C for 24h			10.67	90	
Cu@ZIF-8	➢ Stirring for 15 min ➢ Aging at RT for 7 days ➢ Hydrothermal at 110 °C for 2 days	Catalyst (500 mg), 500 mL of NaOH and Na_2SO_3	500 W Xenon lamp	35.82		[323]
Zn_2GeO_4/ZIF-8	➢ Stirring at RT for 40 min ➢ Hydrothermal at 180 °C for 12 h ➢ Stirring at RT for 2h ➢ Stirring for 1h	Catalyst (200 mg), mass ratio 1:2 of ZIF-8 to Zn_2GeO_4, sodium sulfite (Na_2SO_3, 0.10 M)	500W Xenon lamp	2.44		[324]
ZIF-8 (AM)	➢ Stirring for 24 h at RT ➢ Stirring under reflux at 70 °C for 24 h	Catalyst (50 mg)	125 W mercury vapor lamp	500		[344]
CdSe@ZIF-8	➢ Stirring at 120 °C under N_2 flow ➢ Stirring at RT for 1h	Catalyst (5 mg), $[Ru(bpy)_3]Cl_2 \cdot 6H_2O$ (2 mg), TEOA (1 mL) and 4 mL of acetonitrile, n_{CdSe}/n_{ZIF-8} of 0.42, 12h	300 W Xe lamp with a 420 nm cut-off filter	42.317		[333]

6.6. Key parameters affecting the catalysis for CO_2 conversion

The catalytic performance of ZIFs material depends on several key parameters. Some of these factors are briefly discussed as below:-

6.6.1. Properties of ZIFs Catalysts: Structure, Composition, Morphology, and Synthesis Procedure

The effective ZIFs materials for the cycloaddition reaction should contain active sites of; (1) the presence of metal nodes/metal cluster, i.e., the open metal site or a Lewis acidic center; or (2) an organic linker with a suitable functional organic linker, i.e., Lewis acidic/basic site. These features offered active catalytic sites to achieve a high conversion of CO_2. The presence of an increased number of active sites improved the efficiency of CO_2 fixation reactions.

First-row transition metal ions are good Lewis acids and oxophillic metal centers or nodes for effective ZIFs catalysts. For example, ZIF-8 was doped with other transition metals such as Co [245], and Fe[246]. The doping of Zn^{2+} into ZIF-67 (bimetallic (Co, Zn) ZIF-67, molar ratio Zn: Co of 1:9) showed good CO_2 cycloaddition reactions without using a co-catalyst under solvent-free conditions [242]. IL@ZIF-8(Zn/Co) showed higher yield (99%) compared to IL@ZIF-8(Zn), ZIF-8(Zn/Co), and ZIF-8 that exhibited yield of 67%, 52% and 37%, respectively [345]. 70% mass fraction of $Co(NO_3)_2 \cdot 6H_2O$ showed the highest yield (94.8%) for ZIF-8 compared to other mass fractions (20%, 50%, and 90%)[245]. Fe, Ni, Cu, and Co, are the superior transition elements among different transition elements. Based on yield, the catalysts can be ordered as Fe/ZIF-8 > Ni/ZIF-8 > ZIF-8 > Cu/ZIF-8 > Co/ZIF-8[246]. The study showed yield of 94.3%, 91.9%, 78.9%, 70.2% and 72.6% for Fe/ZIF-8, Ni/ZIF-8, pure ZIF-8, Co/ZIF-8 and Cu/ZIF-8 catalysts, respectively [246]. Polymetallic ZIF containing metals of Zn^{2+}, Co^{2+}, Cd^{2+}, Ni^{2+}, and Cu^{2+} was synthesized via entropy-driven room-temperature mechanochemistry (denoted as high-entropy zeolitic

imidazolate framework, HE-ZIF)[346]. The metal ions in HE-ZIF were dispersed randomly in the frameworks. HE-ZIF exhibited higher catalytic activity compared to single metal ZIF catalyst[346].

ZnO/ZIF-8 photocatalyst exhibited the highest photocatalytic reduction of CO_2 to methanol with a production rate of 6700 μmol•g^{-1}•h^{-1}. It demonstrated the best performance compared to other photocatalysts such as Pt/ZIF-8 (5300 μmol•g^{-1}•h^{-1}), Au/ZIF-8 (426 μmol•g^{-1}•h^{-1}), and Cu/ZIF-8 (232 μmol•g^{-1}•h^{-1}). The ZnO/Pt@ZIF-8 hybrid showed a CH3OH evolution rate of 1.13 μmol•g^{-1}•h^{-1}, 16 and 1.8 times higher than the pristine ZnO and binary ZnO/Pt nanorods, respectively[335].

ZIF-8, ZIF-67, and Co/Zn-ZIF showed yield of 51%, 44%, and 73%, respectively. On the other side, carbonization (at a temperature of 600 ºC, 700 ºC, 800 ºC, and 900 ºC, NPC-X, X refers to the carbonization temperature) of these materials offered metal oxide embedded carbon with high light absorbance. On the other side, NPC-600 and NPC-900 showed high catalytic activities of 93–94% yield, while NPC-700 and NPC-800 exhibited a yield of 84–86% [248]. At low carbonization temperature (600°C), N-C layers can well wrap the Co NPs leading to the formation of smaller grains and high metallic Co^0 content due to the effective inhibition of surface oxidation. In contrast, there is a high probability of surface oxidation at high carbonization temperature leading to a surface with CoO_x oxides that inhibit the charge separation and transfer. Thus, the N-C/Co-600 sample exhibited the best photocatalytic activity [347].

The quaternary ammonium group functionalized ZIF-90 (F-ZIF-90) exhibited high catalytic performance compared to ZIF-90 (consist of Zn^{2+} and imidazole-2-carboxaldehyde (ICA))[238]. Two-dimensional (2D) ZIF-67 with a leaf-like morphology showed the highest photocatalytic CO_2 adsorption as a co-catalyst for photosensitizer $[Ru(bpy)_3]^{2+}$ [328]. It improved the activity and stability due to the highest charge separation (electron transfer)[328].

The synthesis procedure of the photocatalyst affects the materials' performance. Among different Zn salts, ZIF-8, synthesized using $ZnSO_4$, showed the best catalytic activity towards CO_2 electroreduction, with a yield of 65 % CO[293]. The authors explain this observation due to low interaction between the SO_4^{2-} anion and Zn nodes that exhibited high diffusion for SO_4^{2-}.TiO_2/ZIF-8 was synthesized via two different methods; the grinding method and the solid-synthesis method[339]. The grinding method offered high distribution of ZIF-8 particles on the surface of TiO_2 providing extra spaces for CO_2 adsorption. Thus, the composite synthesized via grinding offered high photoreduction CO_2 performances compared solid-synthesis method. The former synthesis method showed a CO formation rate of 21.74 μmol• g^{-1}• h^{-1} with a selectivity of 99% compared to a latter method, which showed only 10.67 μmol•g^{-1}• h^{-1} with 90% selectivity[339]. ZIF-8 and its photocatalytic activities. ZIF-8 was synthesized using different solvents e.g., deionized (DI) water (ZIF-8(W)), methanol (ZIF-8(M)), and ammonia/ethanol (ZIF-8(A) at room temperature (**Figure 19**)[344]. ZIF-8(A) was also soaked in methanol for 2h to evacuate the pores, named ZIF-8(AM). ZIF-8(AM) exhibited the highest amount of methanol with a rate of 500 μmol/g_{cat}. In contrast, ZIF-8(M) is almost inactive[344]. The authors explain the high catalytic performance of level of ZIF-8(M) due to the surface heterogeneity (**Figure 19**)[344].

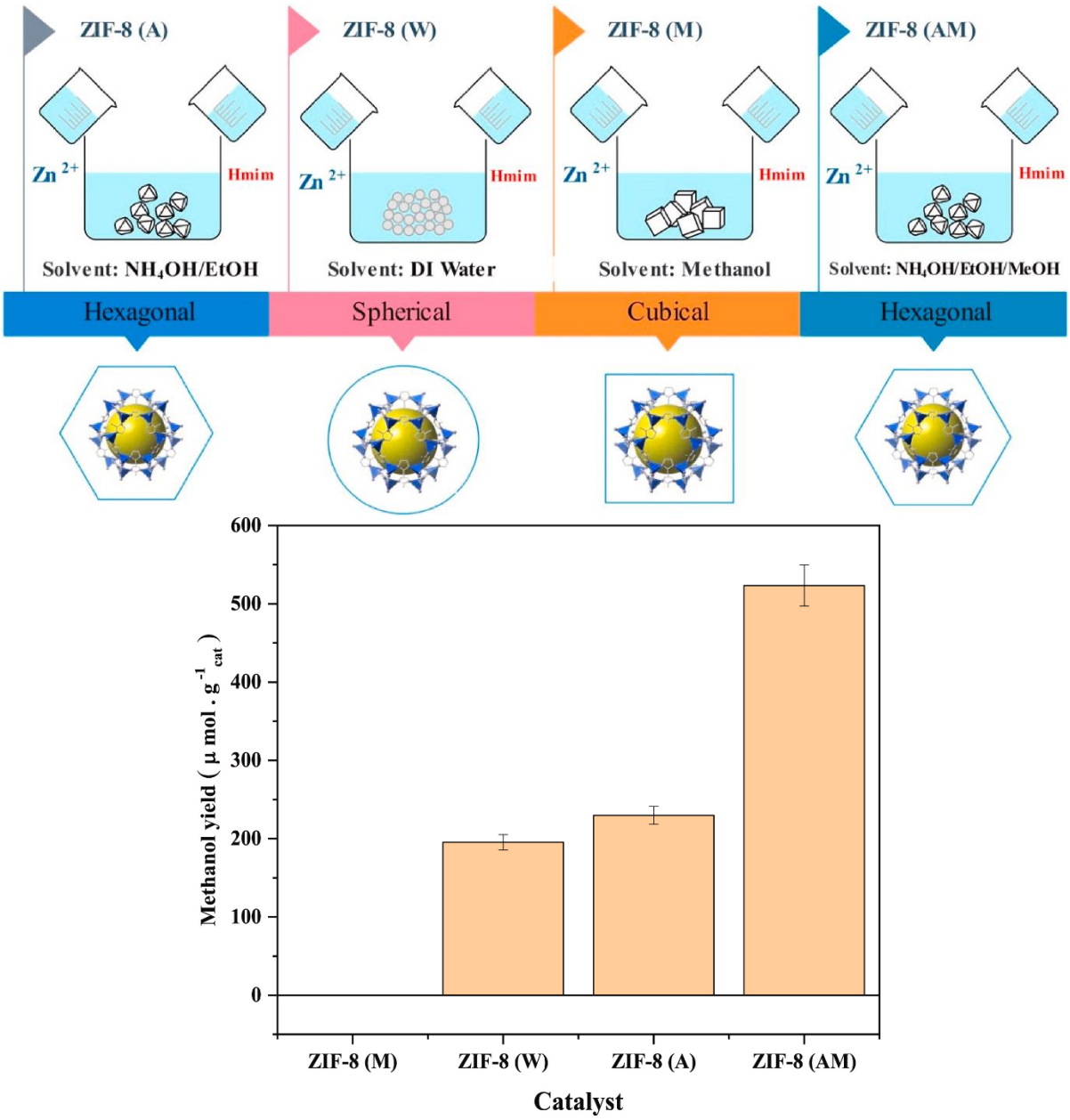

Figure 19. Scheme diagram for the synthesis of ZIF-8 samples using different methods and their methanol yield. Figure reprinted with permission from Ref. [344]. Copyright belongs to Elsevier.

6.6.2. Defects

The presence of defects in the structure of ZIFs plays an essential role in catalytic performance. Missing linkers during the co-assembly process offer open metal sites, which facilitate cycloaddition catalysis. The defects inside ZIF can be determined using several techniques such

as temperature-programmed desorption (TPD), high-resolution transmission electron microscopy (HR-TEM), and thermogravimetric analysis (TGA). ZIF-8 with uncoordinated N-sites on the framework showed a high chemical fixation of CO_2 [279,348]. Unfortunately, so far, the defects in the frameworks are uncontrollable and lack high reproducibility.

6.6.3. Additives, Solvent, and Co-catalysts

The cycloaddition of CO_2 depends on several parameters. The catalytic performance can be improved via the addition of a co-catalyst, e.g., TBAB[279], or gold (Au) [349]. Co-catalysts such as *n*-Bu_4NBr (TBAB), *n*-Pr_4NBr, *n*-Pr_4NBr, Me_4NBr showed a carbonate yields of 91%, 68%, 33%, and 6%, respectively, using hollow-structured Zn−Co based ZIF[244]. The catalytic performance of these co-catalysts can be ordered in the sequence of nBu_4N^+>*n*-Pr_4N^+>Et_4N^+>Me_4N^+. The high performance of TBAB is due to the low interaction between nBu_4N^+ and Br^-.

The cycloaddition of CO_2 and ECH can be performed without solvents [234,239]. Ionic metalloporphyrin encapsulated ZIF-8 offered a solvent-free synthesis of cyclic carbonates from CO_2 (1 atm) and epoxides without co-catalyst [350]. The presence of dehydrating agents is vital for the reaction that produces water[260]. $MgCO_3$ and CH_3CN are the common dehydrating agents. The activation energy of using $MgCO_3$ (5.4 kJ/mol) is lower than that of using CH_3CN (7.8 kJ/mol)[260]. The electrolytes for the electrochemical method are essential. NaCl showed the highest electrochemical reduction of CO_2 to the CO selectivity[293].

The catalytic performance of ZIF-8 can be improved by incorporating an amine such as ethylenediamine [234]. Water molecules can be dissociative into the external surface of ZIF-8, causing Zn-N bond dissociation, i.e., creating active sites of Zn-OH[254].

6.6.4. Substrates and Reaction conditions

F-ZIF-90 for various epoxides e.g., styrene oxide, propylene oxide, epichlorohydrin (ECH), phenyl glycidyl ether, cyclohexene oxide with conversion (%) of 62.8%, 89%, 95.2%, 95.2%, 96.7%, and 2.4%, respectively[238]. It showed selectivity of 99.3%, 98.6%, 99.1%, 98.7%, and 98%, respectively[238]. Oxirane (ECH or propylene oxide (2-methyl oxirane)) was also the optimal substrate for ZIF-67 in terms of time, reaction temperature and conversion[240].

Photocatalysis CO_2 cycloaddition requires a catalyst with good light absorption. High CO_2 concentration is usually required for high conversion and yield. The CO_2 cycloaddition reaction can be accelerated under solar-driven cycloaddition using a Xenon lamp with 320 mW/cm^2 [196]. The N-doped carbon catalyst is an effective photocatalyst for photothermally-driven CO_2 cycloaddition [351].

Substrate plays an essential role in electrocatalytic and photocatalysis. Porous substrate such as Ni foam (NF) offers a 3D platform for electron transmission with good chemical/physical stability. NF exhibits high electron mobility offering good performance as a photocatalyst.

Outlook

ZIFs-based adsorbents offer several advantages. ZIFs-based membranes exhibit good thermal stability for gas separation [352,353]. ZIFs materials such as ZIF-78, ZIF-79, ZIF-80, ZIF-81, and ZIF-82, showed high selectivity for separation of CO_2 and CH_4 with selectivity of 10.6:1 to 9.1:1 for ZIF-78 to ZIF-82, respectively [354]. They retain high CO_2 gas compared to other materials such as zeolite **gme**linite (GME) series and BPL-activated carbon [354]. ZIFs-based materials exhibit high adsorption efficiency toward CO_2 over other gases. They can be used as powder and membranes. The adsorption performance can be enhanced via several methods ensuring high

capacity and better selectivity. The synthesis of ZIF-based membranes on tubular support is promising for research and pilot-scale production before their actual deployment in industrial and commercialization applications. Most of the current methods for fabricating ZIFs-based membranes lack high reproducibility. This is a significant challenge that should be circumvented to enable consistent performance. Solving the challenges such as reproducibility and lab-scale production will enable commercialization and application on an industrial scale.

The conversion of CO_2 into valuable compounds is promising. Several reactions were reported, including photocatalytic reduction, the transformation of CO_2, electrocatalytic conversion, formation of dimethyl carbonate, and hydrogenation. The products of these reactions are valuable industrial compounds. For example, cyclic carbonates are essential intermediates for producing other substances and polymers. They can be used as aprotic polar solvents or electrolytes for lithium-ion batteries (LIBs). Further investigation should be carried out to improve the catalytic performance of ZIFs-based materials enabling large-scale production.

Processing ZIFs materials into the custom design are essential. Most of the reported synthesis procedure produces powder materials limiting their applications. The uses of biopolymers such as cellulose[355–358] and chitosan [359–366] enable to processing of ZIFs materials into commercial forms using well-established technologies. Biopolymers enable processing MOFs into forms such as foam[367].

References

[1] J. M. Kolle, M. Fayaz, A. Sayari, *Chem. Rev.* **2021**, *121*, 7280.
[2] C. Dhoke, A. Zaabout, S. Cloete, S. Amini, *Ind. Eng. Chem. Res.* **2021**, *60*, 3779.
[3] L. Keshavarz, M. R. Ghaani, J. M. D. MacElroy, N. J. English, *Chem. Eng. J.* **2021**, *412*, 128604.
[4] J. Y. Lai, L. H. Ngu, S. S. Hashim, *Greenh. Gases Sci. Technol.* **2021**, *11*, 1076.
[5] A. Sattari, A. Ramazani, H. Aghahosseini, M. K. Aroua, *J. CO2 Util.* **2021**, *48*, 101526.
[6] M. Sai Bhargava Reddy, D. Ponnamma, K. K. Sadasivuni, B. Kumar, A. M. Abdullah,

RSC Adv. **2021**, *11*, 12658.
[7] X. Wang, T. He, J. Hu, M. Liu, *Environ. Sci. Nano* **2021**, *8*, 890.
[8] A. Sharma, J. Jindal, A. Mittal, K. Kumari, S. Maken, N. Kumar, *Environ. Chem. Lett.* **2021**, *19*, 875.
[9] Z. Sun, J. Dong, C. Chen, S. Zhang, Y. Zhu, *J. Chem. Technol. Biotechnol.* **2021**, *96*, 1161.
[10] S. Saeidi, S. Najari, V. Hessel, K. Wilson, F. J. Keil, P. Concepción, S. L. Suib, A. E. Rodrigues, *Prog. Energy Combust. Sci.* **2021**, *85*, 100905.
[11] M. Takht Ravanchi, S. Sahebdelfar, *Process Saf. Environ. Prot.* **2021**, *145*, 172.
[12] M. Pera-Titus, *Chem. Rev.* **2014**, *114*, 1413.
[13] H. N. Abdelhamid, *Advanced Functional Porous Materials* (Eds.: Uthaman, A.; Thomas, S.; Li, T.; Maria, H.), Springer International Publishing, Cham, **2022**.
[14] A. I. A. Soliman, H. N. Abdelhamid, Aboel-Magd A. Abdel-Wahab, *ChemRxiv. Cambridge Cambridge Open Engag. 2022;* **2022**, 10.26434/chemrxiv.
[15] A. F. Abdel-Magied, H. N. Abdelhamid, R. M. Ashour, L. Fu, M. Dowaidar, W. Xia, K. Forsberg, *J. Environ. Chem. Eng.* **2022**, 107467.
[16] H. N. Abdelhamid, A. Mathew, *Coord. Chem. Rev.* **2022**, *451*, 214263.
[17] M. N. Goda, A. E.-A. A. Said, H. N. Abdelhamid, *J. Environ. Chem. Eng.* **2021**, *9*, 106336.
[18] H. N. Abdelhamid, *Appl. Organomet. Chem.* **2021**, *35*, e6319.
[19] H. N. Abdelhamid, A. P. Mathew, *Carbohydr. Polym.* **2021**, *274*, 118657.
[20] H. N. Abdelhamid, *Curr. Med. Chem.* **2021**, *28*, 7023.
[21] Q. Yao, A. Bermejo Gómez, J. Su, V. Pascanu, Y. Yun, H. Zheng, H. Chen, L. Liu, H. N. Abdelhamid, B. Martín-Matute, X. Zou, *Chem. Mater.* **2015**, *27*, 5332.
[22] H. E. Emam, H. N. Abdelhamid, R. M. Abdelhameed, *Dye. Pigment.* **2018**, *159*, 491.
[23] H. Furukawa, K. E. Cordova, M. O'Keeffe, O. M. Yaghi, *Science (80-.).* **2013**, *341*, 1230444.
[24] N. Stock, S. Biswas, *Chem. Rev.* **2012**, *112*, 933.
[25] M. Eddaoudi, J. Kim, N. Rosi, D. Vodak, J. Wachter, M. O'Keeffe, O. M. Yaghi, *Science (80-.).* **2002**, *295*, 469.
[26] Z. Wang, S. M. Cohen, *J. Am. Chem. Soc.* **2007**, *129*, 12368.
[27] H. Deng, C. J. Doonan, H. Furukawa, R. B. Ferreira, J. Towne, C. B. Knobler, B. Wang, O. M. Yaghi, *Science (80-.).* **2010**, *327*, 846.
[28] K. S. Park, Z. Ni, A. P. Cote, J. Y. Choi, R. Huang, F. J. Uribe-Romo, H. K. Chae, M. O'Keeffe, O. M. Yaghi, *Proc. Natl. Acad. Sci.* **2006**, *103*, 10186.
[29] J. Yu, L.-H. Xie, J.-R. Li, Y. Ma, J. M. Seminario, P. B. Balbuena, *Chem. Rev.* **2017**, *117*, 9674.
[30] H. N. Abdelhamid, *Nanotechnology* **2019**, *30*, 435601.
[31] T. K. Pal, D. De, P. K. Bharadwaj, *Fuel* **2022**, *320*, 123904.
[32] G. Singh, J. Lee, A. Karakoti, R. Bahadur, J. Yi, D. Zhao, K. AlBahily, A. Vinu, *Chem. Soc. Rev.* **2020**, *49*, 4360.
[33] J. W. Maina, C. Pozo-Gonzalo, L. Kong, J. Schütz, M. Hill, L. F. Dumée, *Mater. Horizons* **2017**, *4*, 345.
[34] X. Liu, J. Li, N. Li, B. Li, X. Bu, *Chinese J. Chem.* **2021**, *39*, 440.
[35] H. He, J. A. Perman, G. Zhu, S. Ma, *Small* **2016**, *12*, 6309.
[36] M. Ding, R. W. Flaig, H.-L. Jiang, O. M. Yaghi, *Chem. Soc. Rev.* **2019**, *48*, 2783.

[37] A. A. Olajire, *Renew. Sustain. Energy Rev.* **2018**, *92*, 570.
[38] I. Hazra Chowdhury, A. Hazra Chowdhury, P. Sarkar, S. M. Islam, *ChemNanoMat* **2021**, *7*, 580.
[39] D. Kim, D. W. Kim, O. Buyukcakir, M.-K. Kim, K. Polychronopoulou, A. Coskun, *Adv. Funct. Mater.* **2017**, *27*, 1700706.
[40] J. Liang, Y.-B. Huang, R. Cao, *Coord. Chem. Rev.* **2019**, *378*, 32.
[41] Y.-T. Liao, V. C. Nguyen, N. Ishiguro, A. P. Young, C.-K. Tsung, K. C.-W. Wu, *Appl. Catal. B Environ.* **2020**, *270*, 118805.
[42] R.-X. Yang, Y.-T. Bieh, C. H. Chen, C.-Y. Hsu, Y. Kato, H. Yamamoto, C.-K. Tsung, K. C.-W. Wu, *ACS Sustain. Chem. Eng.* **2021**, *9*, 6541.
[43] H. Konnerth, B. M. Matsagar, S. S. Chen, M. H. G. Prechtl, F.-K. Shieh, K. C.-W. Wu, *Coord. Chem. Rev.* **2020**, *416*, 213319.
[44] C.-C. Chueh, C.-I. Chen, Y.-A. Su, H. Konnerth, Y.-J. Gu, C.-W. Kung, K. C.-W. Wu, *J. Mater. Chem. A* **2019**, *7*, 17079.
[45] H. N. Abdelhamid, A. Bermejo-Gómez, B. Martín-Matute, X. Zou, *Microchim. Acta* **2017**, *184*, 3363.
[46] Y. Yang, K. Shen, J. Lin, Y. Zhou, Q. Liu, C. Hang, H. N. Abdelhamid, Z. Zhang, H. Chen, *RSC Adv.* **2016**, *6*, 45475.
[47] H. N. Abdelhamid, Lanthanide Metal-Organic Frameworks and Hierarchical Porous Zeolitic Imidazolate Frameworks: Synthesis, Properties, and Applications, Stockholm University, Faculty of Science, Stockholm, **2017**.
[48] H. N. Abdelhamid, W. Sharmoukh, *Microchem. J.* **2021**, *163*, 105873.
[49] A. A. Kassem, H. N. Abdelhamid, D. M. Fouad, S. A. Ibrahim, *Int. J. Hydrogen Energy* **2019**, *44*, 31230.
[50] H. N. Abdelhamid, *Dalt. Trans.* **2020**, *49*, 4416.
[51] H. M. El-Bery, H. N. Abdelhamid, *J. Environ. Chem. Eng.* **2021**, *9*, 105702.
[52] H. N. Abdelhamid, *Dalt. Trans.* **2020**, *49*, 10851.
[53] H. N. Abdelhamid, *Energy & Fuels* **2021**, *35*, 10322.
[54] H. N. Abdelhamid, A. M. El-Zohry, J. Cong, T. Thersleff, M. Karlsson, L. Kloo, X. Zou, *R. Soc. Open Sci.* **2019**, *6*, 190723.
[55] A. A. Kassem, H. N. Abdelhamid, D. M. Fouad, S. A. Ibrahim, *J. Environ. Chem. Eng.* **2021**, *9*, 104401.
[56] A. A. Kassem, H. N. Abdelhamid, D. M. Fouad, S. A. Ibrahim, *Microporous Mesoporous Mater.* **2020**, *305*, 110340.
[57] H. N. Abdelhamid, *J. Environ. Chem. Eng.* **2021**, *9*, 104404.
[58] M. N. Goda, H. N. Abdelhamid, A. E.-A. A. Said, *ACS Appl. Mater. Interfaces* **2020**, *12*, 646.
[59] H. N. Abdelhamid, M. N. Goda, A. E.-A. A. Said, *Nano-Structures & Nano-Objects* **2020**, *24*, 100605.
[60] Y.-C. Liu, L.-H. Yeh, M.-J. Zheng, K. C.-W. Wu, *Sci. Adv.* **2021**, *7*.
[61] S. Sultan, H. N. Abdelhamid, X. Zou, A. P. Mathew, *Adv. Funct. Mater.* **2018**, 1805372.
[62] A. F. Abdel-Magied, H. N. Abdelhamid, R. M. Ashour, X. Zou, K. Forsberg, *Microporous Mesoporous Mater.* **2019**, *278*, 175.
[63] J.-P. Zhang, Y.-B. Zhang, J.-B. Lin, X.-M. Chen, *Chem. Rev.* **2012**, *112*, 1001.
[64] B. Chen, Z. Yang, Y. Zhu, Y. Xia, *J. Mater. Chem. A* **2014**, *2*, 16811.
[65] H. N. Abdelhamid, *Biointerface Res. Appl. Chem.* **2021**, *11*, 8283.

[66] H. N. Abdelhamid, **2022**, pp. 431–447.
[67] H. K. Chae, D. Y. Siberio-Pérez, J. Kim, Y. Go, M. Eddaoudi, A. J. Matzger, M. O'Keeffe, O. M. Yaghi, *Nature* **2004**, *427*, 523.
[68] H. N. Abdelhamid, M. Dowaidar, Ü. Langel, *Microporous Mesoporous Mater.* **2020**, *302*, 110200.
[69] H. N. Abdelhamid, M. Dowaidar, M. Hällbrink, Ü. Langel, *SSRN Electron. J.* **2019**.
[70] H. N. Abdelhamid, M. Dowaidar, M. Hällbrink, Ü. Langel, *Microporous Mesoporous Mater.* **2020**, *300*, 110173.
[71] H. N. Abdelhamid, G. A.-E. Mahmoud, W. Sharmouk, *J. Mater. Chem. B* **2020**, *8*, 7548.
[72] H. N. Abdelhamid, G. A.-E. Mahmoud, W. Sharmouk, W. Sharmoukh, *J. Mater. Chem. B* **2020**, *8*, 7557.
[73] H. N. Abdelhamid, X. Zou, *Green Chem.* **2018**, *20*, 1074.
[74] A. I. A. Soliman, A.-M. A. Abdel-Wahab, H. N. Abdelhamid, *RSC Adv.* **2022**, *12*, 7075.
[75] H. Nasser Abdelhamid, D. Georgouvelas, U. Edlund, A. P. Mathew, *Chem. Eng. J.* **2022**, 136614.
[76] H. Abdelhamid, D. Georgouvelas, U. Edlund, A. Mathew, *ChemRxiv. Cambridge Cambridge Open Engag* **2022**.
[77] H. N. Abdelhamid, *J. Solid State Chem.* **2021**, *297*, 122034.
[78] H. N. Abdelhamid, *Int. J. Hydrogen Energy* **2021**, *46*, 726.
[79] H. N. Abdelhamid, S. A. Al Kiey, W. Sharmoukh, *Appl. Organomet. Chem.* **2021**.
[80] A. K. Davey, X. Gao, Y. Xia, Z. Li, M. N. Dods, S. Delacruz, A. Pan, S. Swamy, D. Gardner, C. Carraro, R. Maboudian, *Sensors Actuators B Chem.* **2021**, *344*, 130313.
[81] J. C. Tan, T. D. Bennett, A. K. Cheetham, *Proc. Natl. Acad. Sci.* **2010**, *107*, 9938.
[82] A. Phan, C. J. Doonan, F. J. Uribe-Romo, C. B. Knobler, M. O'Keeffe, O. M. Yaghi, *Acc. Chem. Res.* **2010**, *43*, 58.
[83] R. Grau-Crespo, A. Aziz, A. W. Collins, R. Crespo-Otero, N. C. Hernández, L. M. Rodriguez-Albelo, A. R. Ruiz-Salvador, S. Calero, S. Hamad, *Angew. Chemie Int. Ed.* **2016**, *55*, 16012.
[84] H. Zhang, M. Zhao, Y. S. Lin, *Microporous Mesoporous Mater.* **2019**, *279*, 201.
[85] M. Taheri, D. Ashok, T. Sen, T. G. Enge, N. K. Verma, A. Tricoli, A. Lowe, D. R. Nisbet, T. Tsuzuki, *Chem. Eng. J.* **2020**, 127511.
[86] S. Tanaka, Y. Tanaka, *ACS Omega* **2019**, *4*, 19905.
[87] C. Zhang, R. P. Lively, K. Zhang, J. R. Johnson, O. Karvan, W. J. Koros, *J. Phys. Chem. Lett.* **2012**, *3*, 2130.
[88] T. Ueda, T. Yamatani, M. Okumura, *J. Phys. Chem. C* **2019**, *123*, 27542.
[89] Y. Pan, Y. Liu, G. Zeng, L. Zhao, Z. Lai, *Chem. Commun.* **2011**, *47*, 2071.
[90] S. Tanaka, K. Kida, M. Okita, Y. Ito, Y. Miyake, *Chem. Lett.* **2012**, *41*, 1337.
[91] K. Kida, M. Okita, K. Fujita, S. Tanaka, Y. Miyake, *CrystEngComm* **2013**, *15*, 1794.
[92] X.-C. Huang, Y.-Y. Lin, J.-P. Zhang, X.-M. Chen, *Angew. Chemie Int. Ed.* **2006**, *45*, 1557.
[93] J. Cravillon, S. Münzer, S.-J. Lohmeier, A. Feldhoff, K. Huber, M. Wiebcke, *Chem. Mater.* **2009**, *21*, 1410.
[94] M. He, J. Yao, L. Li, K. Wang, F. Chen, H. Wang, *Chempluschem* **2013**, *78*, 1222.
[95] T. D. Bennett, P. J. Saines, D. A. Keen, J.-C. Tan, A. K. Cheetham, *Chem. - A Eur. J.* **2013**, *19*, 7049.
[96] T. Yang, T.-S. Chung, *J. Mater. Chem. A* **2013**, *1*, 6081.

[97] H. N. Abdelhamid, Z. Huang, A. M. El-Zohry, H. Zheng, X. Zou, *Inorg. Chem.* **2017**, *56*, 9139.
[98] J. Cravillon, C. A. Schröder, H. Bux, A. Rothkirch, J. Caro, M. Wiebcke, *CrystEngComm* **2012**, *14*, 492.
[99] D. Peralta, G. Chaplais, A. Simon-Masseron, K. Barthelet, G. D. Pirngruber, *Microporous Mesoporous Mater.* **2012**, *153*, 1.
[100] S. Głowniak, B. Szczęśniak, J. Choma, M. Jaroniec, *Mater. Today* **2021**.
[101] C.-A. Tao, J.-F. Wang, *Crystals* **2020**, *11*, 15.
[102] M. Taheri, I. Di Bernardo, A. Lowe, D. R. Nisbet, T. Tsuzuki, *Cryst. Growth Des.* **2020**, *20*, 2761.
[103] P. Ji, R. Tian, H. Zheng, J. Jiang, J. Sun, J. Peng, *Dalt. Trans.* **2020**, *49*, 12555.
[104] H. T. Kwon, H.-K. Jeong, *J. Am. Chem. Soc.* **2013**, *135*, 10763.
[105] H. T. Kwon, H.-K. Jeong, *Chem. Commun.* **2013**, *49*, 3854.
[106] L. Ge, W. Zhou, A. Du, Z. Zhu, *J. Phys. Chem. C* **2012**, *116*, 13264.
[107] L. Fan, M. Xue, Z. Kang, H. Li, S. Qiu, *J. Mater. Chem.* **2012**, *22*, 25272.
[108] Y.-S. Li, F.-Y. Liang, H. Bux, A. Feldhoff, W.-S. Yang, J. Caro, *Angew. Chemie* **2010**, *122*, 558.
[109] Y. Pan, T. Li, G. Lestari, Z. Lai, *J. Memb. Sci.* **2012**, *390–391*, 93.
[110] M. Shah, M. C. McCarthy, S. Sachdeva, A. K. Lee, H.-K. Jeong, *Ind. Eng. Chem. Res.* **2012**, *51*, 2179.
[111] Y.-S. Li, H. Bux, A. Feldhoff, G.-L. Li, W.-S. Yang, J. Caro, *Adv. Mater.* **2010**, *22*, 3322.
[112] H. Bux, A. Feldhoff, J. Cravillon, M. Wiebcke, Y.-S. Li, J. Caro, *Chem. Mater.* **2011**, *23*, 2262.
[113] H. N. Abdelhamid, *Mater. Today Chem.* **2020**, *15*, 100222.
[114] H. P. Paudel, W. Shi, D. Hopkinson, J. A. Steckel, Y. Duan, *React. Chem. Eng.* **2021**, *6*, 990.
[115] S. K. Nune, P. K. Thallapally, A. Dohnalkova, C. Wang, J. Liu, G. J. Exarhos, *Chem. Commun.* **2010**, *46*, 4878.
[116] C. Chen, J. Kim, D.-A. Yang, W.-S. Ahn, *Chem. Eng. J.* **2011**, *168*, 1134.
[117] Z. Shi, Y. Yu, C. Fu, L. Wang, X. Li, *RSC Adv.* **2017**, *7*, 29227.
[118] H. N. Abdelhamid, *Macromol. Chem. Phys.* **2020**, *221*, 2000031.
[119] R. Chen, J. Yao, Q. Gu, S. Smeets, C. Baerlocher, H. Gu, D. Zhu, W. Morris, O. M. Yaghi, H. Wang, *Chem. Commun.* **2013**, *49*, 9500.
[120] H. Nasser Abdelhamid, A. P. Mathew, *Chem. Eng. J.* **2021**, *426*, 131733.
[121] A. G. Kontos, G. E. Romanos, C. M. Veziri, A. Gotzias, M. K. Arfanis, E. Kouvelos, V. Likodimos, G. N. Karanikolos, P. Falaras, *Appl. Surf. Sci.* **2020**, *529*, 147058.
[122] S. Lijuan, Q. Kai, W. Haonan, L. Jie, Q. Mingyue, Y. Qun, *Fuel* **2021**, *298*, 120875.
[123] M. Shahnawaz Khan, H. N. Abdelhamid, H.-F. Wu, *Colloids Surf. B. Biointerfaces* **2015**, *127C*, 281.
[124] R. M. Ashour, H. N. Abdelhamid, A. F. Abdel-Magied, A. A. Abdel-khalek, M. Ali, A. Uheida, M. Muhammed, X. Zou, J. Dutta, *Solvent Extr. Ion Exch.* **2017**, *35*, 91.
[125] H. N. Abdelhamid, K. H. Hussein, *Biointerface Res. Appl. Chem.* **2021**, *11*, 14726.
[126] M. Dowaidar, H. N. Abdelhamid, M. Hällbrink, X. Zou, Ü. Langel, *Biochim. Biophys. Acta - Gen. Subj.* **2017**, *1861*, 2334.
[127] H. N. Abdelhamid, M. S. Khan, H. F. Wu, *RSC Adv.* **2014**, *4*, 50035.
[128] B.-S. Wu, H. N. Abdelhamid, H.-F. Wu, *RSC Adv.* **2014**, *4*, 3722.

[129] H. Nasser Abdelhamid, B.-S. Wu, H.-F. Wu, *Talanta* **2014**, *126*, 27.
[130] K. H. Hussein, H. N. Abdelhamid, X. Zou, H.-M. Woo, *Mater. Sci. Eng. C* **2019**, *94*, 484.
[131] H. N. Abdelhamid, H.-F. Wu, *Microchim. Acta* **2015**, *182*, 1609.
[132] P.-Y. Hua, M. Manikandan, H. N. Abdelhamid, H.-F. Wu, *J. Mater. Chem. B* **2014**, *2*, 7334.
[133] H. N. Abdelhamid, H.-F. Wu, *Analyst* **2015**, *140*, 1555.
[134] J. Pokhrel, N. Bhoria, S. Anastasiou, T. Tsoufis, D. Gournis, G. Romanos, G. N. Karanikolos, *Microporous Mesoporous Mater.* **2018**, *267*, 53.
[135] S. Xian, F. Xu, C. Ma, Y. Wu, Q. Xia, H. Wang, Z. Li, *Chem. Eng. J.* **2015**, *280*, 363.
[136] S. Wang, X. Wang, *Angew. Chemie Int. Ed.* **2016**, *55*, 2308.
[137] H. N. Abdelhamid, *TrAC Trends Anal. Chem.* **2015**, *77*, 122.
[138] H. N. Abdelhamid, *TrAC Trends Anal. Chem.* **2017**, *89*, 68.
[139] H. N. Abdelhamid, M. S. Khan, H.-F. F. Wu, *Anal. Chim. Acta* **2014**, *823*, 51.
[140] M. Mohamedali, H. Ibrahim, A. Henni, *Chem. Eng. J.* **2018**, *334*, 817.
[141] A. Thomas, M. Prakash, *J. Phys. Chem. C* **2020**, *124*, 26203.
[142] A. Thomas, M. Prakash, *Appl. Surf. Sci.* **2019**, *491*, 633.
[143] A. Mohamed, P. Krokidas, I. G. Economou, *J. Comput. Sci.* **2018**, *27*, 183.
[144] H. N. Abdelhamid, *J. Environ. Chem. Eng.* **2020**, *8*, 104008.
[145] Y. Ban, Y. Li, Y. Peng, H. Jin, W. Jiao, X. Liu, W. Yang, *Chem. - A Eur. J.* **2014**, *20*, 11402.
[146] P. Zhao, G. I. Lampronti, G. O. Lloyd, E. Suard, S. A. T. Redfern, *J. Mater. Chem. A* **2014**, *2*, 620.
[147] E. Pantatosaki, G. Megariotis, A.-K. Pusch, C. Chmelik, F. Stallmach, G. K. Papadopoulos, *J. Phys. Chem. C* **2012**, *116*, 201.
[148] Y. Liu, A. Kasik, N. Linneen, J. Liu, Y. S. Lin, *Chem. Eng. Sci.* **2014**, *118*, 32.
[149] M. Ghahramaninezhad, F. Mohajer, M. Niknam Shahrak, *Front. Chem. Sci. Eng.* **2020**, *14*, 425.
[150] A. Huang, Y. Chen, N. Wang, Z. Hu, J. Jiang, J. Caro, *Chem. Commun.* **2012**, *48*, 10981.
[151] Y. Liu, E. Hu, E. A. Khan, Z. Lai, *J. Memb. Sci.* **2010**, *353*, 36.
[152] Y. Yoo, Z. Lai, H.-K. Jeong, *Microporous Mesoporous Mater.* **2009**, *123*, 100.
[153] Y. Liu, Z. Ng, E. A. Khan, H.-K. Jeong, C. Ching, Z. Lai, *Microporous Mesoporous Mater.* **2009**, *118*, 296.
[154] H. Bux, F. Liang, Y. Li, J. Cravillon, M. Wiebcke, J. Caro, *J. Am. Chem. Soc.* **2009**, *131*, 16000.
[155] V. M. Aceituno Melgar, H. Ahn, J. Kim, M. R. Othman, *J. Ind. Eng. Chem.* **2015**, *21*, 575.
[156] V. M. Aceituno Melgar, H. T. Kwon, J. Kim, *J. Memb. Sci.* **2014**, *459*, 190.
[157] M. Z. Ahmad, V. Martin-Gil, V. Perfilov, P. Sysel, V. Fila, *Sep. Purif. Technol.* **2018**, *207*, 523.
[158] L. Hu, J. Liu, L. Zhu, X. Hou, L. Huang, H. Lin, J. Cheng, *Sep. Purif. Technol.* **2018**, *205*, 58.
[159] X. Zhang, T. Zhang, Y. Wang, J. Li, C. Liu, N. Li, J. Liao, *J. Memb. Sci.* **2018**, *560*, 38.
[160] Y. Zhang, Y. Tong, X. Li, S. Guo, H. Zhang, X. Chen, K. Cai, L. Cheng, W. He, *ACS Omega* **2021**, *6*, 18566.
[161] G. Li, W. Kujawski, A. Tonkonogovas, K. Knozowska, J. Kujawa, E. Olewnik-Kruszkowska, N. Pedišius, A. Stankevičius, *Chem. Eng. Res. Des.* **2022**, *181*, 195.
[162] M. Essen, L. Akker, R. Thür, M. Houben, I. F. J. Vankelecom, Z. Borneman, K.

Nijmeijer, *Adv. Mater. Interfaces* **2021**, *8*, 2001478.
[163] C. W. M. Ch'ng, Y. F. Yeong, N. Jusoh, N. H. Suhaimi, L. S. Lai, *J. Chem. Technol. Biotechnol.* **2022**, *97*, 995.
[164] S. Shahid, K. Nijmeijer, *Sep. Purif. Technol.* **2017**, *189*, 90.
[165] H. Shin, W. S. Chi, S. Bae, J. H. Kim, J. Kim, *J. Ind. Eng. Chem.* **2017**, *53*, 127.
[166] Y. Pan, B. Wang, Z. Lai, *J. Memb. Sci.* **2012**, *421–422*, 292.
[167] M. Shah, H. T. Kwon, V. Tran, S. Sachdeva, H.-K. Jeong, *Microporous Mesoporous Mater.* **2013**, *165*, 63.
[168] S. R. Venna, M. A. Carreon, *J. Am. Chem. Soc.* **2010**, *132*, 76.
[169] A. Huang, W. Dou, J. Caro, *J. Am. Chem. Soc.* **2010**, *132*, 15562.
[170] Z. Xie, J. Yang, J. Wang, J. Bai, H. Yin, B. Yuan, J. Lu, Y. Zhang, L. Zhou, C. Duan, *Chem. Commun.* **2012**, *48*, 5977.
[171] A. Huang, J. Caro, *Angew. Chemie Int. Ed.* **2011**, *50*, 4979.
[172] J. Yao, L. Li, W. H. Benjamin Wong, C. Tan, D. Dong, H. Wang, *Mater. Chem. Phys.* **2013**, *139*, 1003.
[173] H. Bux, C. Chmelik, R. Krishna, J. Caro, *J. Memb. Sci.* **2011**, *369*, 284.
[174] Y.-L. Li, J.-H. Xu, Y. Xu, *J. Mol. Catal. B Enzym.* **2010**, *64*, 48.
[175] Y. Liu, G. Zeng, Y. Pan, Z. Lai, *J. Memb. Sci.* **2011**, *379*, 46.
[176] A. Huang, F. Liang, F. Steinbach, J. Caro, *J. Memb. Sci.* **2010**, *350*, 5.
[177] A. Huang, N. Wang, C. Kong, J. Caro, *Angew. Chemie Int. Ed.* **2012**, *51*, 10551.
[178] A. Huang, Q. Liu, N. Wang, J. Caro, *Microporous Mesoporous Mater.* **2014**, *192*, 18.
[179] X. Zhang, Y. Liu, L. Kong, H. Liu, J. Qiu, W. Han, L.-T. Weng, K. L. Yeung, W. Zhu, *J. Mater. Chem. A* **2013**, *1*, 10635.
[180] A. D. Wiheeb, M. A. Ahmad, M. N. Murat, J. Kim, M. R. Othman, *Transp. Porous Media* **2014**, *104*, 133.
[181] J. Gascon, F. Kapteijn, B. Zornoza, V. Sebastián, C. Casado, J. Coronas, *Chem. Mater.* **2012**, *24*, 2829.
[182] L. Zhang, G. Wu, J. Jiang, *J. Phys. Chem. C* **2014**, *118*, 8788.
[183] W.-H. Lai, G.-L. Zhuang, H.-H. Tseng, M.-Y. Wey, *J. Memb. Sci.* **2019**, *572*, 410.
[184] R. Aniruddha, V. M. Shama, I. Sreedhar, C. M. Patel, *J. Clean. Prod.* **2022**, *350*, 131478.
[185] G. Kaur, R. K. Rai, D. Tyagi, X. Yao, P.-Z. Li, X.-C. Yang, Y. Zhao, Q. Xu, S. K. Singh, *J. Mater. Chem. A* **2016**, *4*, 14932.
[186] C.-W. Tsai, E. H. G. Langner, R. A. Harris, *Microporous Mesoporous Mater.* **2019**, *288*, 109613.
[187] J. A. Thompson, N. A. Brunelli, R. P. Lively, J. R. Johnson, C. W. Jones, S. Nair, *J. Phys. Chem. C* **2013**, *117*, 8198.
[188] M. A. Hussain, Y. Soujanya, G. N. Sastry, *J. Phys. Chem. C* **2015**, *119*, 23607.
[189] F. Yang, T. Ge, X. Zhu, J. Wu, R. Wang, *Sep. Purif. Technol.* **2022**, *287*, 120535.
[190] A. Thomas, R. Ahamed, M. Prakash, *Mater. Lett.* **2021**, *303*, 130575.
[191] B. Zheng, F. Fu, L. L. Wang, L. Yang, Y. Zhu, H. Du, *J. Phys. Chem. C* **2018**, *122*, 7203.
[192] X.-J. Hou, H. Li, *J. Phys. Chem. C* **2010**, *114*, 13501.
[193] C.-W. Tsai, J. W. Niemantsverdriet, E. H. G. Langner, *Microporous Mesoporous Mater.* **2018**, *262*, 98.
[194] Y. Liu, J. Liu, M. Chang, C. Zheng, *J. Phys. Chem. C* **2012**, *116*, 16985.
[195] H. Amrouche, S. Aguado, J. Pérez-Pellitero, C. Chizallet, F. Siperstein, D. Farrusseng, N. Bats, C. Nieto-Draghi, *J. Phys. Chem. C* **2011**, *115*, 16425.

[196] M. Li, J. Liu, S. Deng, Q. Liu, N. Qi, Z. Chen, *ACS Appl. Energy Mater.* **2021**, *4*, 7983.
[197] C. Fan, J. Xu, H. Jiang, R. Chen, *J. Solid State Chem.* **2022**, *309*, 123017.
[198] K. Kenyotha, K. Chanapattharapol, S. McCloskey, P. Jantaharn, *Crystals* **2020**, *10*, 599.
[199] Y. W. Abraha, C.-W. Tsai, J. W. H. Niemantsverdriet, E. H. G. Langner, *ACS Omega* **2021**, *6*, 21850.
[200] F. Akbari Beni, M. Niknam Shahrak, *Polyhedron* **2020**, *178*, 114338.
[201] A. Thomas, K. R. Maiyelvaganan, S. Kamalakannan, M. Prakash, *ACS Omega* **2019**, *4*, 22655.
[202] A. Thomas, M. Prakash, *Appl. Surf. Sci.* **2021**, *562*, 150173.
[203] A. Atash Jameh, T. Mohammadi, O. Bakhtiari, *Sep. Purif. Technol.* **2020**, *231*, 115900.
[204] A. A. Jameh, T. Mohammadi, O. Bakhtiari, M. Mahdyarfar, *J. Environ. Chem. Eng.* **2019**, *7*, 103058.
[205] H. Bux, C. Chmelik, J. M. van Baten, R. Krishna, J. Caro, *Adv. Mater.* **2010**, *22*, 4741.
[206] X. Dong, K. Huang, S. Liu, R. Ren, W. Jin, Y. S. Lin, *J. Mater. Chem.* **2012**, *22*, 19222.
[207] M. Zia ul Mustafa, H. bin Mukhtar, N. A. H. Md Nordin, H. A. Mannan, R. Nasir, N. Fazil, *Chem. Eng. Technol.* **2019**, *42*, 2580.
[208] M. C. McCarthy, V. Varela-Guerrero, G. V. Barnett, H.-K. Jeong, *Langmuir* **2010**, *26*, 14636.
[209] A. Huang, H. Bux, F. Steinbach, J. Caro, *Angew. Chemie* **2010**, *122*, 5078.
[210] M. He, J. Yao, L. Li, Z. Zhong, F. Chen, H. Wang, *Microporous Mesoporous Mater.* **2013**, *179*, 10.
[211] A. J. Brown, J. R. Johnson, M. E. Lydon, W. J. Koros, C. W. Jones, S. Nair, *Angew. Chemie Int. Ed.* **2012**, *51*, 10615.
[212] S. Wang, J. Cui, S. Zhang, X. Xie, W. Xia, *Mater. Res. Express* **2020**, *7*, 025304.
[213] M. van Essen, L. van den Akker, R. Thür, M. Houben, I. F. J. Vankelecom, Z. Borneman, K. Nijmeijer, *Sep. Purif. Technol.* **2021**, *260*, 118103.
[214] M.-T. Vu, R. Lin, H. Diao, Z. Zhu, S. K. Bhatia, S. Smart, *J. Memb. Sci.* **2019**, *587*, 117157.
[215] Q. Li, J. Guo, H. Zhu, F. Yan, *Small* **2019**, *15*, 1804874.
[216] R. Dahmani, S. Grubišić, I. Djordjević, S. Ben Yaghlane, S. Boughdiri, G. Chambaud, M. Hochlaf, *J. Chem. Phys.* **2021**, *154*, 024303.
[217] J. Hu, Y. Liu, J. Liu, C. Gu, *Fuel* **2017**, *200*, 244.
[218] L. Li, D. Yang, T. R. Fisher, Q. Qiao, Z. Yang, N. Hu, X. Chen, L. Huang, *Langmuir* **2017**, *33*, 11543.
[219] R. Chanajaree, T. Chokbunpiam, J. Kärger, S. Hannongbua, S. Fritzsche, *Microporous Mesoporous Mater.* **2019**, *274*, 266.
[220] L. Li, G. Zhou, Z. Yang, F. Fang, Q. Qiao, N. Hu, L. Huang, X. Chen, *J. Chem. Eng. Data* **2019**, *64*, 484.
[221] Z. Wan, G. Zhou, Z. Dai, L. Li, N. Hu, X. Chen, Z. Yang, *J. Chem. Inf. Model.* **2020**, *60*, 2208.
[222] E. M. Forman, B. R. Pimentel, K. J. Ziegler, R. P. Lively, S. Vasenkov, *Microporous Mesoporous Mater.* **2017**, *248*, 158.
[223] P. F. Rosen, M. S. Dickson, J. J. Calvin, N. L. Ross, T. Friščić, A. Navrotsky, B. F. Woodfield, *J. Am. Chem. Soc.* **2020**, *142*, 4833.
[224] A. Arami-Niya, G. Birkett, Z. Zhu, T. E. Rufford, *J. Mater. Chem. A* **2017**, *5*, 21389.
[225] B. A. Russell, A. D. Migone, *Microporous Mesoporous Mater.* **2017**, *246*, 178.

[226] K. G. Ray, D. Olmsted, N. He, Y. Houndonougbo, B. B. Laird, M. Asta, *Phys. Rev. B* **2012**, *85*, 085410.
[227] A. G. Kontos, V. Likodimos, C. M. Veziri, E. Kouvelos, N. Moustakas, G. N. Karanikolos, G. E. Romanos, P. Falaras, *ChemSusChem* **2014**, *7*, 1696.
[228] S. Ghosh, A. Modak, A. Samanta, K. Kole, S. Jana, *Mater. Adv.* **2021**, *2*, 3161.
[229] F. N. Al-Rowaili, U. Zahid, S. Onaizi, M. Khaled, A. Jamal, E. M. AL-Mutairi, *J. CO2 Util.* **2021**, *53*, 101715.
[230] Z. Li, H. Li, S. Yang, *Adv. Sustain. Syst.* **2022**, *6*, 2100380.
[231] J. Ma, J. Liu, Z. Zhang, B. Han, *Green Chem.* **2012**, *14*, 2410.
[232] F. Castro-Gómez, G. Salassa, A. W. Kleij, C. Bo, *Chem. - A Eur. J.* **2013**, *19*, 6289.
[233] S. Foltran, R. Mereau, T. Tassaing, *Catal. Sci. Technol.* **2014**, *4*, 1585.
[234] C. M. Miralda, E. E. Macias, M. Zhu, P. Ratnasamy, M. A. Carreon, *ACS Catal.* **2012**, *2*, 180.
[235] H. Ryu, R. Roshan, M.-I. Kim, D.-W. Kim, M. Selvaraj, D.-W. Park, *Korean J. Chem. Eng.* **2017**, *34*, 928.
[236] J. Tharun, G. Mathai, A. C. Kathalikkattil, R. Roshan, Y.-S. Won, S. J. Cho, J.-S. Chang, D.-W. Park, *Chempluschem* **2015**, *80*, 715.
[237] J. Tharun, K.-M. Bhin, R. Roshan, D. W. Kim, A. C. Kathalikkattil, R. Babu, H. Y. Ahn, Y. S. Won, D.-W. Park, *Green Chem.* **2016**, *18*, 2479.
[238] T. Jose, Y. Hwang, D.-W. Kim, M.-I. Kim, D.-W. Park, *Catal. Today* **2015**, *245*, 61.
[239] K. M. Bhin, J. Tharun, K. R. Roshan, D.-W. Kim, Y. Chung, D.-W. Park, *J. CO2 Util.* **2017**, *17*, 112.
[240] B. Mousavi, S. Chaemchuen, B. Moosavi, Z. Luo, N. Gholampour, F. Verpoort, *New J. Chem.* **2016**, *40*, 5170.
[241] R. R. Kuruppathparambil, T. Jose, R. Babu, G.-Y. Hwang, A. C. Kathalikkattil, D.-W. Kim, D.-W. Park, *Appl. Catal. B Environ.* **2016**, *182*, 562.
[242] A. Zanon, S. Chaemchuen, B. Mousavi, F. Verpoort, *J. CO2 Util.* **2017**, *20*, 282.
[243] R. R. Kuruppathparambil, R. Babu, H. M. Jeong, G.-Y. Hwang, G. S. Jeong, M.-I. Kim, D.-W. Kim, D.-W. Park, *Green Chem.* **2016**, *18*, 6349.
[244] B. Tang, S. Li, W. Song, Y. Li, E. Yang, X. Zhao, L. Li, *Chem. – An Asian J.* **2019**, *14*, 4375.
[245] L. Hu, Z. Yan, X. Mo, X. Peng, L. Chen, *Microporous Mesoporous Mater.* **2020**, *294*, 109917.
[246] L. Hu, L. Chen, X. Peng, J. Zhang, X. Mo, Y. Liu, Z. Yan, *Microporous Mesoporous Mater.* **2020**, *299*, 110123.
[247] L. Yang, L. Yu, G. Diao, M. Sun, G. Cheng, S. Chen, *J. Mol. Catal. A Chem.* **2014**, *392*, 278.
[248] P. Ma, M. Ding, X. Liu, W. Rong, J. Yao, *Chem. Eng. Sci.* **2022**, *252*, 117530.
[249] S. Chaemchuen, X. Xiao, M. Ghadamyari, B. Mousavi, N. Klomkliang, Y. Yuan, F. Verpoort, *J. Catal.* **2019**, *370*, 38.
[250] W. Xiang, Z. Sun, Y. Wu, L.-N. He, C. Liu, *Catal. Today* **2020**, *339*, 337.
[251] T. Toyao, M. Fujiwaki, K. Miyahara, T.-H. Kim, Y. Horiuchi, M. Matsuoka, *ChemSusChem* **2015**, *8*, 3905.
[252] M. Ding, S. Chen, X. Liu, L. Sun, J. Lu, H. Jiang, *ChemSusChem* **2017**, *10*, 1898.
[253] C. Duan, M. Ding, Y. Feng, M. Cao, J. Yao, *Sep. Purif. Technol.* **2022**, *285*, 120359.
[254] G. Lee, M. Lee, Y. Jeong, E. Jang, H. Baik, J. Chul Jung, J. Choi, *Chem. Eng. J.* **2022**,

435, 134964.
[255] A. Gu, Y. Zhang, Z. Wu, H. Cui, T. Hu, B. Zhao, *Angew. Chemie Int. Ed.* **2022**, *61*.
[256] M. Zhang, Y. Xu, B. L. Williams, M. Xiao, S. Wang, D. Han, L. Sun, Y. Meng, *J. Clean. Prod.* **2021**, *279*, 123344.
[257] A. Poungsombate, T. Imyen, P. Dittanet, B. Embley, P. Kongkachuichay, *J. Taiwan Inst. Chem. Eng.* **2017**, *80*, 16.
[258] C. Hu, M. Yoshida, H.-C. Chen, S. Tsunekawa, Y.-F. Lin, J.-H. Huang, *Chem. Eng. Sci.* **2021**, *235*, 116451.
[259] J. Shi, L. Zhang, N. Sun, D. Hu, Q. Shen, F. Mao, Q. Gao, W. Wei, *ACS Appl. Mater. Interfaces* **2019**, *11*, 28858.
[260] C. Hu, C.-W. Chang, M. Yoshida, K.-H. Wang, *J. Mater. Chem. A* **2021**, *9*, 7048.
[261] W. Li, H. Wang, X. Jiang, J. Zhu, Z. Liu, X. Guo, C. Song, *RSC Adv.* **2018**, *8*, 7651.
[262] P. Sharma, J. Sebastian, S. Ghosh, D. Creaser, L. Olsson, *Catal. Sci. Technol.* **2021**, *11*, 1665.
[263] L. Guo, J. Sun, Q. Ge, N. Tsubaki, *J. Mater. Chem. A* **2018**, *6*, 23244.
[264] J. Wei, R. Yao, Y. Han, Q. Ge, J. Sun, *Chem. Soc. Rev.* **2021**, *50*, 10764.
[265] T. A. Atsbha, T. Yoon, P. Seongho, C.-J. Lee, *J. CO2 Util.* **2021**, *44*, 101413.
[266] S. Nieß, U. Armbruster, S. Dietrich, M. Klemm, *Catalysts* **2022**, *12*, 374.
[267] J. Ashok, S. Pati, P. Hongmanorom, Z. Tianxi, C. Junmei, S. Kawi, *Catal. Today* **2020**, *356*, 471.
[268] S. Zhang, Z. Wu, X. Liu, K. Hua, Z. Shao, B. Wei, C. Huang, H. Wang, Y. Sun, *Top. Catal.* **2021**, *64*, 371.
[269] S. Wickramasinghe, J. Wang, B. Morsi, B. Li, *Energy & Fuels* **2021**, *35*, 11820.
[270] A. Modak, A. Ghosh, A. Bhaumik, B. Chowdhury, *Adv. Colloid Interface Sci.* **2021**, *290*, 102349.
[271] T. Zhao, Y. Hui, Niamatullah, Z. Li, *Mol. Catal.* **2019**, *474*, 110421.
[272] S. Fan, H. Cheng, M. Feng, X. Wu, Z. Fan, D. Pan, G. He, *Chinese J. Chem. Eng.* **2021**, *39*, 144.
[273] J. Liang, Q. Wu, Y. Huang, R. Cao, *EnergyChem* **2021**, *3*, 100064.
[274] W. K. Fan, M. Tahir, *Ind. Eng. Chem. Res.* **2021**, *60*, 13149.
[275] S. Hu, M. Liu, F. Ding, C. Song, G. Zhang, X. Guo, *J. CO2 Util.* **2016**, *15*, 89.
[276] J. Liu, Y. Sun, X. Jiang, A. Zhang, C. Song, X. Guo, *J. CO2 Util.* **2018**, *25*, 120.
[277] Z. Dong, J. Zhao, Y. Tian, B. Zhang, Y. Wu, *Catalysts* **2020**, *10*, 455.
[278] W. Li, A. Zhang, X. Jiang, C. Chen, Z. Liu, C. Song, X. Guo, *ACS Sustain. Chem. Eng.* **2017**, *5*, 7824.
[279] M.-Y. Li, F. Wang, J. Zhang, *Cryst. Growth Des.* **2020**, *20*, 2866.
[280] X. Hu, M. Luo, M. ur Rehman, J. Sun, H. A. S. M. Yaseen, F. Irshad, Y. Zhao, S. Wang, X. Ma, *J. CO2 Util.* **2022**, *60*, 101992.
[281] S. E. M. Elhenawy, M. Khraisheh, F. AlMomani, G. Walker, *Catalysts* **2020**, *10*, 1293.
[282] H. Zhang, J. Li, Q. Tan, L. Lu, Z. Wang, G. Wu, *Chem. – A Eur. J.* **2018**, *24*, 18137.
[283] T. Zhan, Y. Zou, Y. Yang, X. Ma, Z. Zhang, S. Xiang, *ChemCatChem* **2022**, *14*.
[284] X. Li, Q.-L. Zhu, *EnergyChem* **2020**, *2*, 100033.
[285] J. Ma, Ed., *Photo- and Electro-Catalytic Processes*, Wiley, **2022**.
[286] D. Narváez-Celada, A. S. Varela, *J. Mater. Chem. A* **2022**, *10*, 5899.
[287] Y. Zhao, L. Zheng, D. Jiang, W. Xia, X. Xu, Y. Yamauchi, J. Ge, J. Tang, *Small* **2021**, *17*, 2006590.

[288] E. O. Eren, S. Özkar, *J. Power Sources* **2021**, *506*, 230215.
[289] S. S. A. Shah, T. Najam, M. Wen, S.-Q. Zang, A. Waseem, H.-L. Jiang, *Small Struct.* **2021**, 2100090.
[290] R. Wang, F. Kapteijn, J. Gascon, *Chem. – An Asian J.* **2019**, *14*, 3452.
[291] X. Huang, Y.-B. Zhang, *Coord. Chem. Rev.* **2021**, *427*, 213564.
[292] Y. Quan, R. Yu, J. Zhu, A. Guan, X. Lv, C. Yang, S. Li, J. Wu, G. Zheng, *J. Colloid Interface Sci.* **2021**, *601*, 378.
[293] Y. Wang, P. Hou, Z. Wang, P. Kang, *ChemPhysChem* **2017**, *18*, 3142.
[294] J.-X. Wu, W.-W. Yuan, M. Xu, Z.-Y. Gu, *Chem. Commun.* **2019**, *55*, 11634.
[295] X. Jiang, H. Li, J. Xiao, D. Gao, R. Si, F. Yang, Y. Li, G. Wang, X. Bao, *Nano Energy* **2018**, *52*, 345.
[296] R. Zhang, J. Yang, X. Zhao, H. Yang, H. Li, B. Ji, G. Zhou, X. Ma, D. Yang, *ChemCatChem* **2022**, *14*.
[297] A. Ahmad, N. Iqbal, T. Noor, A. Hassan, U. A. Khan, A. Wahab, M. A. Raza, S. Ashraf, *J. CO2 Util.* **2021**, *48*, 101523.
[298] H. Qi, Y. Zhou, Y. Li, F. Liao, Z. Wang, X. Wang, H. Huang, M. Shao, Y. Liu, Z. Kang, *Nanoscale* **2021**, *13*, 14089.
[299] J.-X. Gu, X. Zhao, Y. Sun, J. Zhou, C.-Y. Sun, X.-L. Wang, Z.-H. Kang, Z.-M. Su, *J. Mater. Chem. A* **2020**, *8*, 16616.
[300] Y. Hu, H. Wu, Y. Yang, X. Lin, H. Cheng, R. Zhang, X. Jiang, J. Wang, *J. Nanoparticle Res.* **2021**, *23*, 133.
[301] C. Yan, Y. Ye, L. Lin, H. Wu, Q. Jiang, G. Wang, X. Bao, *Catal. Today* **2019**, *330*, 252.
[302] X.-L. Chen, L.-S. Ma, W.-Y. Su, L.-F. Ding, H.-B. Zhu, H. Yang, *Electrochim. Acta* **2020**, *331*, 135273.
[303] Y. Guan, Y. Liu, J. Yi, J. Zhang, *Dalt. Trans.* **2022**.
[304] P. Shao, L. Yi, S. Chen, T. Zhou, J. Zhang, *J. Energy Chem.* **2020**, *40*, 156.
[305] L. Zhang, J. Zhang, *Front. Energy* **2019**, *13*, 221.
[306] A. Crake, *Mater. Sci. Technol.* **2017**, *33*, 1737.
[307] M. Nemiwal, V. Subbaramaiah, T. C. Zhang, D. Kumar, *Sci. Total Environ.* **2021**, *762*, 144101.
[308] I. I. Alkhatib, C. Garlisi, M. Pagliaro, K. Al-Ali, G. Palmisano, *Metal-organic frameworks for photocatalytic CO2 reduction under visible radiation: A review of strategies and applications*, Vol. 340, Elsevier B.V., **2020**, pp. 209–224.
[309] G. Y. Shinde, A. S. Mote, M. B. Gawande, *Catalysts* **2022**, *12*, 94.
[310] X. Li, J. Yu, M. Jaroniec, X. Chen, *Chem. Rev.* **2019**, *119*, 3962.
[311] R. R. Ikreedeegh, M. Tahir, *J. CO2 Util.* **2021**, *43*, 101381.
[312] W. Zhang, R. Huang, L. Song, X. Shi, *Nanoscale* **2021**, *13*, 9075.
[313] M. Aggarwal, N. P. Shetti, S. Basu, T. M. Aminabhavi, *J. Environ. Manage.* **2022**, *313*, 114916.
[314] H. L. Nguyen, *Adv. Energy Mater.* **2020**, *10*, 2002091.
[315] D. Li, M. Kassymova, X. Cai, S.-Q. Zang, H.-L. Jiang, *Coord. Chem. Rev.* **2020**, *412*, 213262.
[316] D. Qin, Y. Zhou, W. Wang, C. Zhang, G. Zeng, D. Huang, L. Wang, H. Wang, Y. Yang, L. Lei, S. Chen, D. He, *J. Mater. Chem. A* **2020**, *8*, 19156.
[317] X. Li, L. Wang, W. Su, Y. Xing, *New J. Chem.* **2021**, *45*, 2315.
[318] B. Wang, W. Chen, Y. Song, G. Li, W. Wei, J. Fang, Y. Sun, *Catal. Today* **2018**, *311*, 23.

[319] K. Guo, I. Hussain, G. Jie, Y. Fu, F. Zhang, W. Zhu, *J. Environ. Sci.* **2023**, *125*, 290.
[320] C.-C. Wang, Y.-Q. Zhang, J. Li, P. Wang, *J. Mol. Struct.* **2015**, *1083*, 127.
[321] J. W. Maina, J. A. Schütz, L. Grundy, E. Des Ligneris, Z. Yi, L. Kong, C. Pozo-Gonzalo, M. Ionescu, L. F. Dumée, *ACS Appl. Mater. Interfaces* **2017**, *9*, 35010.
[322] C. I. Ezugwu, S. Liu, C. Li, S. Zhuiykov, S. Roy, F. Verpoort, *Coord. Chem. Rev.* **2022**, *450*, 214245.
[323] S. Goyal, M. Shaharun, C. Kait, B. Abdullah, M. Ameen, *Catalysts* **2018**, *8*, 581.
[324] Q. Liu, Z.-X. Low, L. Li, A. Razmjou, K. Wang, J. Yao, H. Wang, *J. Mater. Chem. A* **2013**, *1*, 11563.
[325] S. Liu, J. Wang, J. Yu, *RSC Adv.* **2016**, *6*, 59998.
[326] J. Qin, S. Wang, X. Wang, *Appl. Catal. B Environ.* **2017**, *209*, 476.
[327] Z.-C. Kong, J.-F. Liao, Y.-J. Dong, Y.-F. Xu, H.-Y. Chen, D.-B. Kuang, C.-Y. Su, *ACS Energy Lett.* **2018**, *3*, 2656.
[328] M. Wang, J. Liu, C. Guo, X. Gao, C. Gong, Y. Wang, B. Liu, X. Li, G. G. Gurzadyan, L. Sun, *J. Mater. Chem. A* **2018**, *6*, 4768.
[329] Y. Su, H. Xu, J. Wang, X. Luo, Z. Xu, K. Wang, W. Wang, *Nano Res.* **2019**, *12*, 625.
[330] J.-J. Li, Q. Zhang, L.-Y. Zhang, J.-Y. Zhang, Y. Liu, N. Zhang, Y.-Z. Fang, *Catal. Sci. Technol.* **2022**.
[331] Y. Liu, L. Deng, J. Sheng, F. Tang, K. Zeng, L. Wang, K. Liang, H. Hu, Y.-N. Liu, *Appl. Surf. Sci.* **2019**, *498*, 143899.
[332] H.-J. Peng, L. Zhu, Y.-L. Wang, H.-Y. Chao, L. Jiang, Z.-P. Qiao, *Inorg. Chem. Commun.* **2020**, *117*, 107943.
[333] H.-J. Peng, P.-Q. Zheng, H.-Y. Chao, L. Jiang, Z.-P. Qiao, *RSC Adv.* **2020**, *10*, 551.
[334] M. Izadpanah Ostad, M. Niknam Shahrak, F. Galli, *J. CO2 Util.* **2021**, *43*, 101373.
[335] X. Li, W. He, C. Li, B. Song, S. Liu, *Appl. Catal. B Environ.* **2021**, *287*, 119934.
[336] Z. Tang, F. Zhu, J. Zhou, W. Chen, K. Wang, M. Liu, N. Wang, N. Li, *Appl. Catal. B Environ.* **2022**, *309*, 121267.
[337] J. Becerra, D.-T. Nguyen, V.-N. Gopalakrishnan, T.-O. Do, *ACS Appl. Energy Mater.* **2020**, *3*, 7659.
[338] E. Pipelzadeh, V. Rudolph, G. Hanson, C. Noble, L. Wang, *Appl. Catal. B Environ.* **2017**, *218*, 672.
[339] Y.-H. Zou, H.-N. Wang, X. Meng, H.-X. Sun, Z.-Y. Zhou, *Nanoscale Adv.* **2021**, *3*, 1455.
[340] S. Yan, S. Ouyang, H. Xu, M. Zhao, X. Zhang, J. Ye, *J. Mater. Chem. A* **2016**, *4*, 15126.
[341] Y.-J. Dong, Y. Jiang, J.-F. Liao, H.-Y. Chen, D.-B. Kuang, C.-Y. Su, *Sci. China Mater.* **2022**.
[342] Y. Ke, Q. Liang, S. Zhao, Z. Zhang, X. Li, Z. Li, *Inorg. Chem.* **2022**, *61*, 2652.
[343] W. Chen, B. Han, C. Tian, X. Liu, S. Liang, H. Deng, Z. Lin, *Appl. Catal. B Environ.* **2019**, *244*, 996.
[344] M. Izadpanah Ostad, M. Niknam Shahrak, F. Galli, *Microporous Mesoporous Mater.* **2021**, *326*, 111363.
[345] Y. Sun, X. Jia, H. Huang, X. Guo, Z. Qiao, C. Zhong, *J. Mater. Chem. A* **2020**, *8*, 3180.
[346] W. Xu, H. Chen, K. Jie, Z. Yang, T. Li, S. Dai, *Angew. Chemie* **2019**, *131*, 5072.
[347] F.-F. Chen, J. Chen, Y.-N. Feng, L. Li, Y. Yu, *Sci. China Mater.* **2022**, *65*, 413.
[348] Z.-W. Wang, Z.-Y. Zhu, S. Li, F. Wang, *CrystEngComm* **2022**.
[349] L. Tang, S. Zhang, Q. Wu, X. Wang, H. Wu, Z. Jiang, *J. Mater. Chem. A* **2018**, *6*, 2964.
[350] H. He, Q. Zhu, C. Zhang, Y. Yan, J. Yuan, J. Chen, C. Li, M. Du, *Chem. – An Asian J.*

2019, *14*, 958.
[351] Y. Liu, Y. Chen, Y. Liu, Z. Chen, H. Yang, Z. Yue, Q. Fang, Y. Zhi, S. Shan, *J. Catal.* **2022**, *407*, 65.
[352] J. B. James, Y. S. Lin, *J. Memb. Sci.* **2017**, *532*, 9.
[353] A. Kasik, X. Dong, Y. S. Lin, *Microporous Mesoporous Mater.* **2015**, *204*, 99.
[354] R. Banerjee, H. Furukawa, D. Britt, C. Knobler, M. O'Keeffe, O. M. Yaghi, *J. Am. Chem. Soc.* **2009**, *131*, 3875.
[355] D. Georgouvelas, H. N. Abdelhamid, J. Li, U. Edlund, A. P. Mathew, *Carbohydr. Polym.* **2021**, *264*, 118044.
[356] M. Soliman, A. A. Sadek, H. N. Abdelhamid, K. Hussein, *Res. Vet. Sci.* **2021**, *137*, 262.
[357] H. N. Abdelhamid, A. P. Mathew, *Front. Chem. Eng.* **2021**, *3*, 790314.
[358] H. N. . Abdelhamid, A. P. . Mathew, *Preprints* **2022**, 2022010035.
[359] H. N. Abdelhamid, H.-F. Wu, *J. Mater. Chem. B* **2013**, *1*, 3950.
[360] H. N. Abdelhamid, H.-F. Wu, *J. Mater. Chem. B* **2013**, *1*, 6094.
[361] J. Gopal, H. N. Abdelhamid, P.-Y. Hua, H.-F. Wu, *J. Mater. Chem. B* **2013**, *1*, 2463.
[362] H. N. Abdelhamid, H.-F. Wu, *Mater. Sci. Eng. C* **2014**, *45*, 438.
[363] M. Dowaidar, H. Nasser Abdelhamid, M. Hällbrink, Ü. Langel, X. Zou, *J. Biomater. Appl.* **2018**, *33*, 392.
[364] H. N. Abdelhamid, Y. C. Lin, H.-F. Wu, *Microchim. Acta* **2017**, *184*, 1517.
[365] H. N. Abdelhamid, H.-F. Wu, *Spectrochim. Acta Part A Mol. Biomol. Spectrosc.* **2018**, *188*, 50.
[366] H. N. Abdelhamid, In *Nanoengineering of Biomaterials*, Wiley, **2022**, pp. 91–105.
[367] L. Valencia, H. N. Abdelhamid, *Carbohydr. Polym.* **2019**, *213*, 338.